Depsi-Peptide functionalized Biopolymers for Hydrogel Synthesis

---

Masterthesis

For the Academic Degree of Master of Science (M.Sc.)

in the Course of Study Chemistry

in the Department of Chemistry, Pharmacy, Geography and Geosciences

of the Johannes Gutenberg-University Mainz

By

Patrick Roth

Born in Wiesbaden

2707110

Mainz, 2020

Diese Arbeit wurde unter der Leitung von Prof. Dr. Tanja Weil im Zeitraum von Oktober 2019 bis April 2020 am Max-Planck-Institut für Polymerforschung im Bereich “Synthese von Makromolekülen” angefertigt

Erstgutachter: Prof. Dr. Tanja Weil
Zweitgutachter: Prof. Dr. Holger Frey

Abgabe der Arbeit am 17.04.2020

Eigenständigkeitserklärung

Ich, Patrick Roth, Matrikelnummer 2707110 versichere, dass ich meine Masterarbeit selbstständig verfasst und keine anderen als die angegebenen schriftlichen und elektronischen Quellen sowie andere Hilfsmittel benutzt habe. Alle Ausführungen, die anderen Schriften wörtlich oder sinngemäß entnommen wurden, habe ich kenntlich gemacht.

Mainz, den 17.04.2020	Roth
(Ort, Datum)	(Unterschrift)

Zusammenfassung

Das Thema dieser Masterarbeit ist die Synthese von Depsi-Peptid funktionalisierten Biopolymeren für die Herstellung von Hydrogelen. Hierbei ermöglichen die Depsi-Peptide durch ihre pH Responsivität einen Sol-zu-Gel Übergang, indem sie durch eine Änderung des pH-Werts einen *O,N*-Acylshift vollziehen, welcher es den Peptidketten ermöglicht β-Faltblätter und anschließend Fibrillen auszubilden. Diese supramolekularen Wechselwirkungen führen letztendlich zur Vernetzung einzelner Polymerketten und potenziell zu einem Hydrogel.

Das Depsi-Peptid mit der Sequenz KIKI(O-C(O))SQINC (D3) soll mit Hilfe einer Thiol-En Click Reaktion an unterschiedliche Polymerrückgrate gekuppelt werden, um potentiell bioabbaubare und -kompatible Hydrogele herzustellen.

Da die Synthese von Peptiden über die Festphase mit Hilfe der Fmoc-Strategie trotz ihrer langen Geschichte immer noch Probleme birgt, wurde die Synthese des Depsi-Peptids D3 optimiert. Dabei lag der Fokus vor allem auf der Reduktion der Nebenprodukte durch den Wechsel des Harzes für die Festphasenpeptidsynthese und die Erhöhung der Äquivalente für die Veresterung des Serins. Der Wechsel von einem Wang- zu einem 2-Chlortrityl-Harz ermöglichte sterische Abschirmung des α-Kohlenstoffatoms des Cysteins und damit eine Unterdrückung der Deprotonierung durch Piperidin während der Fmoc-Abspaltung. Weiterhin wurden Nebenprodukte umgangen, die während der Abspaltung des Peptids vom Wang-Harz entstanden. Das synthetisierte Peptid wurde auf seine Reinheit mittels MALDI-ToF-MS und LCMS untersucht. Anschließend wurden die pH-responsiven Eigenschaften des Peptids mithilfe von ATR-FTIR, TEM Aufnahmen, CD-Spektroskopie, ThT-Assay und Conversion-Assay untersucht.

Um die Auswirkung verschiedener Polymerrückgrate auf die physikalischen und chemischen Eigenschaften der resultierenden Hybridmaterialien zu testen, wurden jeweils zwei Poly(phosphonat)e und zwei Dextrane mit niedrigen und hohen Molekulargewichten für die Hybridsynthese verwendet. Die Dextrane wurden mit GMA funktionalisiert, um eine Thiol-En Click Reaktion zu ermöglichen. Da eines der verwendeten Monomere zur Synthese der Poly(phosphonat)e bereits eine Allyl-Funktion trug, war eine Funktionalisierung dieser Polymere nicht nötig. Das Molekulargewicht und der Funktionalisierungsgrad mit Alken-Gruppen der Polymerrückgrate wurde über GPC und/oder NMR-Spektroskopie bestimmt.

Zuletzt wurden die Polymerrückgrate mit dem Depsi-Peptid D3 über eine Thiol-En-Click Reaktion funktionalisiert und über NMR-Spektroskopie ihr Molekulargewicht und ihr Funktionalisierungsgrad mit Peptid bestimmt. Zudem wurden die pH-responsiven Eigenschaften und das Aggregationsverhalten über ATR-FTIR, TEM Aufnahmen und ThT-Asssay bestimmt. Die Fähigkeit zur Ausbildung von Hydrogelen und die mechanischen Eigenschaften der synthetisierten Hybride wurden über rheologische Messungen bestimmt. Dafür wurden diese mit einem Phosphatpuffer (pH 7.4) versetzt und mechanischer Belastung ausgesetzt. Es zeigten sich deutliche Unterschiede der Hybridmaterialien, je nachdem welches Rückgrat verwendet wurde: Die Polyphosphonat-Peptid Hybridmaterialien besaßen nur geringe Stabilität und wurden deshalb als Flüssigkeit eingestuft. Der niedermolekulare Dextran-Hybrid ergab ein weiches Hydrogel mit scherverdünnenden Eigenschaften und der Fähigkeit zur selbstständigen Regeneration.

Table of Contents

1. Introduction

1.1 Peptides

Peptides and proteins consisting of amino acids (AA) are key molecules in living systems. Their importance in biological processes like oxygen transport, proliferation and differentiation of cells and many other processes are undeniable. The structures of proteins can be subdivided in four categories: Primary, secondary, tertiary and quaternary structure. The primary structure is the sequence of AA connected via amide bonds. Peptides and proteins fold into three-dimensional structures through interactions such as hydrogen bonds, hydrophobic interactions, etc. between the AA in the linear sequence close to each other. This structure is called secondary structure, which is distinguished between in α-helix, β-sheet, β-turn and random coil. The tertiary structure is built by further interactions between functional groups of the AA of the same sequence as Coulomb-interactions, hydrogen bonds, etc. and disulfide bridges between two cysteines. The connection of several polypeptides is called quaternary structure and forms often the final structure of the protein.[1] Peptides can be synthesized in different ways. J. L. Bailey established a peptide synthesis via α-amino acid *N*-carboxyanhydrides (NCA) and R. B. Merrifield via a solid phase synthesis.[2,3]

Natural proteins usually consist of the 20 natural AA, which function as building blocks for peptides. AA are composed of a carboxylic acid and an amine function, which are positioned at the α-position of the carboxylic acid and have a defined side chain. The α-carbon atom in every AA is a chiral center, except in glycin, which is the simplest AA with two hydrogen atoms at the α-carbon atom. Proteinogenic AA generally have a L-configuration and possess a corresponding side chain. There are a lot of non-proteinogenic AA besides the natural AA, which also occur in nature. Well known representatives of the approximately 400 non-proteinogenic AA are L-thyroxin, L-DOPA and L-ornithine. Due to the high number of natural occurring AA and the even higher amount of synthetic AA, there is no limit to the possible peptide sequences.[4,5]

Two AA formally react via a condensation reaction to form an amide/peptide bond. This bond is rigid and fixed in one plane, while the C-C- and C-N-bonds are freely rotating. This yields a reduced flexibility of the peptide chain and corresponding superstructures. Associated AA of around 10 monomers build an oligopeptide, up to 100 monomers a macro peptide or protein. Peptides with higher amounts of AA are called protein.[5]

Since the condensation of AA has an energy barrier, the reaction must be induced by catalysis via enzymes or derivatives of the educts. The chemical synthesis of defined peptides is only possible, if the functional groups of the AA are protected in order to allow the reaction of the carboxylic acid and the amino function. Those protecting groups can be cleaved off after successful synthesis of the peptide.[5,4]

There are different possibilities of superstructures for peptides and proteins depending on the sequence of AA. The primary structure of peptides and proteins is the order of AA, the amino acid sequence. Twenty proteinogenic AA yield a number of structural alternatives $A_{\mathrm{PS}} = 20^{\mathrm{N}}$. In this connection N is the number of built-in AA. Peptides are not threadlike molecules in contrast to classical synthetic polymers like polystyrene. They form a fixed spatial shape defined by their primary structure. The chain links are rotatable around their covalent single bond of the -C-C-N back bone and thus can form a stable structural state. Furthermore, the non-covalent bonds are crucial for the structure of peptides. The backbone and side chains of AA can interact with each other through hydrogen bonds, van-der-Waals forces and Coulomb interactions. Areas with the same charge repel each other and must be spatially separated, while differently charged areas attract each other to stabilize bonds. In the case of cysteine, it is possible to form disulfide bridges between two thiol groups.[5]

The secondary structure is called α-helix, if a peptide backbone forms a tightly convoluted rod, while the side chains are turned outside in a screw-like order (Figure 1A). Hydrogen bonds between the NH- and the CO-groups of the backbone stabilize the helix, while the CO-group of an AA interacts with the NH-group of the following fourth AA. Thus, all CO- and NH-groups except for the last are responsible for the stabilization of the secondary structure. Each side chain is shifted by 0.15 nm along the axis (translation) and turned by 100°; therefore, one full turn of the helix takes 3.6 AA. Since the natural occurring AA are in the L-configuration, a right-handed turn of the helix is energetically favored.[1]

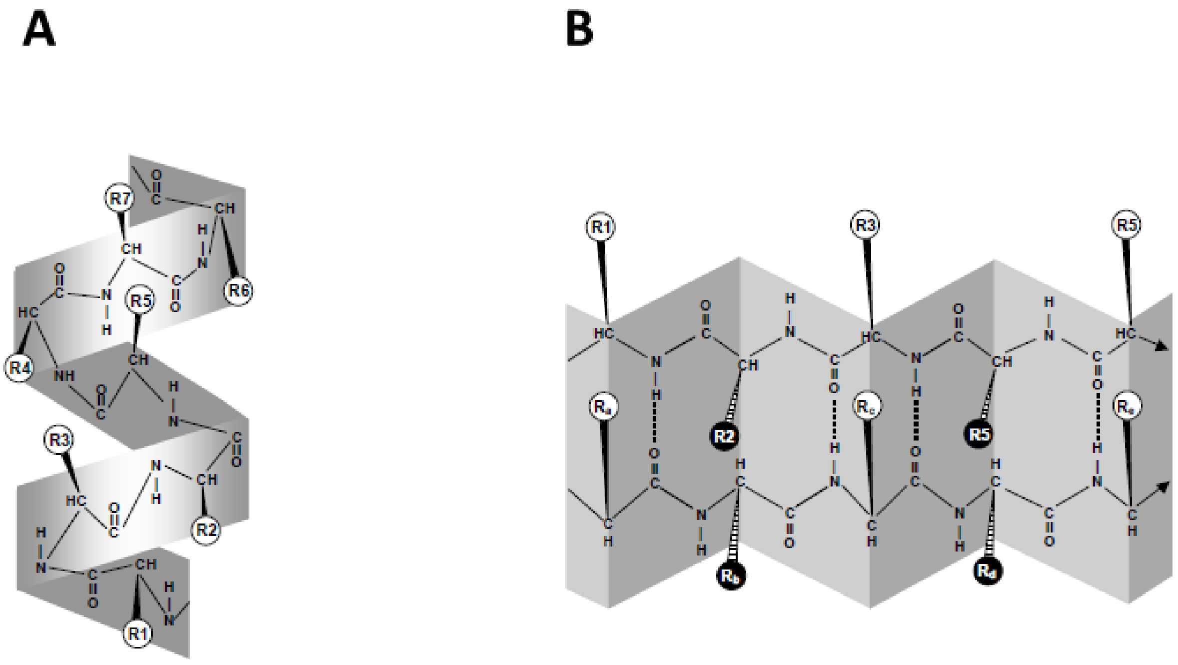

Figure 1:Scheme of an α-helical winded peptide sequence (A) and a β-sheet structure (B).[5]

Relatively uniform peptide chains of similar amino acids aggregate next to each other in sections and form a β-sheet structure through hydrogen bonds (Figure 1B).[5] The sequences can be either oriented parallel, which means, adjacent peptide sequences have the same direction, or antiparallel, which means, adjacent peptide sequences have the opposite direction. Amphiphilic peptides, such as RADA 16 and EAK 16, exhibit high aggregation behavior, due to their “ionic complementation”.[6] A special and well known kind of those aggregates are amyloid fibrils. These fibrils consist of cross-β-sheet bilayer of peptides, where the hydrophobic side chains are turned inside of the fibril and the hydrophilic side chains are exposed to the solvent (Figure 2).[7–9]

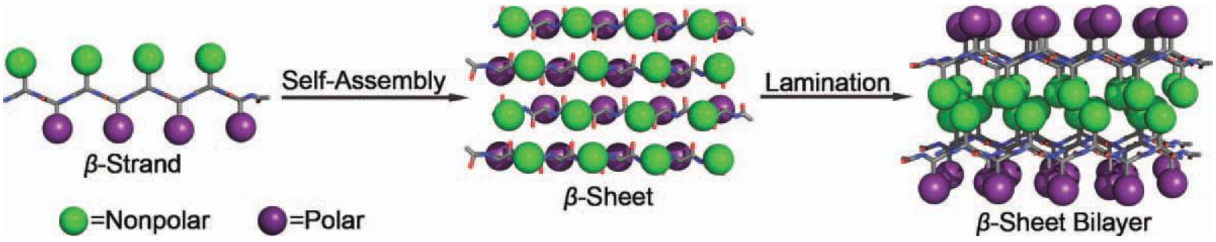

Figure 2: Proposed mode of amphiphilic peptide self-assembly and arrangement of AA side chains in the β-sheet bilayer.[7]

Thus, they are called fibrillar polypeptide aggregates with a cross-β-structure, which consists of, in principle, infinitely continued β-sheets. Those β-sheets form the central structured backbone of the fibrils. The β-strands of the polypeptides are ordered perpendicularly to the fibril axis and the hydrogen bonds parallel to the fibril axis (Figure 3). Therefore, amyloid fibrils encompass a structural superfamily, which shares a common protofilament substructure, regardless to the nature of their precursor proteins.[10]

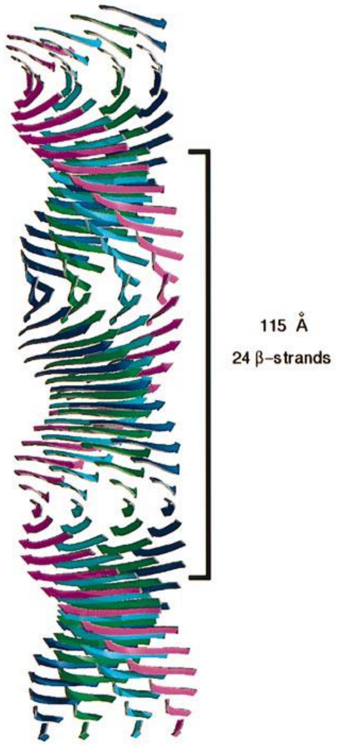

Figure 3: Model of the common core protofilament structure of amyloid fibrils. Several β-sheets (four illustrated here) form the protofilament structure. If the β-strands twist normally, than the β-sheets twist around a common helical axis, which coincides with the axis of the protofilament, yielding a helical repeat of 115.5 Å containing 24 β-strands (boxed region).[10]

If two β-sheets are connected via two to five AA, then this structure is called β-hairpin. The flexible chain or the rigid bend between both β-sheets yields an antiparallel structure of them (Figure 4).[11]

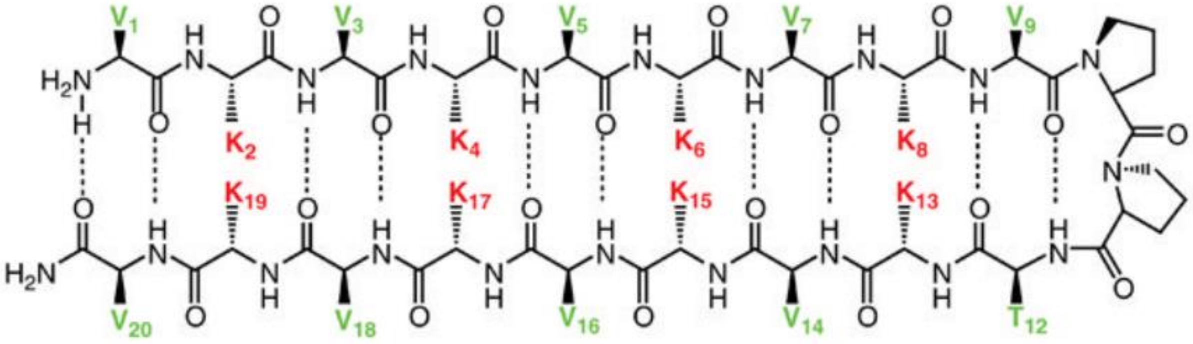

Figure 4: β-hairpin structure of a peptide consisting of valine (green) and lysine (red) units with a connection vie two proline units.[12]

The definition of the random coil structure of peptides is similar to the definition of the random coil structure of polymers with a few limitations. Random coils of polymers are defined as a complete set of spatial arrangements of chain molecules, where the mutual orientation of the segments is randomly changed with time, while they are free from external constraints that could affect their conformation.[13] However, because of the planar and rigid amide bond, peptides have restrictions to their flexibility that are not occurring in typical synthetic polymers. Thus, the mainchain path of the peptide can be described as a series of peptide planes connecting the α-carbon atoms. The orientation of these planes can be defined by their torsion angles ϕ and ψ. Assigning a value to each torsion angle for every AA in a peptide chain is sufficient to define a complete conformation.[14]

The spatial assignment of those chain links into the secondary structures determines the whole structure of a peptide. Those segments are present as loops and bends of the peptide chain and in combination with α-helices and β-sheets yield a compact, folded and ordered coil (tertiary structure). A combination of several peptide chains yields the quaternary structure, which is also stabilized through hydrogen bonds, van-der-Waals forces, Coulomb interactions and disulfide bridges.[5]

1.1.1 Merrifield solid-phase peptide synthesis

In 1963 R. B. Merrifield published a new approach to synthesize peptides. In his approach, the first AA is bound to a solid phase and every new AA is protected at the *N*-terminus and their functional group, leading to a much faster and simpler synthesis procedure.[3] A particle made of a copolymer of styrene and divinylbenzene with a chloromethyl function was used as a solid phase by Merrifield. The chloromethyl function can be used as linker to the solid phase for the *C*-terminal AA.[3] Today there are three widely used resins as solid phases: (1) Polystyrene based, (2) poly(ethylene glycol)-grafted polystyrene and (3) poly(ethylene glycol) resins without polystyrene.[15] As mentioned, there is the need for a linker group to connect the first AA to the resin. Since there are different requirements for the linker (stability at coupling and deprotection pH, end group functionalization and steric protection of the α-C hydrogen atom), a diversity of functional groups were developed. The most popular ones are the Rink(**1**)- and the Wang(**2**)-resins followed by 2-chlorotrityl(**3**)- (Clt) and XAL(**4**)-resins.[15] Peptides can be cleaved under mild acidic conditions from Rink-resins to yield a peptide amide, while the side chain protecting groups remain intact.[16] Wang-resins serve a similar purpose: The side chain protection also remains intact during cleavage from the resin, while the resulting peptide possesses a free carboxyl group.[17] AA can be quantitively anchored on Clt-resins with diisopropylethylamine and later fully cleaved as AA or peptide in 15-60 min, while the side chain protecting groups remain intact.[18] Peptides can be cleaved from XAL-resins with excellent yields and purities, while using low concentrations of trifluoro acetic acid (1-5% v/v) in dichloromethane.[19]

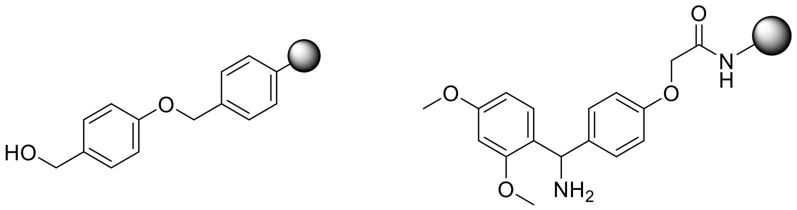

1 Wang-resin **2** Rink-resin

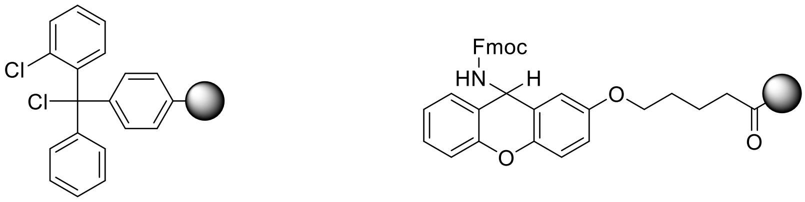

3 2-Chlorotrityl-resin **4** XAL-resin

Figure 5: Commonly used linkers for solid phase peptide synthesis.[15]

While Merrifield used benzyloxy carbonyl (Cbz) and also later *tert*-butyloxy carbonyl (Boc) as a protecting group for the amino function, the newer approach with fluorenylmethylenoxycarbonyl (Fmoc) protection is more suitable for peptide synthesis on solid phases. Fmoc is easily cleaved with a base like piperidine (Figure 6) instead of hydrogen bromide in glacial acetic acid (Cleavage of Cbz) or trifluoroacetic acid (TFA)(Cleavage of Boc) and therefore acid-labile protecting groups are available for the AA protection. This also leads to new acid labile linker for the *C*-terminal AA on the solid phase.[20]

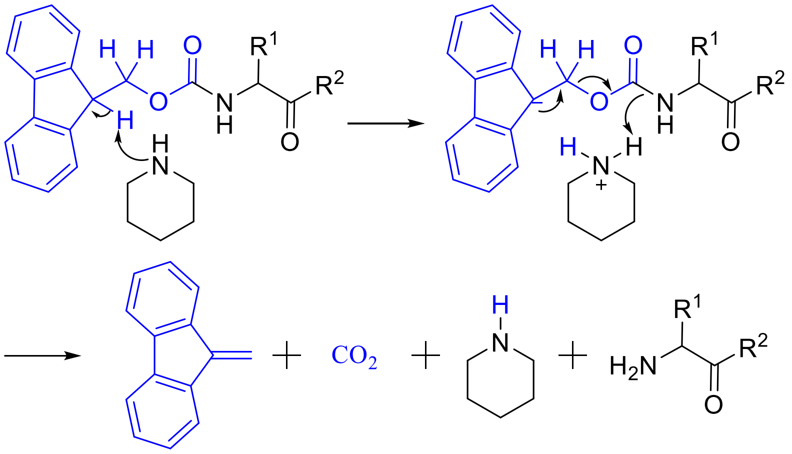

Figure 6: Deprotection of Fmoc-protected AA with piperidine.[4]

Likewise, the so-called coupling agents for amid bond formation developed over time, which convert the carboxylic acid function of an AA into a reactive acyl derivative.[4] The activator reacts with the carboxylic acid and functions as electron withdrawing group. The activator can be improved through the use of an activator base, which can accelerate the coupling, suppress racemization and inhibit the dehydration of the carboxamide side chains of asparagine and glutamine to the corresponding nitriles.[21]

Merrifield used *N,N′*-dicyclohexylcarbodiimide (DCC) as a coupling agent, which precipitated as carbamide and is therefore not suitable for automation of the peptide synthesis.[3] Thus, new coupling agents like other carbodiimides or onium salt-based reagents were developed. Diisopropylcarbodiimide (DIC) forms a carbamide that is soluble in dimethylformamide (DMF) and is therefore more suitable for SPPS.[22] The development of onium salt-based coupling agents like 1-hydroxy-7-azabenzotriazole (HOAt) replaced the carbodiimides because of the reduction of side reactions during the coupling step and better handling as a solution. Especially HOAt increases the yields of the desired product and reduces the configuration loss at the *C*-terminal carboxy acid residue.[23] Since the well-established onium salt-based coupling agents exhibit explosive properties, alternative oxime based reagents were developed.[24] Ethyl 2-cyano-2-(hydroxyimino)acetate (Oxyma) can be used in combination with DIC as a base, to form a reactive Fmoc-protected AA for peptide coupling (Figure 7).[25]

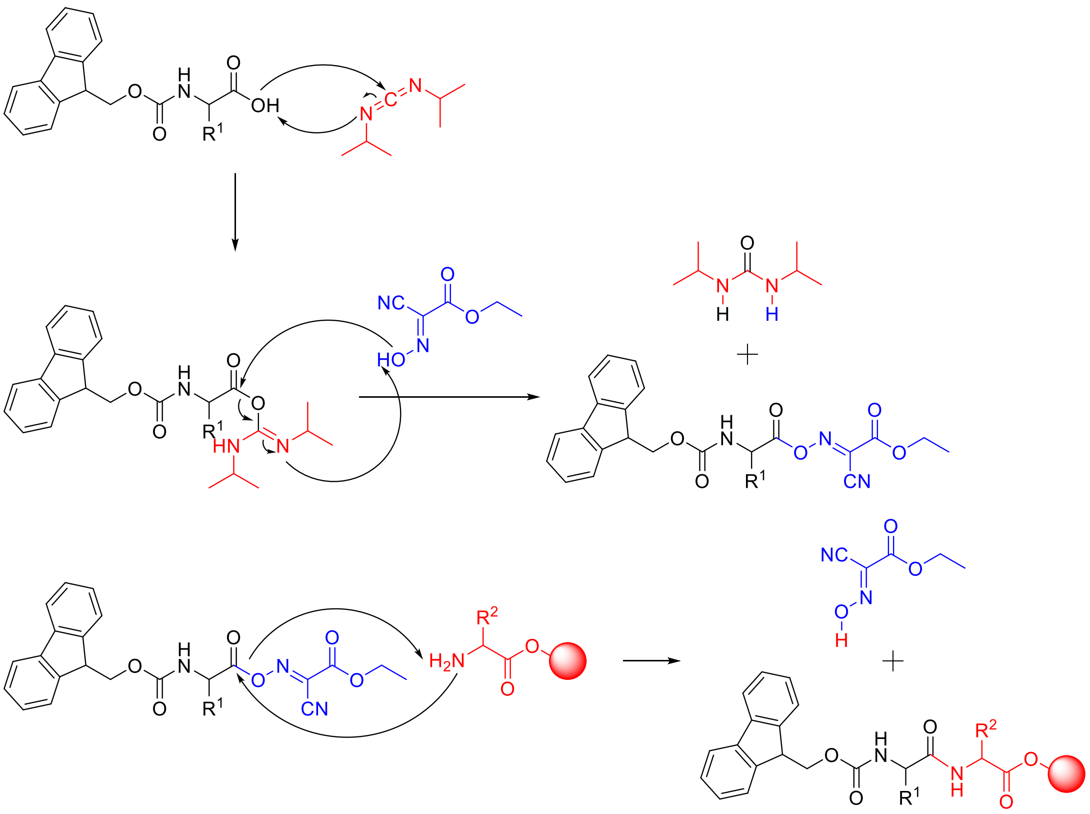

Figure 7: Activation and coupling of Fmoc-protected AA with DIC/Oxyma during solid phase synthesis.[25]

For the cleavage of the peptide from the resin, a wide range of different cleavage cocktails are used. The previously mentioned resins for the Fmoc-strategy are unstable under the acidic conditions of TFA depicted in Figure 8, which usually enable the simultaneous cleavage of the peptide from the resin as well as the protecting groups from the peptide itself, which produces degradation products. Triisopropylsilane (TIPS) works as a scavenger that reacts with carbocations generated during cleavage of the protecting groups. Other widely used cleavage cocktails use ethane-1,2-dithiol (EDT) as an additive to scavenge the degradation product of the Wang- and Rink-resin. To yield the protected peptide, Wang-, Rink- or Clt-resin and milder conditions are used: Acetic acid/trifluoroethanol/dichloromethane (DCM). After cleavage for usually 2 h the peptide is precipitated in cold diethyl ether and purified via high performance liquid chromatography (HPLC) after freeze drying and dissolving in a suitable solvent.[15]

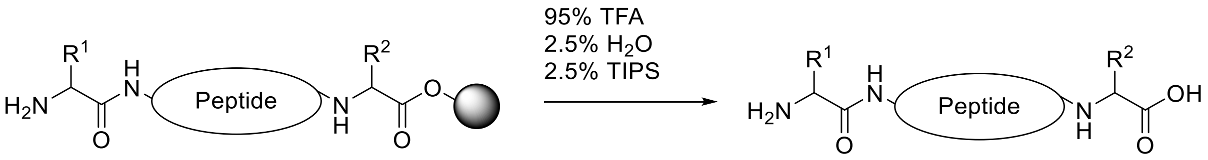

Figure 8: Cleavage of a peptide from the solid phase with a mixture of TFA, water and TIPS after synthesis.

1.1.2 Side reactions during peptide synthesis

Despite these methods for mild cleavage conditions, the racemization of AA during solid-phase peptide synthesis is still an issue. Especially cysteine is a problematic AA, because its α-proton can be acidic depending on the protecting group of the thiol and the linker used to connect the peptide to the solid phase. Particularly Wang-linker can promote deprotonation of the α-carbon of the cysteine. Deprotonation enables racemization of the stereocenter and β-elimination when piperidine is added during Fmoc-deprotection step and forms 3-(1-piperidinyl)alanine (A^{Pip})(Figure 9). This side reactions can be suppressed by using optimal protecting groups and linkers for the synthesis of C-terminal cysteine-containing peptides. The use of Clt-resin and trityl as protecting group for the thiol functionality reduces the amount of side reactions to 5% during 4 hours of exposure to 20% piperidine solution, while peptides with a Wang-linker are prone to side reactions between 10-90% in the same time span.[26,27]

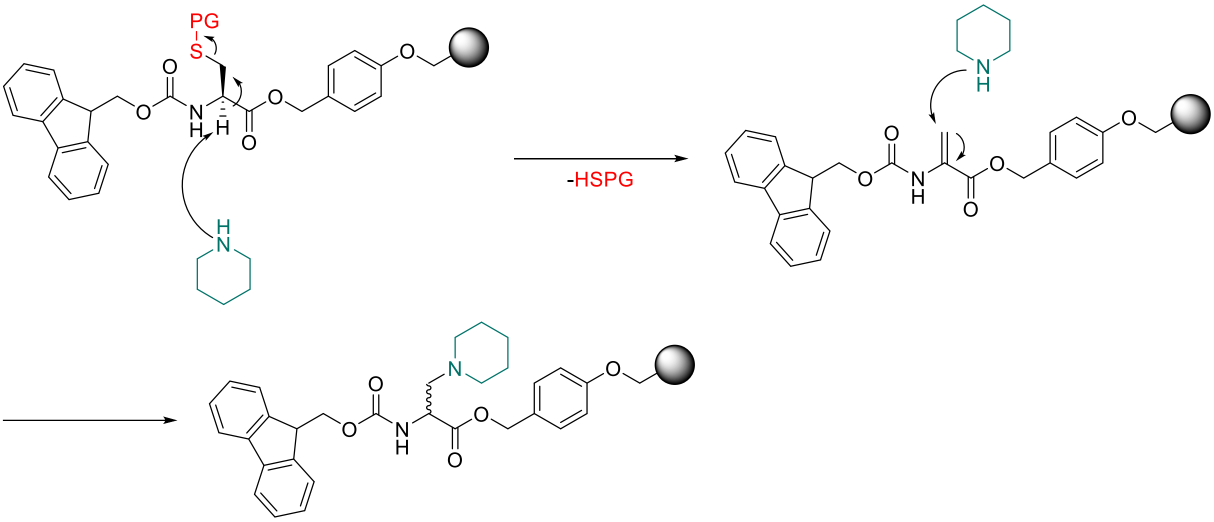

Figure 9: Side reaction of C-terminal cysteine during Fmoc-deprotection with piperidine.

Further reasons to avoid Wang-resins for peptides with a C-terminal cysteine is the potential side reaction with the degradation product of the linker during TFA-cleavage of the peptide. As pictured in Figure 10, the *p*-hydroxy benzyl group can react with the thiol group of the cysteine, yielding a thioether in the former thiol position. This thiol group can either intra- or intermolecularly attack the cationic benzyl group of the degradation product of the Wang-linker.[28]

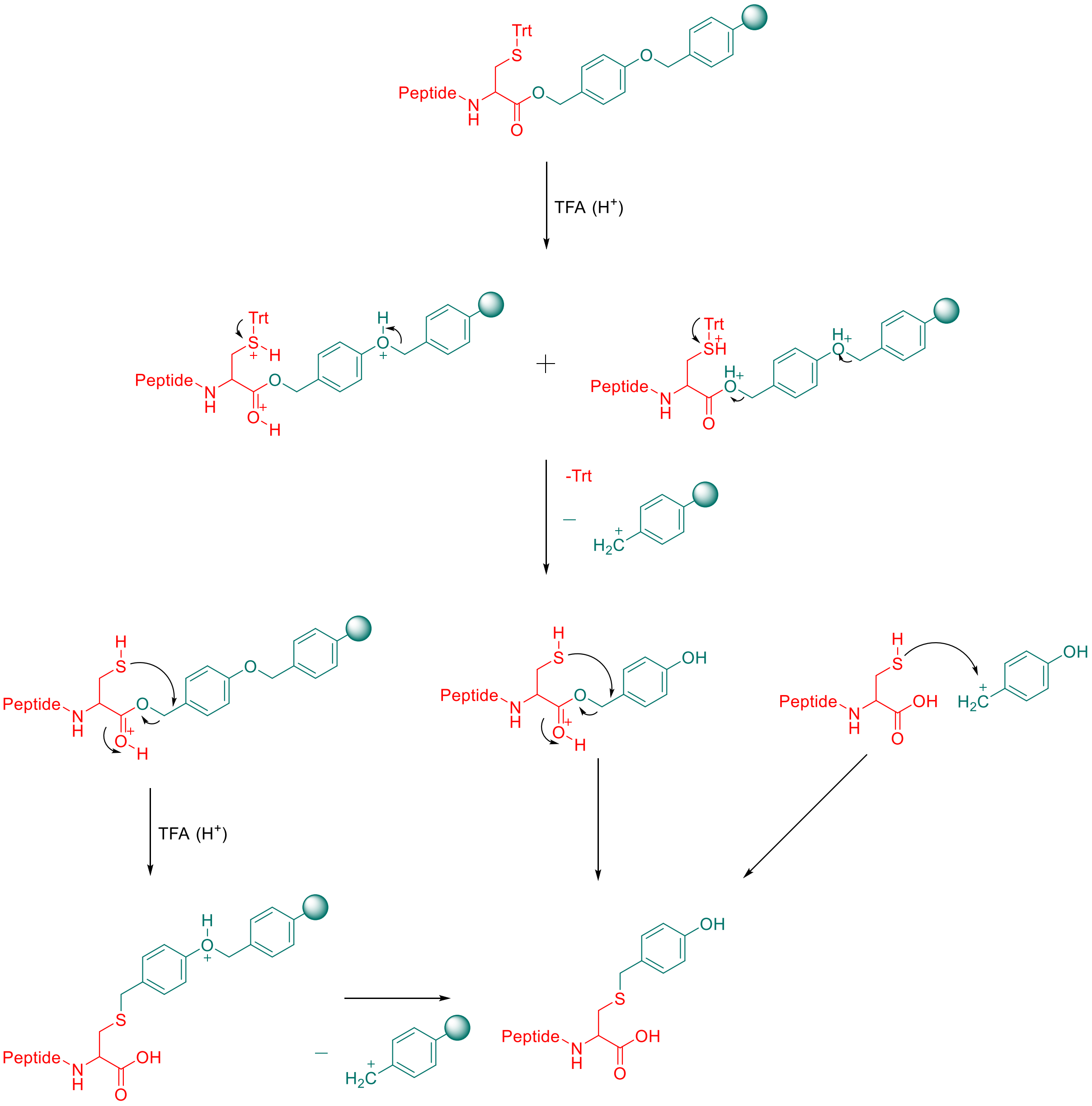

Figure 10: Suggested intramolecular and intermolecular mechanisms for S-alkylated side product formation, in case that cysteine is at the C-terminus on Wang-resins.[28]

1.1.3 Self-assembling peptides

Peptides can fold themselves in different structures like α-helix or β-sheet via hydrogen bonds. This behavior can be used for the design of synthetic, self-assembling peptides, which form one of those structures instantly or in response to specific triggers. Such triggers can be a change in pH or oxidation/reduction of functional groups.[29a,8,29b] For example, serine and threonine containing peptides can form so called depsi-peptides, which have an ester bond instead of an amide bond at the serine/threonine. Depsi-peptides are derived from natural peptides, which can be isolated from bacteria and algae. The ester bond enables the biosynthesis of cyclic peptides, which usually exhibit toxic properties.[30] Later the depsi-peptide method was adapted for chemical synthesis of peptides. The ester bond disturbs the formation of peptide aggregates and enables the synthesis of longer, more complex peptides.[31] These kind of peptides are stable under acidic conditions and can perform an intramolecular *O,N*-acyl shift upon change of the pH to neutral conditions (Figure 11).[32,8] The novel method to use the pH-induced shift for the formation of supramolecular structures like β-sheet fibrils and the cross-linking of polymers with them to yield hydrogels was introduced by the Weil group.[8]

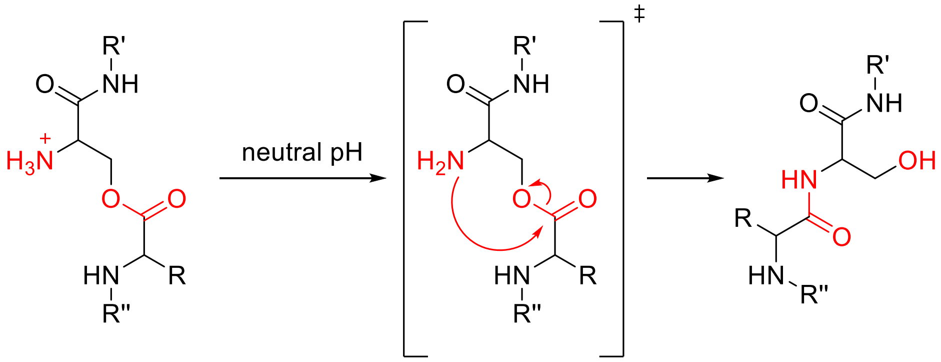

Figure 11: pH induced intramolecular *O,N*-acyl of depsi-peptides yielding linear peptides.[8]

The driving force for the formation of supramolecular structures is to reach a thermodynamic minimum, which can be achieved by coulomb interactions, π-stacks, van-der-Waal interaction or the formation of hydrogen bonds.[9] These interactions and a resulting long range order can enable high aspect ratios for the formed aggregates. As an example, tripeptides must be amphiphilic with the hydrophobic AA residue in the middle of the sequence in order to form fibril-like aggregates. Further, an introduced aromatic group must not be bulky or has large substitutions to enable the formation.[33] However, the formation of these structures is also coupled with the release of solvent molecules during assembly and therefore driven by entropy, which explains the dependency on temperature and concentration.[9] Amyloid fibrils mimic the fibrous part of the extracellular matrix and can support the survival and growth of cells in hydrogels or coatings. The high stability of those supramolecular structures can be used in hydrogel preparation. For example, supramolecular fibril alignment of charged amphiphilic peptides is possible due to temperature elevation resulting in a hydrogel.[34] However, the entanglement of high aspect ratio fibrils can also promote hydrogel formation.[34] Also, the formation of hydrogels can be induced upon mixing cell culture media with peptide amphiphiles.[35] The fibril formation can also be exploited as potential cross-linking for the synthesis of hydrogels. Due to the reversible association of those fibrils, such materials can exhibit dynamic and self-healing behavior. In some cases, the gels were reported to recover in relatively short time and in rare cases up to 100% of their original stability.[8]

1.2 Hydrogel

Cross-linked, three-dimensional, hydrophilic polymers, which are able to swell by absorbing large amounts of water or other aqueous fluids, while retaining them, are called hydrogels. Their properties are dependent on the properties of the cross-linker of the polymer chains and the hydrophilicity. The latter is influenced by the functional groups like hydroxylic, carboxylic, amidic, and sulphonic groups within the polymer network.[36] Cross-linking can be accomplished via different interactions between the hydrophilic polymer backbones. Polymerizing monomers with an addition of multifunctional molecules yields a covalently cross-linked network, which swells in water. For example, poly(methyl methacrylate) and poly(hydroxyethyl methacrylate) can be crosslinked with ethylene glycol dimethacrylate to form a chemically linked network.[37] Other methods use functional groups in the side chains of the backbone to cross-link them physically via hydrogen bonds, complexation of metal ions, coulomb interactions or chemically via click reactions.[37,38]

The swelling of a hydrogel depends on three forces: polymer-water interactions, electrostatic forces and osmosis. Polymer-water interactions depend on the hydrophilicity of the polymer. Therefore, a more hydrophilic polymer leads to stronger polymer-water interactions. Osmosis is generated in polymers containing ionic groups, due to the difference in ion concentrations between the inside of the gel and the surrounding solution. If the backbone is positively or negatively charged, the similar charges repel each other, which leads to an expansion of the space between the polymers. The effects of these forces are displayed in Figure 12. The hydrogel properties depend not only on the polymer itself but also on the water content, which can be determined by differential scanning calorimetry. On the one hand, hydrogels require a high solid content, when they express superior stability in their swollen state. On the other hand, when a superior swelling capacity is a major requirement, a low solid content is required.[37,39]

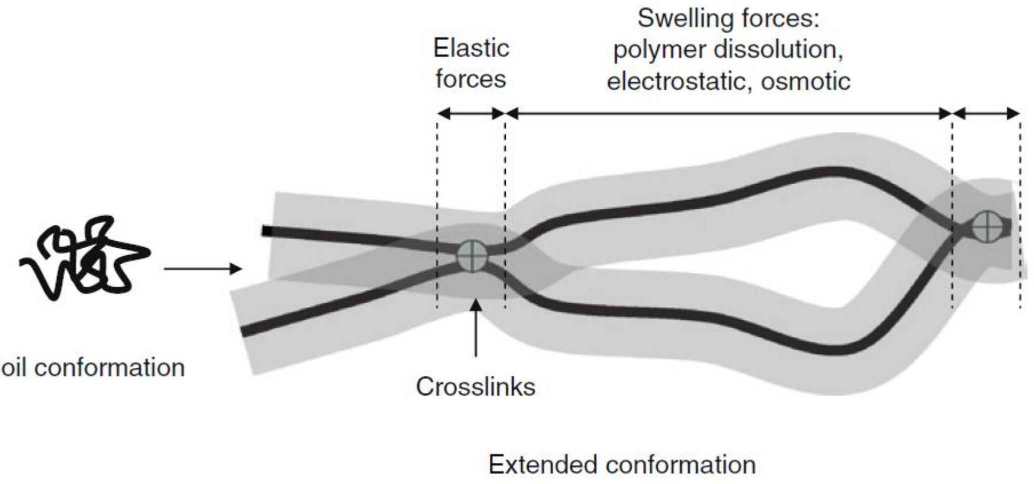

Figure 12: Swelling forces in hydrogels.[37]

The chemical structure of hydrogels can be characterized via FTIR and NMR. Hydrogen bonds, complexation of metal ions and coulomb interactions can be revealed via analyzing the vibrations of the corresponding bonds with FTIR. The number of crosslinks, in relation to the length of the backbone, can be characterized with NMR. Hydrogels can be non-porous, microporous or superporous, which affects the physical properties of the material. Density, refractive index and mechanical properties change depending on the porosity, pore size and size distribution. The porosity of a hydrogel can be determined by scanning electron microscopy, liquid intrusion and image analysis. But for most applications, the important requirement is usually the wet-state stability of the hydrogel; a measure of how well the hydrogel maintains its shape in the swollen/wet state. Analyzing the deswelling under mechanical stress, desorption of water and the viscoelasticity with a rheometer gives a better understanding of the wet-state stability of the hydrogel.[37,39]

Hydrogels can be classified into different categories depending on their origin, composition, ionic charge, physical structure and nature of cross-links. Classified by their origin, hydrogels are either natural (proteins and polysaccharides), synthetic or hybrids. Synthetic hydrogels are chemically polymerized using man-made monomers and can be homo-, copolymers. Hydrogels prepared with natural and synthetic polymers are called hybrid hydrogels. Classified by their composition, hydrogels can be homo- or copolymeric or interpenetrating networks. Homopolymer hydrogels are derived from one type of monomer and cross-linked during polymerization. The structural network of homopolymeric hydrogels is dependent on the cross-linker, monomer and polymerization technique. Copolymer hydrogels are synthesized by polymerizing two or more types of monomers where at least one monomer is hydrophilic and responsible for the swell ability of the hydrogel. The copolymers can have different configurations like graft, random, block or alternate types. They are prepared by polymerization or cross-linking the monomers by using an initiator and a cross-linker. Physical cross-linking via chain aggregation, hydrogen bonding, ionic interaction and ion-polymer complexation is also possible. Interpenetrating networks are made up of two intertwined polymer networks. Classified by their ionic charge, hydrogels can be either neutral, ionic or ampholytic. Classified by their physical structure, hydrogels have different pore sizes, configurations and appearance. As mentioned before, hydrogels can be non-porous, microporous and superporous. Depending on the polymerization method, hydrogels can be a matrix, film or microsphere. The configuration of hydrogels is based on their physical structure and chemical composition; thus, a hydrogel can be classified as amorphous or semi-crystalline. Amorphous hydrogels are isotropic and contain randomly arranged macromolecular chains. Semi-crystalline hydrogels consist of crystalline and amorphous phases. Classified based on their cross-linking, hydrogels can be either physically or chemically cross-linked. Chemical cross-linked hydrogels contain covalently linked polymer chains, whereas physical linked hydrogels can be cross-linked via crystallization, hydrogen bonding, complexation of metal ions or coulomb interactions.[36]

The goal of tissue engineering is the control of the growth, differentiation and behavior of cells in such a way, that they organize into functional tissue.[40] For that, local regeneration of lost or malfunctioning tissues and organs should be promoted by culturing the patient’s own cells in a polymer matrix. In this context, the cell-matrix interactions and the biological environment of the matrix play an important role in the implanted biomaterial. The effective combination of tunable mechanical properties, degradability and the ability to afford excellent biological environment for encapsulating bioactive moieties like growth factors and cells can be achieved by supramolecular hydrogels. The result is a biocompatible scaffold in tissue engineering for the support, guidance and stimulation of growth of tissues.[41]

Hydrogels for tissue engineering, aside their necessary physical stability, need to be biocompatible and biodegradable. In detail, they need to be nontoxic, nonallergenic, noncarcinogenic, nonmutagenic and mimic the natural support structures of the cells environment.[40,42,8] These properties should also apply to the degradation products of the hydrogel.[8,42] Since proteins, peptides, polysaccharides and diverse polyphosphonates are natural occurring materials, they are potential candidates for hydrogel synthesis for pharmaceutical applications.[43,42,44] Hydrogels can be prepared by exploiting the host-guest-interactions of cyclodextrin and adamantane. For this purpose, two hyaluronic acid (HA) macromers were synthesized, one functionalized with cyclodextrin and another with adamantane. Upon mixing of those macromers in suitable medium, a shear-thinning hydrogel is formed, which is cross-linked by the host-guest-interactions and can near instantaneously reassemble after deformation.[45] The biodegradability of poly(phosphoester) as hydrogel backbone was demonstrated by functionalizing it with a photoactive acrylate cross-linker and poly(ethylene glycol) spacer.[46] Another hydrogel can be prepared by self-assembly of a pentapeptide hydrogelator (Nap-FFGEY), which can be disassembled by a kinase in the presence of adenosine triphosphate by converting tyrosine into tyrosine phosphate.[47] Combining the stability offered by a covalent backbone of biocompatible polysaccharides, proteins or polyphosphonates with the dynamics of peptide self-assembly, hybrid materials can be developed, which form stable, yet reversible physical connections between polymer backbones. The hydrogel can express potential self-healing properties because of the reversibility of the physical bond between the covalently attached peptides on the backbones.[8]

1.2.1 Depsi-peptides as cross-linker for hydrogel synthesis

The combination of denatured proteins and depsi-peptides to form hybrid hydrogels was introduced in Jasmina Gačanins publication “Autonomous ultrafast self-healing hydrogels by pH responsive functional nanofiber gelators as cell matrices”.[8]

Herein, a polypeptide consisting of human serum albumin (HSA) was used as polymer backbone for the hydrogel synthesis. Therefore, the protein was functionalized with poly(ethylene glycol) (PEG), and denaturized. After denaturization, a maleimide-modified depsi-peptide was attached to the polymer backbone. The peptide sequence KIKI(O-C(O))SQINM transforms to its linear form under physiological pH and tends to form β-sheet fibrils. This aggregation tendency was used for pH induced self-assembling gelation of the hybrid. The sequence was modified with a maleimide function and coupled to the polymer backbone via Michael type thiole-ene click reaction (Figure 13). This combination of peptide and protein bestows upon the resulting hydrogel both biodegradability and biocompatibility. An immediate *in-situ* self-healing and thus thixotropic characteristic could be achieved through the reversible aggregation behavior of the peptide. Due to these properties, the hydrogel is suitable for tissue engineering, which was shown in initial cell vitality tests of different cell lines, including Human umbilical vein endothelial cells (HUVECs).[8]

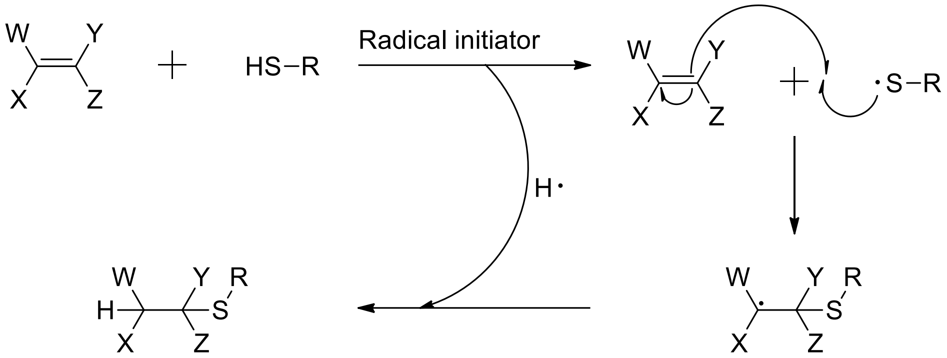

Figure 13: Scheme of a thiol-ene click reaction initiated by a radical starter.[48]

1.2.2 Poly(phosphoester) (PPE) as polymer backbone

Living organisms depend on different kinds of poly- and oligomeric phosphorus derivatives for storing genetic information (deoxyribonucleic acid/ ribonucleic acid (DNA/RNA)) or storing chemical energy (adenosine triphosphate (ATP)). The long-term stability of DNA derives from its negatively charged phosphate linkers, yet can be degraded via hydrolysis with enzymes. The mimicking of those systems can achieve biocompatible and -degradable polymers with similar mechanical and chemical properties. The PPEs consist of pentavalent phosphorus, a backbone containing different kinds of aliphatic chains and the side chain, which can contain different functional groups, yielding poly(phosphate)s, poly(phosphonate)s and poly(phosphoamidate)s (Figure 14). PPEs are degradable by hydrolysis with or without enzymes, thus qualifying as biocompatible and -degradable. By changing the backbone or the side chain, the properties of the PPEs can be manipulated to generate amorphous, water-soluble materials or crystalline, stiff plastics.[44]

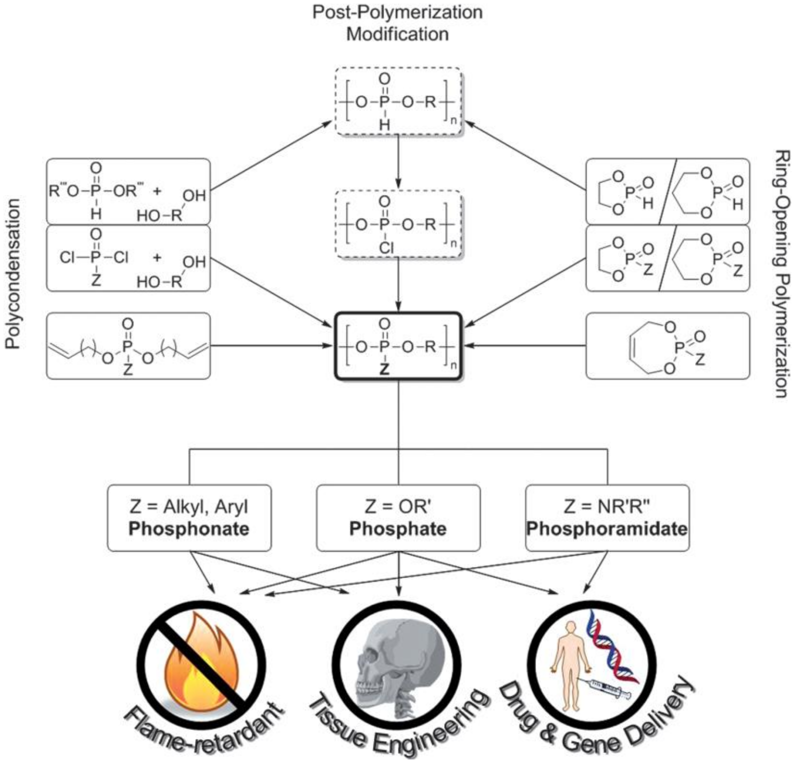

Figure 14: Synthetic pathways toward PPE and fields of application.[44]

Especially the biocompatible and -degradable properties of poly(phosphonate)s make them interesting materials for applications in drug delivery.[49] In comparison to widely used biodegradable polymers like poly(lactic acid), poly(glycolic acid) and poly(ε-caprolactone), PPEs are degraded much faster by hydrolysis or enzymatic degradation. The polymer backbone and side chains of PPE degrade under basic conditions similarly fast, while the side chains also degrade under acidic conditions.[50] The degradation rate can be adjusted by changing the chemical structure of the PPE.[44] The degradation products of poly(phosphonate)s have been studied and show, that there is no toxic effect on COS-7 cells.[51] However, further studies of poly(phosphonate) structures are important to prove general biocompatibility. If the backbone and the side chains are correctly chosen, the formation of hydrogels are possible. Cross-linking of a triblock copolymer of poly(ethyl ethylene phosphate) and poly(ethylene glycol) with a diacrylate yields nanogels as a drug carrier.[52]

1.2.3 Dextran as polymer backbone

Dextran is a homopolysaccharide containing glucose monomer units with α-1,6 glycosidic linkage and a few branches of α-glucopyranose at the positions *O*-2, *O*-3 or *O*-4 (Figure 15). Dextran is synthesized by lactic acid bacteria mainly belonging to *Leuconostoc, Lactobacillus* and *Streptococcus* genera and therefore its molecular weight and branching is dependent on the bacteria strand, pH of the medium and concentration of sucrose in the medium.[53,54]

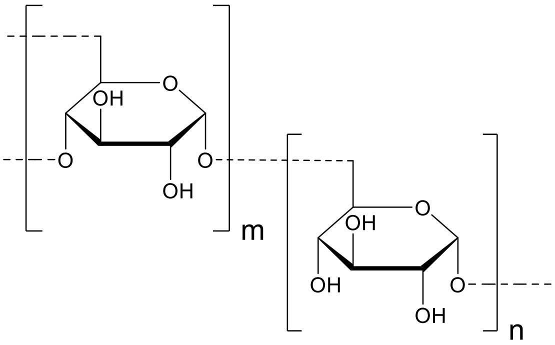

Figure 15: Possible Structure of Dextran.

As a bioproduct, dextran is biocompatible and -degradable and thus has many applications in the food and pharmaceutical industry. The biodegradation is possible through the enzyme dextranase, which can be produced by bacteria.[53] Dextran has a wide range of applications which are derived from the different physicochemical properties of dextran of different molecular weights and degrees of branching. Intrinsic bioactivity of dextran can be shown by dextran sulphate with an antiviral effect against human immunodeficiency virus and dextran as potential antiviral- and immunomodulatory agents in trout.[53] Due to its biocompatibility, nontoxicity and facile chemical modification, crosslinking dextran chains can lead to semi-synthetic hydrogels for tissue engineering. Cross-linking dextran with dithiothreitol yields a hydrogel, which can encapsulate rat bone marrow mesenchymal stem cells.[43]

1.3 Purification and characterization methods

1.3.1 Reversed-phase high performance liquid chromatography (RP-HPLC) and size-exclusion chromatography (SEC)

Several similar chromatography techniques are used for the separation of different molecular species. The molecular species of interest (analyte) must be separated from the matrix (rest of components) in the sample. Therefore, chromatography is used to separate the analyte from the sample by introducing it to a flowing mobile phase that must pass over a stationary phase. The stationary phase shows varying interaction strength with different kinds of molecular species in the sample and thus releases them separately back into the mobile phase. The mobile phase can be either a gas (gas chromatography) or a liquid (liquid chromatography), but it is also possible to have a supercritical fluid, countercurrent or electrochromatography. Focusing on the HPLC, the stationary phase is usually a column packed with porous particles having a diameter ranging from 1-5 µm and the mobile phase (eluent) a solvent that moves through the column by a pump at elevated pressure. The exiting molecular species can be detected by different methods, depending on the physicochemical properties of the analyte. The most commonly used methods for detection use ultraviolet(UV)-absorption, refraction index, fluorescence, molecular mass or fragmentation in a mass spectrometer.[55]

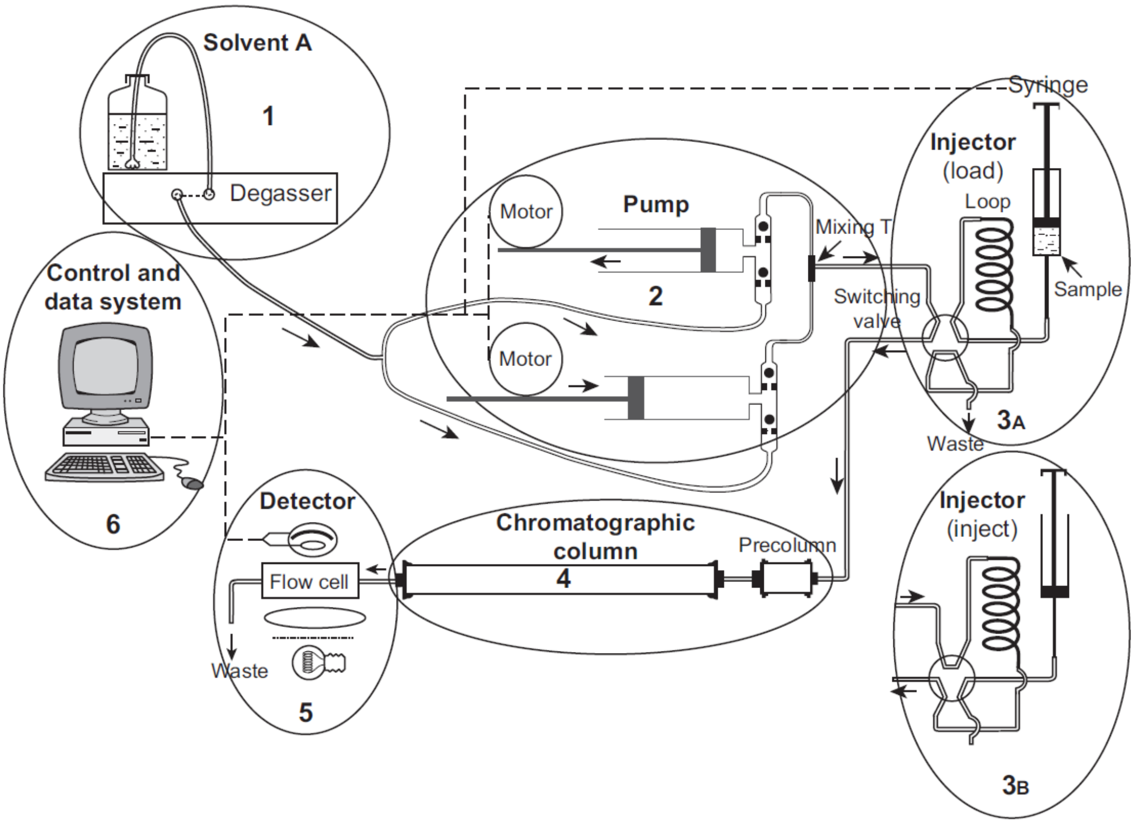

Figure 16: Schematic representation of a simple HPLC system. 1) Solvent supply system with a solvent container and degasser, 2) pumping system for high pressure, 3) injector (syringe) with the sample and switching valve for **A** loading the loop and **B** injecting the sample, 4) chromatographic column with a possible precolumn, 5) one or more possible detectors, 6) controller/ data processing unit.[55]

Figure 16 shows a possible set-up for HPLC instrument. The solvent supply system consists of one or more reservoirs and a possible degasser, to remove gases dissolved in the eluent. The pumping system delivers constant flow of solvent via one or more pumps through the complete HPLC system. They must be able to produce and maintain high pressure, to overcome the resistance to flow of the chromatographic column. This flow is characterized by the *volumetric flow rate U*, which can take up values between 0.1 to 10 mL/min with a pressure between 6000 to 8500 psi. A small, precisely measured volume of a solution containing the sample can be added to the mobile phase through the injector. One method to inject a sample in the system is the loop system pictured in Figure 16. The loop can be filled with the sample and afterward connected to the flow circuit by switching a valve. Depending on the type of HPLC setup that is used, the size of the loop can vary between 20 nL to some milliliters. The role of chromatographic columns in HPLC is to achieve the separation of the analyte. Columns usually consist of a tube made from metal (stainless steel) or plastic (e.g., polyether ketone) and is filled with the stationary phase, which is held in place by two special frits at the ends of the tube. The dimensions of the tube vary depending on the use. The length of a typical chromatographic column can be between 30 to 250 mm and have an internal diameter between 1 to 10 mm. This tube can be filled with different kinds of stationary phases depending on the separation method: Normal phase, reversed phase, ion exchange size exclusion, etc. The stationary phase consists of small, solid particles with different porosity (porous, superficially porous and pellicular) and surface properties. Porous particles have a diameter of 3 to 5 µm and consist of specific porous materials like silica with a surface coating of active components. Those surfactants are physically or chemically bound to the surface and are the components interacting with the mobile phase. The chemical properties of the surface of the particles can be altered by changing the chemical nature of the active surface, chemical stability, surface reactivity or density and distribution of the reactive centers. RP-HPLC for example uses octadecyl (C18) or octyl (C8) groups on the surface of silica. Size-exclusion chromatography uses perfusion particles made from different kinds of polymers or silica with big pores (400-800 nm) connected to a system of small pores (30-100 nm). In some systems, there is more than one column required, to get the desired separation, thus two to four columns are connected in series. Also, there is the option or requirement to heat a column to reach the preferred separation. Therefore, the column is put in a column oven, which can control the temperature between 10-100 °C.[55]

1.3.2 Matrix-assisted laser desorption/ionization-time of flight mass spectroscopy (MALDI-ToF MS)

Besides electrospray ionization, MALDI is one of two soft ionization techniques and allows the detection of large, non-volatile and labile molecules by mass spectrometry. This technique evolved from a diversity of different methods developed over time. In the 1960s Beckey introduced field desorption, which opened the possibility to analyze bioorganic molecules via MS. A step further in the direction of MALDI-ToF MS was taken, when the secondary ion MS introduced by Benninghoven 1975 was combined by Barber 1981 with glycerol as “matrix”, to promote desorption and enhance ion yield. The invention of the laser enabled the generation of ions for MS analysis via laser irradiation. Over several years, MALDI was further improved to measure samples with higher molecular masses like proteins (10-100 kDa) and promote the sensitivity of the detector, which can nowadays detect ions in the attomolar range.[56]

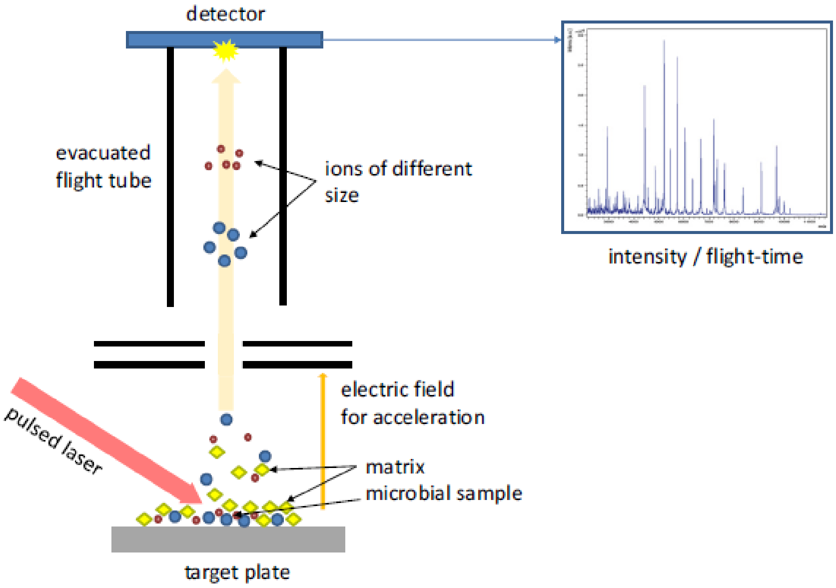

Figure 17: Basic principle of MALDI-ToF MS.[57]

The basic principle of MALDI-ToF MS is the co-crystallization of the molecule of interest with a matrix and ionization of the mixture with a laser. This matrix is used in excess of the sample and enables the efficient absorption of the laser energy at the operated wavelength. The sample desorbs and "gently" ionizes together with the matrix through the energy of the laser, to prevent the fragmentation of the labile sample. After the acceleration through an electric field, the ions are directed across an evacuated flight tube to a detector, which detects the series of impacts of the ions. Therefore, the mass-to-charge ratio of the analyzed molecules can be determined, by knowing the time-of-flight to impact on the detector. The detectors can run in positive or negative ion mode and there are different options for the matrix like α-cyano-4-hydroxycinamic acid (HCCA) and 2,4-dihydroxybenzoic acid (DHBA) and their derivates. Figure 17 shows the basic principle of MALDI-ToF MS from the desorption/ionization of the sample to detection and visualizing the data.[57]

1.3.3 Thioflavin T-Assay

The aggregation of peptide/proteins to form amyloid fibrils can cause a wide range of human disorders like Alzheimer's disease, Parkinsons's disease and type 2 diabetes. Thioflavin T (ThT) is a commonly used dye to monitor amyloid fibril formation. Bound to an β-sheet rich fibril, ThT exhibits a strong fluorescence signal at approximately 482 nm upon excitation at approximately 450 nm. The fluorescence is enhanced through rotational immobilization of the central C-C bond connecting the benzothiazole and the aniline rings upon binding to an β-sheet fibril. ThT binds to the side chain channels (“channel” model) of the fibrils formed by four or more consecutive β-strands along the long axis of the amyloids (Figure 18).[58,59] Besides amyloid fibrils, the C-C bond rotation can be suppressed by cyclodextrin, cucurbit[*n*]uril, polymer membranes, porous silicon and other biomolecules like DNA, which yields in this context to falsely positive results.[60] ThT binds to α-helices with Tyr- and Trp-rich areas due to π-stacking or to hydrophobic pockets of human serum albumin or drug-like molecules.[61]

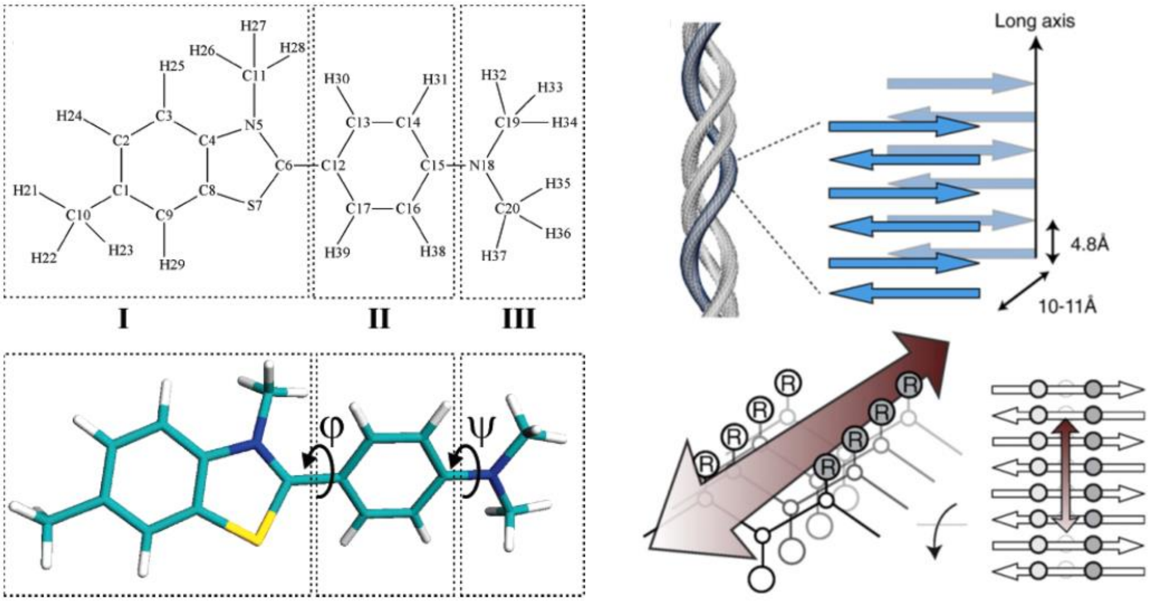

Figure 18: Chemical structure and spatial model of ThT cation (left). Benzthiazole ring (I), benzene ring (II), and dimethylamino group (III) are boxed.[59] Cross-β structure of amyloid fibrils, formed from layers of laminated β-sheets and “Channel” model of ThT binding to fibril-like β-sheets (right).[61]

1.3.4 Conversion-Assay

The conversion of molecularly dissolved peptides to peptide aggregates/β-sheet fibrils is determined by a conversion-assay. For this purpose, an incubated peptide solution is passed through a spin tube with a certain molecular weight cut-off (MWCO) via centrifugation. Aggregates and β-sheet fibrils are too large to pass through the filter, thus only single molecules are collected. As a reference, the same amount of peptide solution is used without filtration (original). Both solutions are lyophilized and re-dissolved in dimethyl sulfoxide (DMSO) to mix with fluorescamine.[8] As a fluorescence marker, fluorescamine reacts with primary amines, like peptides, to exhibit fluorescence (Figure 19).[62]

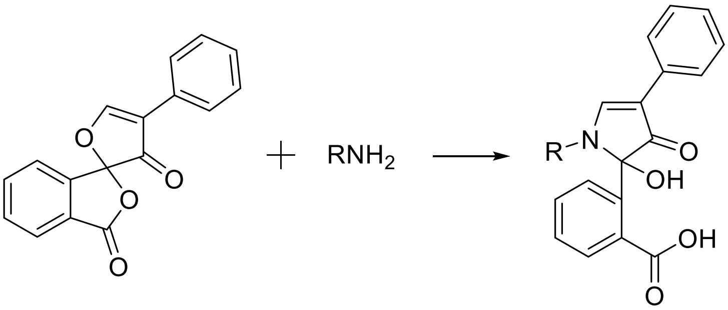

Figure 19: Reaction of fluorescamine with primary amines to form a fluorophore.[62]

Upon excitation ($\lambda_{\mathrm{exc}} = 365\ \mathrm{nm}$), the fluorophore emits light with the emission wavelength $\lambda_{\mathrm{em}} = 470\ \mathrm{nm}$. The fluorescence intensity of the original solution I_{Original} reflects the whole number of peptides, whereas the fluorescence intensity of the filtrate I_{Filtrate} reflects only the non-fibrillated peptides. The conversion rate CR can be calculated with the following formula:

$$CR = 100 - \frac{100 * I_{\mathrm{Filtrate}}}{I_{\mathrm{Original}}}\ [\%] \qquad (1)^{[8]}$$

1.3.5 Transmission electron microscopy (TEM)

A microscope is used to magnify objects too small to see with the naked eye. The smallest distance between two points our eyes can resolve is approximately 0.1 mm and based on the wavelength λ and numerical aperture NA. The numerical aperture consists of the product of the refractive index μ and the sinus of angular aperture $\sin\beta$. This smallest distance between two points that can be resolved is called Abbe limit δ and can be calculated via the Rayleigh criterion:[63]

$$\delta = \frac{0.61\lambda}{NA} \qquad (2)^{[63]}$$

In most cases the sample is measured in air or vacuum, thus the refractive index μ equals 1. The sinus of the angular aperture $\sin\beta$ is usually nearly 1, thus the whole numerical aperture NA can be simplified to 1. With this simplification, the Abbe limit δ is only dependent on the wavelength of the radiated light of the light source. In the case of visible-light microscopes, the highest resolution possible is around 300 nm (green light: $\lambda = 550\ \mathrm{nm}$). To overcome those limits, electrons are used instead of photons, which wavelength is dependent on its energy E.Ignoring the relativistic effects, the wavelength of an electron can be calculated with the following formula:

$$\lambda = \frac{1.22}{E^{\frac{1}{2}}} \qquad (3)^{[63]}$$

The wavelength λ for an electron with energy $E = 100\ \mathrm{keV}$ equals 4 pm and thus the Abbe limit $\delta = 2.4\ \mathrm{pm}$. However, it is not possible to build a perfect TEM because of limits of the electron lenses, thus such high resolutions cannot be reached. The high resolution of TEM imaging brings some limitation with it. It is only possible to look at small part of the sample at any time. Thus, it is important to analyze the sample with other microscopy methods or the eye before looking at small parts of the specimen. Also, TEM imaging presents only 2D images of 3D samples. Therefore, the interpretation of the image is key, before making false conclusions. A further problem is the damage to the sample through ionizing radiation. Particularly polymers and biological specimens are easily destroyed by an electron beam. However, the combination of intense electron beams with sensitive electron detectors and by using computer enhanced noisy images, the total dose of electrons received by the sample can be reduced below the damage threshold. The last limitation of TEM imaging is the thickness of the sample. The specimen must be thin enough for electrons to pass through the sample (electron transparency) and thus should be <100 nm. In the case of high resolution TEM imaging the sample must be 50 nm or even thinner.[63]

Upon impact the electrons produce a wide variety of secondary signals, which can be detected by different TEM methods (Figure 20). Most of those signals are used in analytical electron microscopy to get chemical information and further details of the sample. For TEM imaging especially the direct beam is important to visualize the investigated specimen.[63]

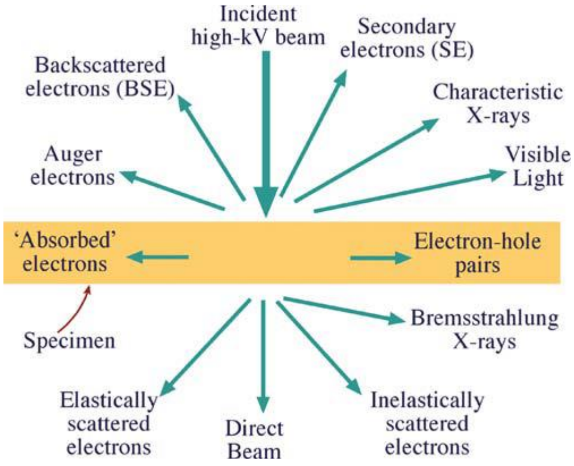

Figure 20: Generated signals by interaction of high-energy beam of electrons with a thin specimen.[63]

The simplest setting for a TEM consist of the electron source, three different lenses and their apertures and the detector. There are two different types of electron sources: thermionic and field-emission sources. The thermionic source consists of either tungsten filaments or lanthanum hexaboride crystals and produce electrons by heating. Field emitters are fine tungsten needles, which produce electrons when large electric potentials are applied between them and an anode. The electron lenses are the TEM's equivalent of glass lenses for visible light microscopy and can be discussed in similar fashion. Lenses, in principle, have two basic functions: 1. Collects all beams radiated from a point in an object and reconstruct a point in an image; 2. Focus parallel beams to a point in the focal plane of the lens. The objective lens is the most important lens in the TEM and forms the images and diffraction pattern that are magnified by the other lenses. The intermediate lens selects either the back-focal plane for the diffraction or the image plane for the image. The projector lens focuses the final image or diffraction pattern on the detector or viewing screen. The condenser, objective and intermediate aperture select only the relevant electron beam after the corresponding lens. Figure 21 shows the two basic operation modes of a TEM imaging system. Depending on the selected aperture, the diffraction or image is projected on the screen. Since the imaging mode is relevant for viewing self-assembled peptides or cross-linked polymer backbones, the diffraction mode is not further explained. The image mode can be differentiated into bright- and dark-field imaging. In the case of the bright-field, only the direct beam is selected to form the bright-field image. The dark-field shows only electrons, that are not in the direct beam.

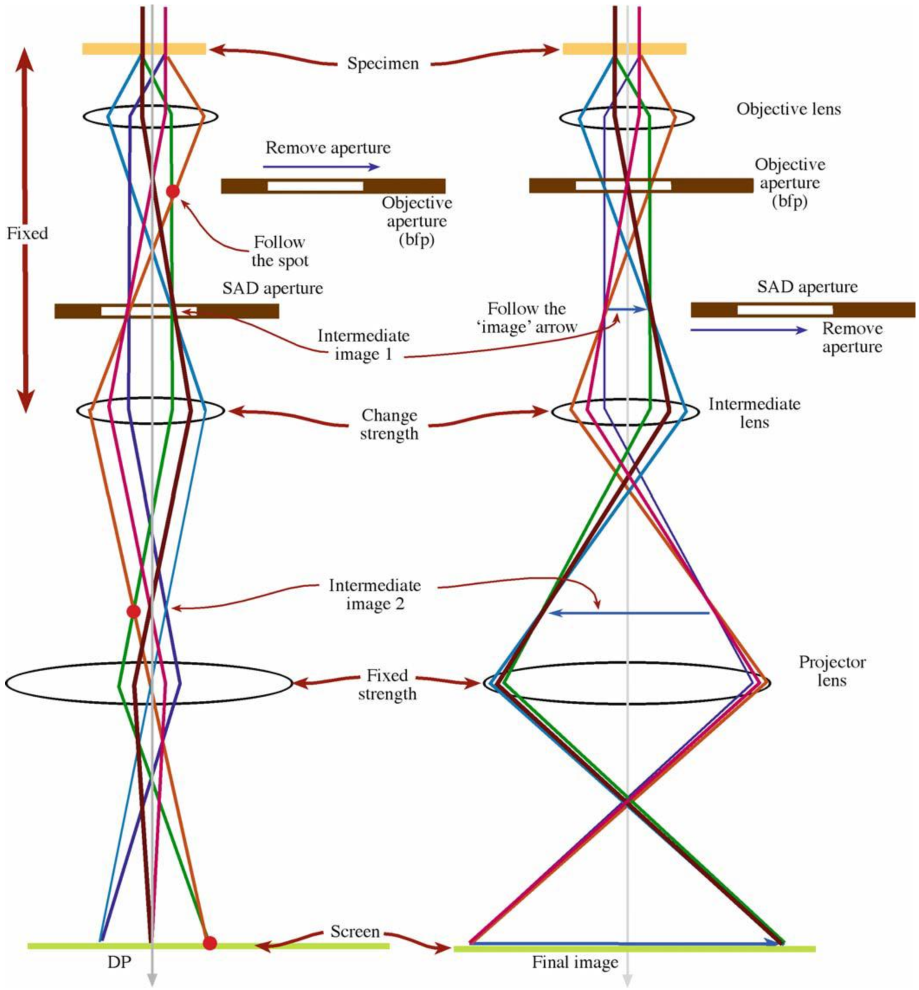

Figure 21: The two basic operations of the TEM imaging system: diffraction (left) and imaging mode (right). Diffraction mode projects the diffraction pattern onto the viewing screen with the intermediate lens selecting the back-focal plane. Imaging mode projects the image onto the viewing screen with the image lens selected (Note: highly simplified diagram).[63]

1.3.6 Attenuated total reflection-Fourier transformation infrared spectroscopy (ATR-FTIR)

IR spectroscopy is utilized to analyze the amide bond of peptides and proteins. The frequencies, at which the amide bond vibrations occur, can be assigned to different secondary structures of the peptide/protein. Especially the Amide I, II and III IR spectral regions can be used for protein structure analysis. Due to the variance of hydrogen bonding among the AA, different vibrations of the amide bonds occur. For example, α-helices and β-sheets have different folded structures and while they both form highly ordered structures, their signal patterns are distinct. This difference in hydrogen bonding and the geometric orientation of the amide bonds in the corresponding structure gives rise to different vibration frequencies associated with the individual secondary structures. The amide bond involves the vibrations of three different groups: C=O, C-N and N-H. Those vibrations can be assigned to three major spectral regions, as mentioned before. The amide I vibration region is located between 1700-1600 cm^{-1} and is widely used due to its strong signal. This region is corresponding to the C=O stretch, C-N stretch and N-H bending. The amide II region involves the frequencies between 1600-1500 cm^{-1} and represents the C-N stretch and the N-H bending. At last, the amide III region represents the N-H in plane bending and the C-N stretching from 1350-1200 cm^{-1}. It also includes C-H and N-H deformation vibration.[64]

The amide I vibration region is mainly used to characterize the secondary structure of peptides and proteins. Therefore, frequencies were determined, which correlate to the secondary structures in proteins. The α-helical structure shows bands around 1661-1647.5 cm^{-1}. Furthermore, the β-sheet structure shows bands around 1689-1682 cm^{-1}, 1637.5-1627.5 cm^{-1} and 1627.5-1615 cm^{-1}. Unordered or random structures can be assigned to the bands between 1644.5-1637.5 cm^{-1} and finally β-turns can be assigned to frequencies between 1682-1661 cm^{-1}.[65]

Due to the O-H vibrations of water (1640 cm^{-1}), it is difficult to measure aqueous peptide/protein solutions.[66] Therefore, peptide/protein solutions can be lyophilized to receive dry powders. Those can be easily measured in low quantities with precise results.[8]

The ATR-unit makes use of the high refractive index of a dielectric, which totally reflects radiation at an angle larger than the critical angle, if a sample is introduced to the surface. The reflection will not be total anymore at frequencies, where the sample absorbs the radiation, thus a reflection spectrum with high contrast and intensity is obtained, which resembles a transmission spectrum. Therefore, if the sample is non-absorbing, the incident beam is reflected without energy loss. However, if the sample absorbs energy, a periodic alternation takes place and the reflection is not total anymore.[67]

1.3.7 Circular dichroism spectroscopy (CD)

The basis of a modern CD spectrometer (Figure 22) was laid by Grosjean and Legrand in 1960. A xenon arc lamp generates non-polarized light, which is modulated by a monochromator and a linear polarizer. The monochromatic, linear polarized beam is further modulated through a Pockels cell (or photo elastic modulator), which is controlled by the computer, to receive left- and right-circularly polarized light. After modulation, the circularly polarized beam is sent through the sample and the transmitted light is detected by a photomultiplier or photodiode. The data is collected and processed by the computer and a CD spectrum is received.[68]

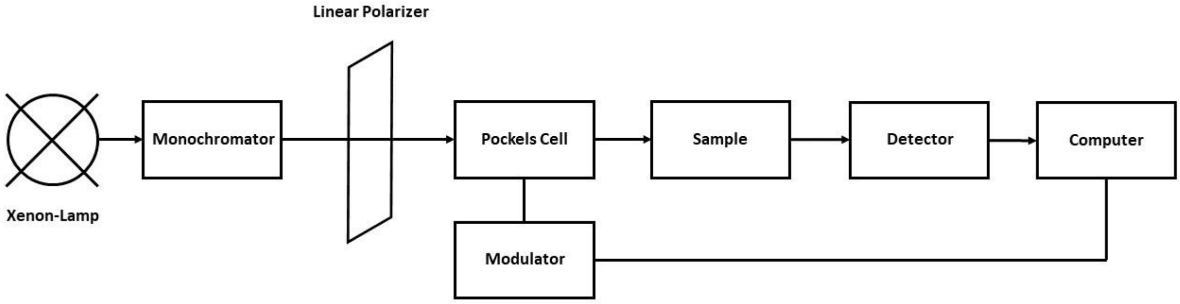

Figure 22: Principal design of a CD spectrometer (modified).[68]

A beam of light can be either linearly or circularly polarized. Linear polarized light can be absorbed by molecules depending on their orientation. This dependence of absorption strength is called linear dichroism. The orientation of the electric field in circularly polarized light rotates with time either clockwise or counterclockwise like left- or right-handed screws. Therefore, the light is “left” or “right” circularly polarized. Especially, biomaterials exhibit different absorbance depending on the direction of the circular polarization. This property is called circular dichroism. If the polarization of the measuring beam is rapidly changed back and forth between right and left circular polarization, this small effect can be measured. Since CD represents the difference between two absorption strengths, the value can either be positive or negative. The units of CD are often expressed in angular units (ellipticity or molar ellipticity) for historical reasons. They relate to the elliptical polarization, which is generated when a beam of linearly polarized light is partially absorbed. Peptides, proteins and nucleic acids generally are distinguishable from their mirror image and thus exhibit CD. For example, the right-handed α-helix of peptides can be distinguished from left-handed α-helix. The individual monomers have little to no influence on the CD, but in this arrangement the oligomers exhibit strong CD. Thus, CD spectroscopy is suitable for the determination of secondary structures in biomolecules. The partial double bond characteristics of the amide bond in peptides leads to a delocalization of π-electrons. In the ground state, the π-orbital is occupied by two electrons and the n-orbital of the nitrogen also by two electrons. These electrons can be excited by incident light through photon absorption. There are two possibilities for this electron transition; either π-π* or n-π* transition. The position of these transitions is dependent on the chemical properties of the measured sample. Typical

CD-spectra can be seen in Figure 23. Peptides in α-helix conformation have a positive band around 195 nm and two characteristic negative bands around 210 and 220 nm. The β-sheet has a positive band around 200 nm and a negative band around 215 nm.[69]

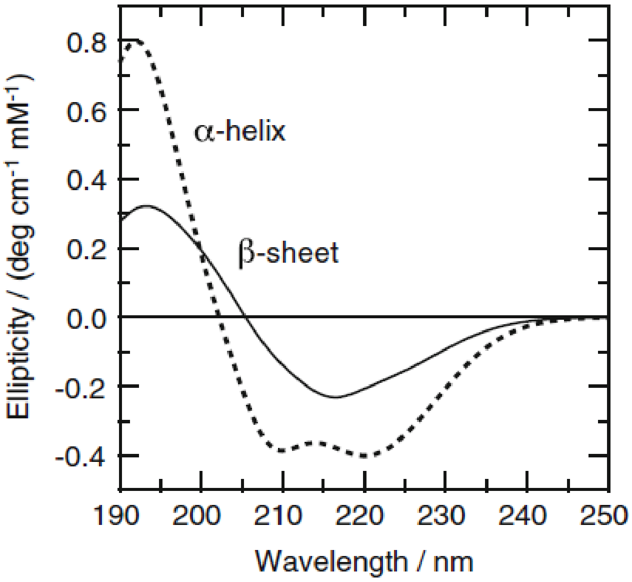

Figure 23: Typical CD-spectra of polypeptides with α-helix and antiparallel β-sheet conformation.[69]

1.3.8 Rheology

Polymeric materials show viscous and elastic properties, depending on time- and length scales of stress-strain-experiments, and can be explained by combining Hooke's and Newton's law, which describe the behavior of ideal solids (Hooke) and the ideal fluid (Newton). Hooke stated that the extension of an ideal solid is proportional to the force used to deform it. Further, stress σ and strain γ can be put into relation with an independent dimension, which is called elastic modulus G.[70]

$$\sigma = G \cdot \gamma \qquad (4)^{[70]}$$

This behavior can be visualized with the elasticity of a spring. As a model for the viscous behavior of such polymeric materials, a "dashpot" is used. It is a piston inside a fluid with the viscosity η and visualizes the reaction of an ideal fluid deformed by force. The stress σ can be put in relation with the shear rate $\dot{\gamma}$ with the following equation:[70]

$$\sigma = \eta \cdot \dot{\gamma} \qquad (5)^{[70]}$$

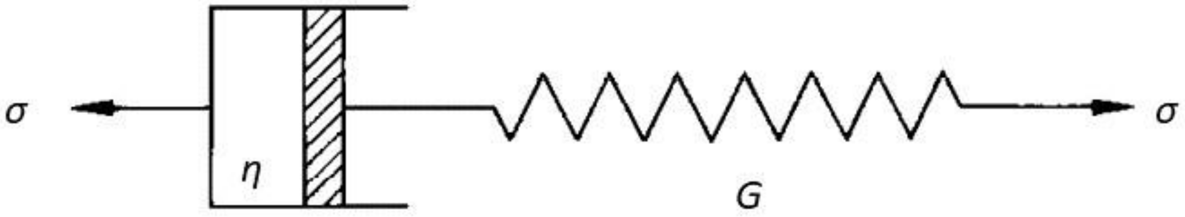

Figure 24: Maxwell model: sequential arrangement of spring and dashpot (modified).[71]

To describe viscoelasticity, a combination of both laws is necessary. If the material is more viscous, a sequential arrangement of both, spring and dashpot, is suitable (Maxwell model), whereas materials with dominant solid-like properties can be better described with a parallel arrangement of the spring and the dashpot (Kelvin-Voigt model). The Maxwell model is displayed in Figure 24. If stress σ is impacted on the system, a strain γ is induced, which can be separated in two part: strain of the spring γ_{s} and strain of the dashpot γ_{d}. Both parts are additive and thus following equation applies:[71]

$$\gamma = \gamma_{\mathrm{s}} + \gamma_{\mathrm{d}} \tag{6}$$

Because of the sequential order, both components are under the same strain σ. Therefore the following equation applies:[71]

$$\sigma = \sigma_{\mathrm{s}} = \sigma_{\mathrm{d}} \qquad (7)^{[71]}$$

The derivative of equation (4) and (6) yields:

$$\dot{\sigma} = G \cdot \dot{\gamma} \qquad (8)^{[71]}$$

$$\dot{\gamma} = \dot{\gamma}_{\mathrm{s}} + \dot{\gamma}_{\mathrm{d}} \qquad (9)^{[71]}$$

Insertion of equation (5) and (8) into equation (9) yields:

$$\dot{\gamma} = \frac{\dot{\sigma}}{G} + \frac{\sigma}{\eta} \qquad (10)^{[71]}$$

The system is put under constant strain in a so-called creep experiment. Thus the change of stress over time $\dot{\sigma}$ should be zero and equation (10) can be simplified:[71]

$$\dot{\gamma} = \frac{\sigma}{\eta} = \gamma_0 \qquad (11)^{[71]}$$

The results of the creep experiment are different from the theoretical results. Immediately after stretching, all stress $\sigma_0 = G_0 \cdot \gamma$ is stored in the spring component and an exponential decrease of stress is caused by the dashpot:[71]

$$\sigma(t) = G_0 \cdot \gamma \cdot \exp\left(-\frac{G_0}{\eta} \cdot t\right) \qquad (12)^{[71]}$$

The corresponding time-dependent modulus $G(t)$ is given as:

$$G(t) = \frac{\sigma(t)}{\gamma} = G_0 \cdot \exp\left(-\frac{t}{\tau_0}\right) \qquad (13)^{[71]}$$

The relation $\tau_0 = \eta/G_0$ is a constant with the dimension of time and is called relaxation time.[71] If periodically oscillating deformation is applied with time ($\gamma(t) = \gamma_0 \cdot \sin(\omega \cdot t)$), the storage modulus G' and the loss modulus G'' can be obtained. This oscillatory deformation of the sample can be expressed mathematically as a complex exponential:[70]

$$\gamma(t) = \gamma_0 \cdot \exp(i \cdot \omega \cdot t) \qquad (14)^{[70]}$$

$$\dot{\gamma} = \frac{d\gamma}{dt} = i \cdot \omega \cdot \gamma_0 \cdot \exp(i \cdot \omega \cdot t) = i \cdot \omega \cdot \gamma(t) \qquad (15)^{[70]}$$

If the viscoelastic sample is at shear equilibrium, the periodic deformation is phase-shifted to the periodic stress by a phase angle δ, thus the stress is given as:[70]

$$\sigma(t) = \sigma_0 \cdot \exp\big(i \cdot (\omega \cdot t + \delta)\big) \qquad (16)^{[70]}$$

$$\dot{\sigma} = \frac{d\sigma}{dt} = i \cdot \omega \cdot \sigma_0 \cdot \exp\big(i \cdot (\omega \cdot t + \delta)\big) = i \cdot \omega \cdot \sigma(t) \qquad (17)^{[70]}$$

Inserting the expressions for $\dot{\gamma}$ and $\dot{\sigma}$ into the Maxwell equation (10) and rewriting the equation yields:

$$G \cdot \frac{\gamma(t)}{\sigma(t)} = 1 + \frac{G}{i \cdot \omega \cdot \eta} \qquad (18)^{[70]}$$

The ratio of time-dependent stress and time-dependent strain is the complex shear modulus:

$$G^* = \frac{\sigma(t)}{\gamma(t)} \qquad (19)^{[70]}$$

Now, the complex modulus can be separated into a real part $G'(\omega)$ (storage modulus) and an imaginary part $G''(\omega)$ (loss modulus), considering that G^* is frequency dependent and using the relaxation time τ_0:[70]

$$G^* = G'(\omega) + i \cdot G''(\omega) = G \cdot \frac{i \cdot \omega \cdot \tau}{1 + i \cdot \omega \cdot \tau} \qquad (20)^{[70]}$$

The storage modulus $G'(\omega)$ corresponds to the part of deformation in phase with applied stress and the loss modulus corresponds to the viscous part of the shear strain, which is shifted by a phase angle of 90° compared to the oscillatory stress:[70]

$$G'(\omega) = G \cdot \frac{(\omega \cdot \tau)^2}{1 + (\omega \cdot \tau)^2} \qquad (21)^{[70]}$$

$$G''(\omega) = G \cdot \frac{\omega \cdot \tau}{1 + (\omega \cdot \tau)^2} \qquad (22)^{[70]}$$

The before mentioned relation between stress σ and shear rate $\dot{\gamma}$ of Newtonian liquids in equation (5) can be clarified by imagining two parallel plates with a fluid in between. Rotating the upper plate with constant velocity v_{x} in x-direction, causes a shear gradient of the velocity due to the adhesion of the liquid to the plates. Therefore, the molecules near the moving plate are moving with the same velocity as the plate v_{x} and the molecules near the fixed plate do not move at all. The resulting shear stress σ on the moving plate is proportional to the shear rate $\dot{\gamma}$ and can be calculated with the proportional constant η, the viscosity. This relation is used in plate-plate rheometer in order to determine important parameters of viscoelastic materials.[70]

Materials, without a linear relation between stress and shear rate, are called non-Newtonian liquids. Besides this relation, a time-dependency during constant shear is possible. In ideal Newtonian liquids, the stress σ is proportional to the shear rate $\dot{\gamma}$ (eq. 5). Shear thickening occurs, when the stress σ is only proportional to the shear rate $\dot{\gamma}$ at small shear rates $\dot{\gamma} \to 0$. Increasing the shear rate $\dot{\gamma}$ yields a reduced rise of the stress σ, thus the viscosity η decreases with higher shear rate $\dot{\gamma}$. A lot amorph polymers show shear thinning, once the molecular weight reaches a critical value. Since the molecular weight is proportional to the length of a polymer, a critical length enables entanglement of the polymer chains, which yields an increase in viscosity. Upon deformation, the entanglements are loosened and the viscosity decreases. Shear thickening materials show similar behavior at low shear rates $\dot{\gamma} \to 0$, but have a rise of stress increase at higher shear rates. This yields a rise of viscosity at increased shear rates. This behavior is shown by polymers, which crystallize upon strain.[70] If the application of finite shear on a system after long rest yields a decrease in viscosity and the decrease persists, than the material is work softening. If the original viscosity is recovered, the behavior is called thixotropic.[13] Thixotropy is a time-dependent decrease of viscosity induced by flow, which is reversible, if the flow is decreased or arrested.[72]

2. Motivation

The objective of this master thesis is the synthesis and comparison of different polymer-peptide hybrids and their ability to form hydrogels. Further, the synthesis of a novel pH-responsive peptide cross-linker for hydrogel synthesis should be optimize, which can be coupled via thiol-ene click reaction to alkene functionalized poly(phosphonates) and dextrans. These polymer backbones are biocompatible and biodegradable and could yield potentially biocompatible and biodegradable polymer-peptide hybrids, when coupled with the before-mentioned peptide (Figure 25).

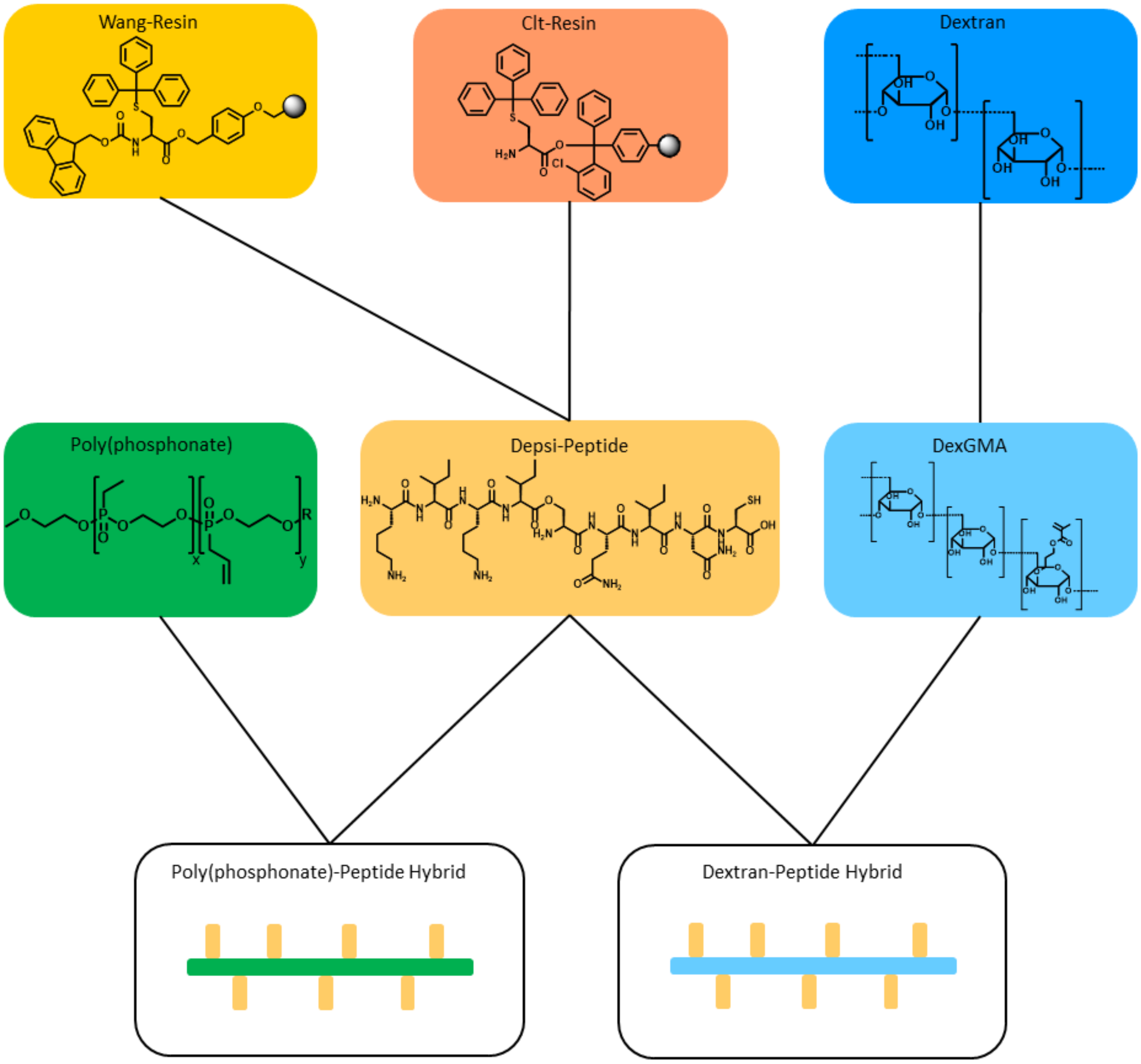

Figure 25: Synthesis route for this master thesis: Synthesis of a pH-responsive depsi-peptide on either a Wang- or Clt-resin, which can be linked to an allyl-functionalized poly(phosphonate) or GMA-functionalized dextran via thiol-ene click reaction to yield a polymer-peptide hybrid.

In general, different polymer-peptide hybrids based on either a poly(phosphonate) or dextran backbone should be synthesized and tested for their gelation propensity, stability of the gel and self-healing properties. This will enable to expand on the types of available backbones and allow a direct comparison to the previously used HSA backbone. Since the dextran backbone must carry an alkene function in order to couple the depsi-peptide via thiol-ene click reaction, the backbone needs to first be functionalized with GMA. The previously introduced depsi-peptide KIKI(O-C(O))SQINC will be synthesized and used as a supramolecular cross-linker, which can be activated by inducing a pH shift from acidic to neutral. Further, the coupling conditions of the peptide to the respective polymer backbone needs to be optimized to occur exclusively in aqueous media.

The fibrillation of the cross-links and the resulting gelation of the polymer-peptide hybrid should be controlled by a pH shift. A thiol-ene click reaction will be used to couple cysteine-containing D3 to alkene-functionalized backbones.

The hydrogel introduced in Jasmina Gačanins publication "Autonomous ultrafast self-healing hydrogels by pH responsive functional nanofiber gelators as cell matrices", which exhibits high stability, thixotropy, biocompatibility and -degradability, was used as a model.[8] Further, the poly(phosphonate)-peptide hybrid introduced by J. Luisa J. L. L. Wiechmann should be improved and used as a model for the synthesis of a novel polymer-peptide hybrid.[73] The established peptide sequence KIKISQINC should be linked as a depsi-peptide to the same poly(phosphonate) and also to a similar polymer with higher molecular weight, which increases the number of entanglements in order to improve the stability. Also, GMA-functionalized dextrans should be synthesized, which could be coupled with the established peptide via thiol-ene click reaction. Both polymer backbones are chosen due to their water-solubility, biodegradability and -compatibility, which facilitates applications in the biomedical field. In addition, the gels can be scaled up due to the lower costs of the polymer backbones. The poly(phosphonate) can be easily adjusted in length and chemical properties by changing the monomer-initiator ratio and the monomers itself containing different functional groups. Due to the various range of different dextrans, the molecular weight of the polymer can be easily adjusted. However, the downside to the wide variety of dextrans is the high polydispersity, since dextran is obtained from bacteria.

The goal of the hydrogel synthesis should be a biodegradable and -compatible material, which exhibits thixotropic properties arising from the physical cross-links due to the peptide-peptide interactions. The thixotropic properties and high stability would make the gel attractive for biomedical applications like tissue engineering in order to cultivate cells in 2D or 3D matrices. In addition, such material could be easily injected into a patient, while instantaneously gelling under physiological conditions. Also, fissures in the gel could be quickly regenerated due to the rearrangement and reassembly of the components.

The synthesized peptides were purified via HPLC and characterized with MALDI-ToF MS and LCMS. The secondary structure and fibrillation of D3 coupled with the pH-responsiveness was analyzed via ThT-assay, conversion assay, TEM and ATR-FTIR.

The polymer backbones and the polymer-peptide hybrids were characterized via ^{1}H- (both) and ^{31}P-NMR (poly(phosphonate)) and analyzed via ThT-assay, TEM, ATR-FTIR and rheology to determine the influence of cross-links on their stability.

3. Results and Discussion

3.1 Design

The design of the depsi-peptide sequence KIKI(O-C(O))SQINC was adopted from the unpublished master thesis of J. Luisa J. L. L. Wiechmann “Novel Responsive Peptide Crosslinker for Hydrogel Synthesis”.[73] Serine was selected to enable esterification in order to prevent aggregation of peptide chains. The remaining AA were selected to promote the formation of β-sheet fibrils. The combination of a hydrophobic and hydrophilic AA in alternating repeating distance like in KIKISQINM (D1) facilitates the formation of β-sheets.[8] Isoleucine has a hydrophobic side chain and promotes in combination with the hydrophilic AA lysine, asparagine and glutamine the formation of β-sheets. The hydrophilic AA are so-called gatekeeper AA and exhibit an important role in β-sheet fibril formation. They inhibit intrinsic aggregation and slow down polymerization. Inhibition of the aggregation allows correct arrangement of β-sheets, thus completion of the nucleation phase of fibrils. Fast aggregation of peptides without gatekeeper leads to misfolding of the β-sheets and therefore few to none fibrils.[74] The depsi-character of the peptide is important for the coupling reaction with a polymer backbone and the necessary solubility. Upon changing the pH from acidic to neutral, the *O*,*N*-acyl shift of the depsi-peptide occurs and the polymer-peptide hybrid can be cross-linked via aggregation of the linear peptide sequences.

The C-terminal cysteine can be linked to polymer backbones via thiole-ene click reaction. Therefore, the introduced poly(phosphonate)[73] and a novel functionalized dextran with an alkene group were used as potential polymer backbones for hydrogel synthesis. Both polymers are promising candidates as alternative backbones to the introduced HSA due to their biocompatibility, -degradability, their lower cost and better availability.

3.2 Synthesis of the hybrid components

The synthesis of the depsi-peptide and polymer backbones needed for the polymer-peptide hybrid preparation is described in the following chapter.

3.2.1 Synthesis of depsi-peptides

The synthesis of the depsi-peptide KIKI(O-C(O))SQINC (D3) was performed on a Wang- and a Clt-resin (Figure 26). All peptides were synthesized via SPPS either with a SPPS-device or in a vial (esterification).

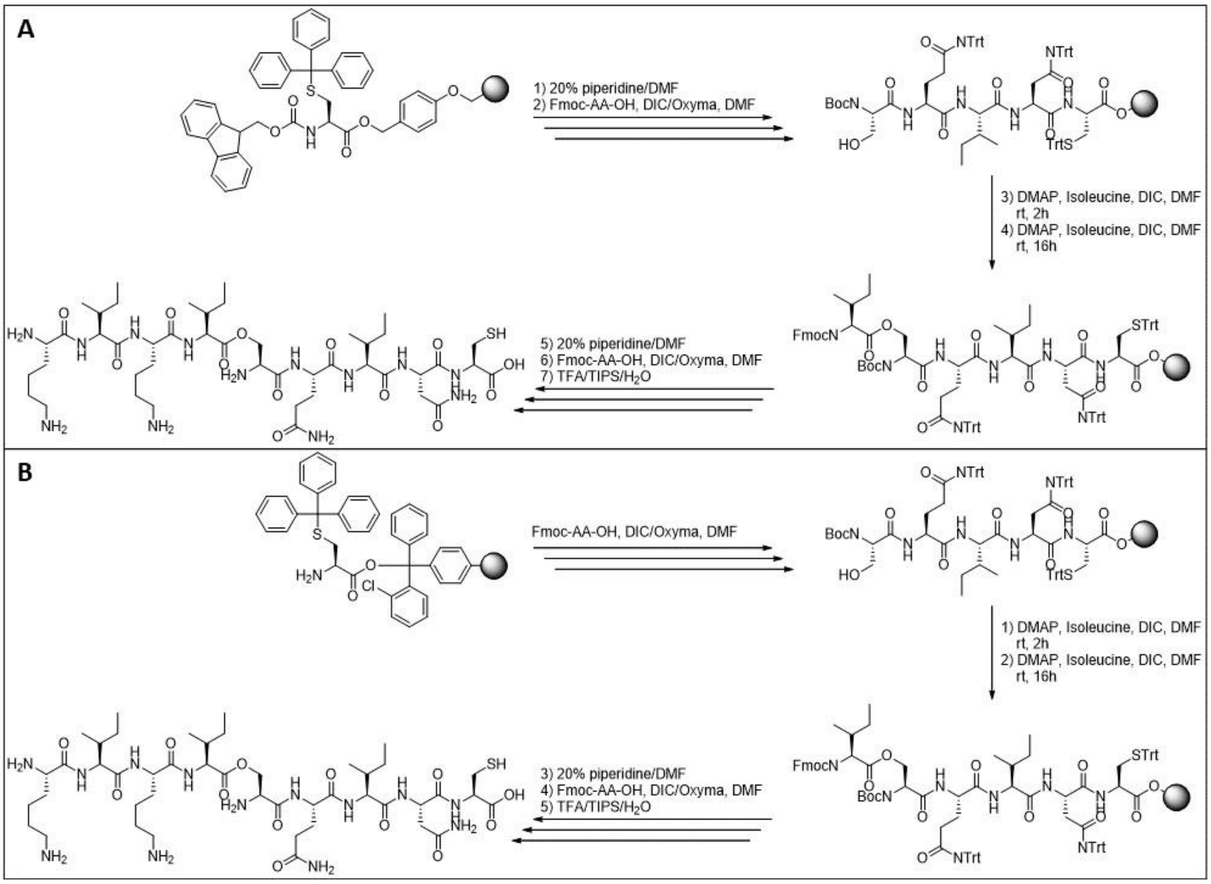

Figure 26: Reaction schemes of the synthesis of D3. (**A**) Synthesis via Wang-resin. 1)+2) alternating Fmoc-deprotection and AA coupling with DIC/Oxyma; 3)+4) double coupling of isoleucine with DMAP/DIC; 5)+6) alternating Fmoc-deprotection and AA coupling with DIC/Oxyma; 7) cleavage of peptide from resin. (**B**) Synthesis via Clt-resin. Multiple AA coupling steps with Fmoc-deprotection with 20% piperidine/DMF; 1)+2) double coupling of isoleucine with DMAP/DIC; 3)+4) alternating Fmoc-deprotection and AA coupling with DIC/Oxyma; 5) cleavage of peptide from resin.

Since Wang-resins are typically used for peptide synthesis in our working group, the same approach was used for the preparation of D3. However, during synthesis of the peptide and cleavage of the peptide D3 from the resin different side reactions were observed. The use of a Clt-resin was tested to evaluate if side reactions could be avoided. Here, the synthesis of D3 on both resins is explained and compared in the following section.

The Wang-resin was loaded with Fmoc-Cys(Trt), while the corresponding Clt-resin was loaded with H-Cys(Trt). For this reason, the synthesis of D3 had an additional deprotection step in the very beginning applying 20% piperidine solution in DMF when loaded on a Wang-resin. The remaining steps were performed in the same manner for both resins. The Fmoc-protected AA was coupled with the growing peptide and Fmoc-deprotected before the next coupling step until the AA serine. Serine was N-terminally Boc-protected, because the next AA (isoleucine) was supposed to react via its carboxy group with the hydroxy group in the side chain of serine to from an ester bond, and ultimately yield a so-called depsi-peptide. The esterification was carried out inside a vial instead of the SPPS-device because the device was not configured for this type of reaction. The coupling step with isoleucine was repeated two times with extended reaction times, because of the missing thermal activation through microwaves. The remaining three AA were again coupled in the SPPS-device in the same way as before, yielding the final product depsi-peptide D3.

D3 was cleaved off from the resin and deprotected with a mixture of TFA/TIPS/H_2O (95/2.5/2.5) and precipitated in cold diethyl ether. D3 was purified via RP-HPLC and freeze dried to yield the dry product. The comparison of the HPLC-traces of the crude product of both synthesis routes reveal that a significant amount of side products arises during the synthesis of D3 on the Wang-resin (Figure 27).

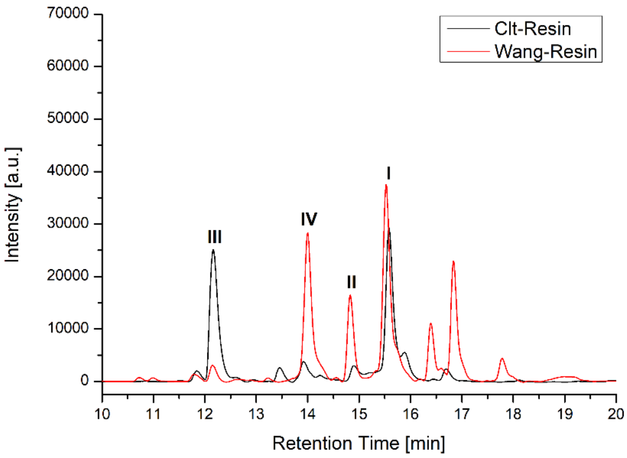

Figure 27: Comparison of HPLC-traces of D3 originating from Clt-resin and Wang-resin. Crude product absorption at 214 nm. Peak (**I**): D3; Peak (**II**): P3; Peak (**III**): SQINC; Peak (**IV**): KIKI(O-C(O))SQINA^{Pip}.

Besides the product D3, also the side products of the reaction could be isolated and identified. The respective products are summarized in Figure 28 and are assigned to the peaks in Figure 27.

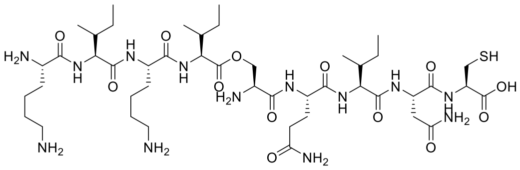

Exact Mass: 1045,60

KIKI(O-C(O))SQINC

I

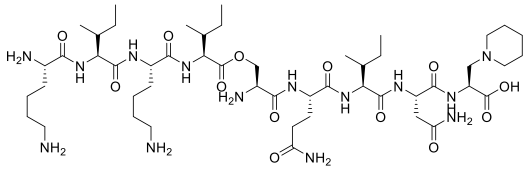

Exact Mass: 1096,70

KIKI(O-C(O))SQINA^{Pip}

IV

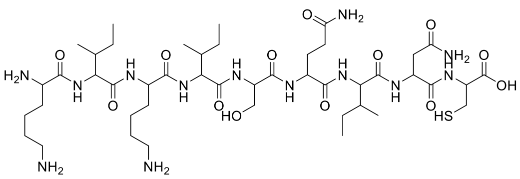

Exact Mass: 1045,60

KIKISQINC

II

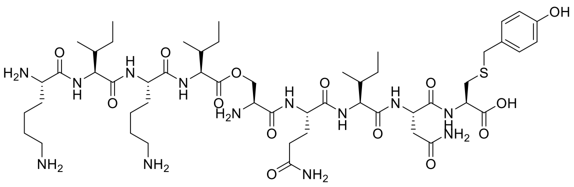

Exact Mass: 1151,64

KIKI(O-C(O))SQINC^{Wang}

V

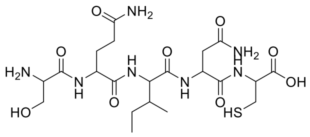

Exact Mass: 563,24

SQINC

III

Figure 28: Sequence of the depsi-peptide D3 (**I**), the linear peptide P3 (**II**), the peptide part before esterification (**III**), the side product formed during Fmoc-cleavage (**IV**) and the side product formed during cleavage from the Wang-resin (**V**).

Especially, the side products originating from the Fmoc-deprotection step and the cleavage step play a major role in case of the Wang-resin. By changing the linker to Clt, side products were significantly reduced. Since the Wang-linker was exchanged, its side product (**V**) could not occur. Also, the amount of formed side product (**IV**) originating from Fmoc-deprotection could be drastically decreased. The yield of the final product could be optimized from 5.8% to 7.8%. Unfortunately, the esterification of SQINC (**III**) was significantly less efficient, because it made up approximately 50% of the side products. However, this reaction was optimized by using higher amounts of equivalents of isoleucine, DIC and 4-dimethylaminopyridine (DMAP) for the coupling.

Looking further into details of the HPLC-trace and analyzing the respective peaks, D3 synthesized on a Wang-resin (D3^{W}), the amount of side product KIKI(O-C(O))SQINA^{Pip} (**IV**) is nearly the same as the product D3^{W} (Figure 29).

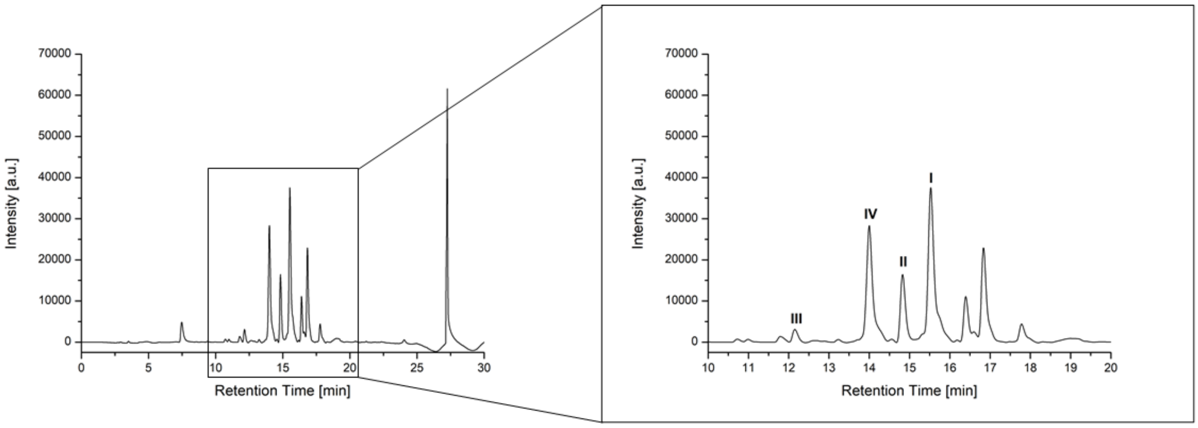

Figure 29: HPLC-trace and enlarged region of interest of D3 synthesized on Wang-resin. Crude product absorption at 214 nm. Peak (**I**): D3^{W}; Peak (**II**): P3^{W}; Peak (**III**): SQINC; Peak (**IV**): KIKI(O-C(O))SQINA^{Pip}.

Due to the poor sterical hinderance and negative inductive effect of the Wang-linker, the α-carbon atom of the cysteine can be deprotonated by piperidine during Fmoc-deprotection, followed by an elimination reaction of the thiol group with its protecting group. The following addition of piperidine yields A^{Pip} at the C-terminus (Figure 9).[26] This side product could be verified via MALDI-ToF-MS in the isolated HPLC fraction of peak **IV** (Figure 30).

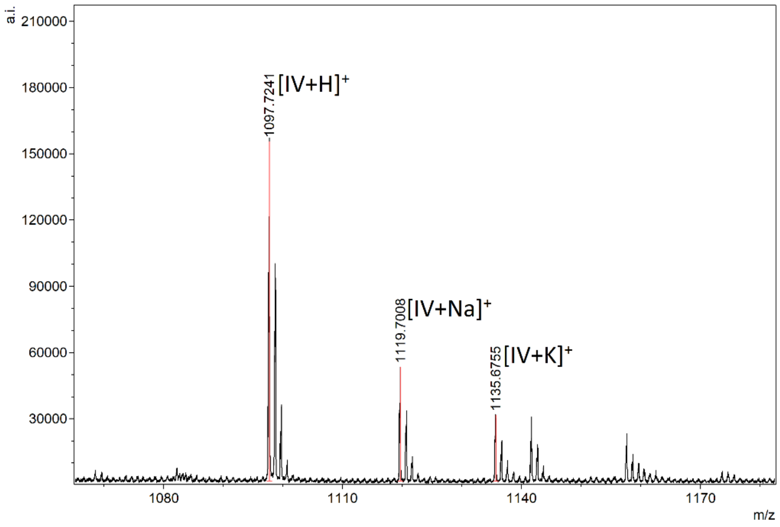

Figure 30: Enlarged region of interest of MALDI-ToF MS data of isolated side product KIKI(O-C(O))SQINA^{Pip} (**IV**). m/z: Calculated: [**IV**+H]$^{+}$ = 1097.71, [**IV**+Na]$^{+}$ = 1119.69, [**IV**+K]$^{+}$ = 1135.66. Found: [**IV**+H]$^{+}$ = 1097.72, [**IV**+Na]$^{+}$ = 1119.70, [**IV**+K]$^{+}$ = 1135.68.

An *O*-*N*-acyl shift can occur during purification of the peptide D3 despite of handling the peptide in acidic solution (0.1% aqueous TFA solution). TEM images (Figure 31 by Luisa Wiechmann) show fibrous aggregates under acidic conditions, which are typically associated with the linear peptide. Since the peptide formed β-sheet fibrils under acidic conditions, the *O*-*N*-acyl shift must have occurred during the purification step.

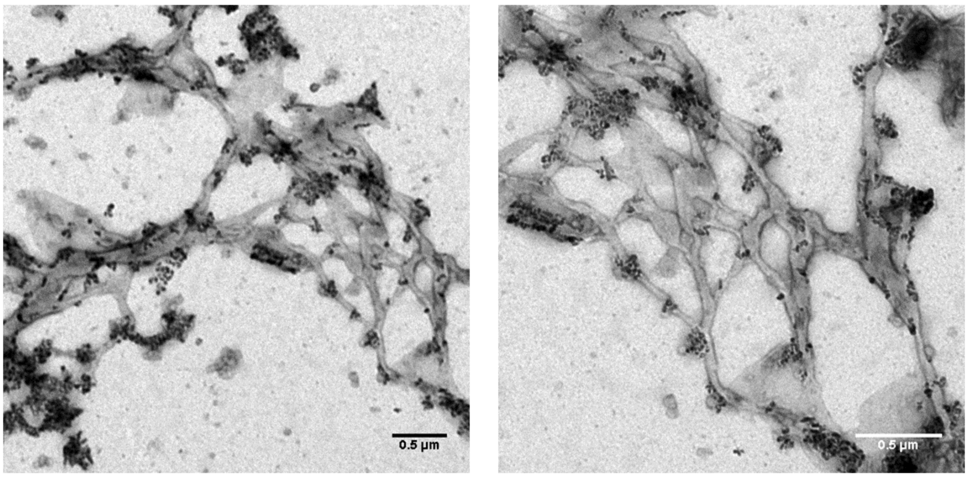

Figure 31: TEM images of P3^{W} (**II**) under acidic conditions (0.1% aqueous TFA). Scalebars 0.5 µm.

Aggregation behavior of the synthesized depsi-peptide sequence is only possible in media with a pH>2 and therefore should not occur in 0.1% aqueous TFA (pH=2). The isolated side product (**II**) was consequently kept under acidic conditions, but was able to form fibril-like aggregates (Figure 31) and thus cannot be a depsi-peptide. Since the isolated material has the same molecular mass as the depsi-peptide (Figure 33) and similar retention times as the crude linear synthesized control peptide P3-Ctrl (Figure 32), the side product could be identified as the linear peptide sequence KIKISQINC (**II**).

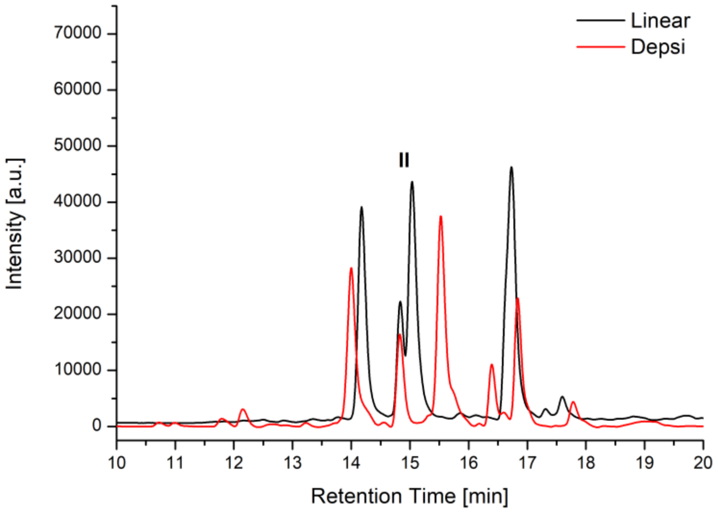

Figure 32: Comparison of crude HPLC-traces of D3 and P3-Ctrl. Peak (**II**): P3^W and P3-Ctrl.

The linear peptide P3^W (**II**) also contained the side product (**V**), which originated from the cleavage step of the peptide from the Wang-resin as depicted in Figure 33.[28]

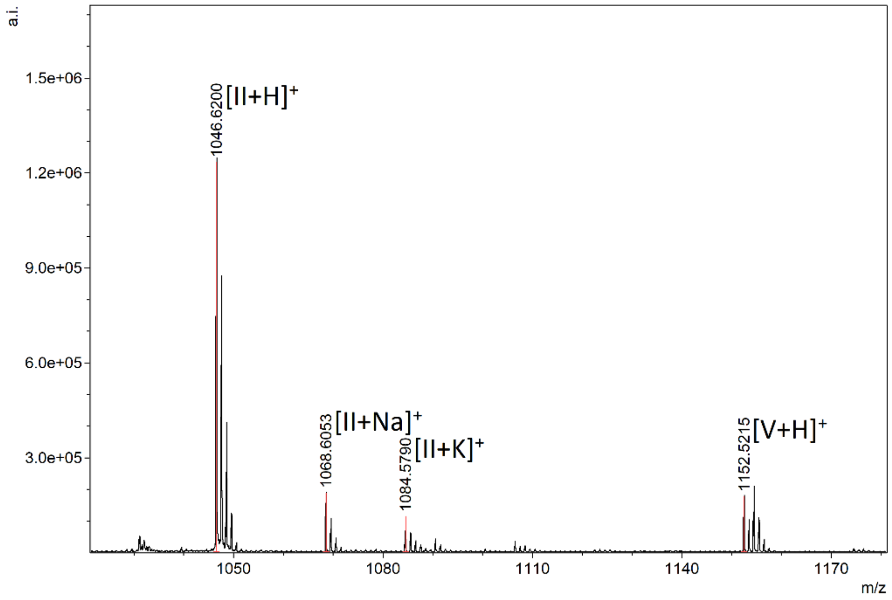

Figure 33: Enlarged region of interest of MALDI-ToF MS data of isolated side product P3^W (**II**) with side product (**V**). m/z: Calculated: [**II**+H]$^+$ = 1046.61, [**II**+Na]$^+$ = 1068.59, [**II**+K]$^+$ = 1084.56, [**V**+H]$^+$ = 1152.64. Found: [**II**+H]$^+$ = 1046.62, [**II**+Na]$^+$ = 1068.61, [**II**+K]$^+$ = 1084.58, [**V**+H]$^+$ = 1152.52.

The isolated product D3^W (**I**) also contained the side product (**V**). This was verified via MALDI-ToF MS (Figure 34). Since the side product (**V**) has different chemical properties than the product(**I**) and side product (**II**) because of the added phenol group, the elution times should be different from product(**I**) and side product (**II**). MALDI-ToF MS is not a quantitative method to analyze samples and neither a peak nor a mass of this substance could be seen in the LCMS spectrum of product (**I**) (Figure 35), thus the amount of the side product (**V**) should be minor.

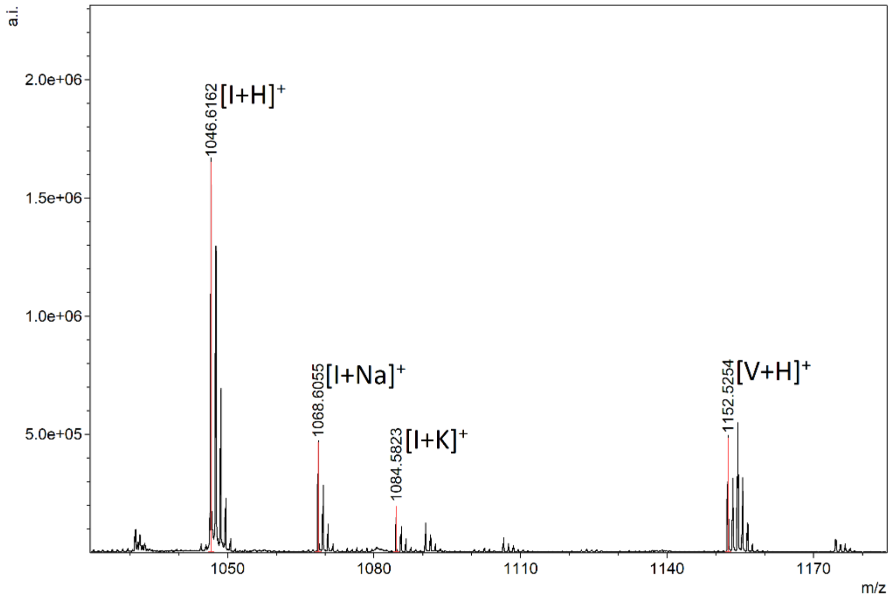

Figure 34: Enlarged region of interest of MALDI-ToF MS data of isolated D3^W (**I**) with side product (**V**). m/z: Calculated: [**I**+H]$^+$ = 1046.61, [**I**+Na]$^+$ = 1068.59, [**I**+K]$^+$ = 1084.56, [**V**+H]$^+$ = 1152.64. Found: [**I**+H]$^+$ = 1046.62, [**I**+Na]$^+$ = 1068.61, [**I**+K]$^+$ = 1084.58, [**V**+H]$^+$ = 1152.52.

The isolated product D3^W contained impurities of another unknown side product (**VI**) as the LCMS results showed. It was not possible to remove this impurity via HPLC, since both peptides had nearly the same retention time. Also, the amount of side product (**VI**) as an impurity varied from batch to batch to the extend, that a batch contained more side product than product D3^W (Figure 35B).

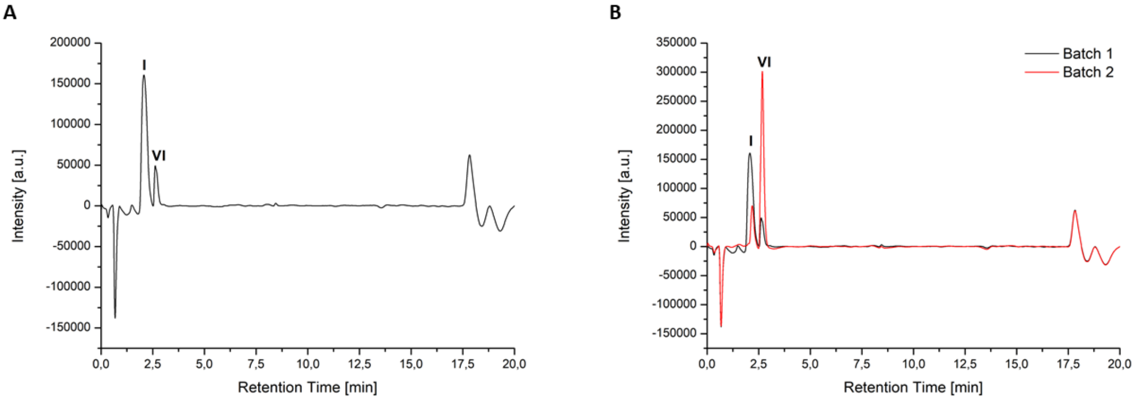

Figure 35: LC-trace of LCMS measurements of the isolated product D3^W. (**A**) Representative LC-trace. (**B**) Representative batch (black) and batch with high side product (**VI**) content (red).

The corresponding MS-spectra of the labeled peaks (**I**) and (**VI**) in Figure 35 are shown in Figure 36.

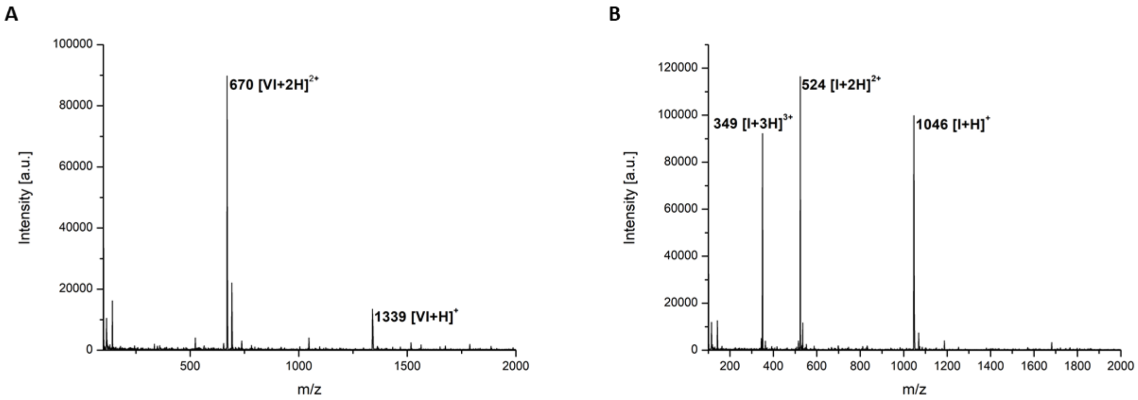

Figure 36: MS-spectra of (**A**) the side product (**VI**) and (**B**) the product D3 (**I**). m/z: Calculated: [**I**+H]$^{+}$ = 1046.61, [**I**+2H]$^{2+}$ = 523.80 [**I**+3H]$^{3+}$ = 349.87. Found: [**VI**+H]$^{+}$ = 1339, [**VI**+2H]$^{2+}$ = 670, [**I**+H]$^{+}$ = 1046, [**I**+2H]$^{2+}$ = 524 [**I**+3H]$^{3+}$ = 349.

Because of the impurity of the isolated product D3 and the decrease in yield (5.8%) through the amount of side products, Clt-resin was used to provide for an alternative with improved purity and overall yield (7.8-8.7%). Figure 37 shows the HPLC-trace of the crude peptide originating from the Clt-resin. While the side products observed during the synthesis of D3^{W} could be eliminated successfully, an increase in side product, namely the D3 fragment SQINC (**III**) was observed during the synthesis of D3 using Clt-resin. Unfortunately, the side product (**III**) makes up 50% of the reaction. However, this problem could be solved by increasing the amount of isoleucine, DMAP and DIC during esterification.

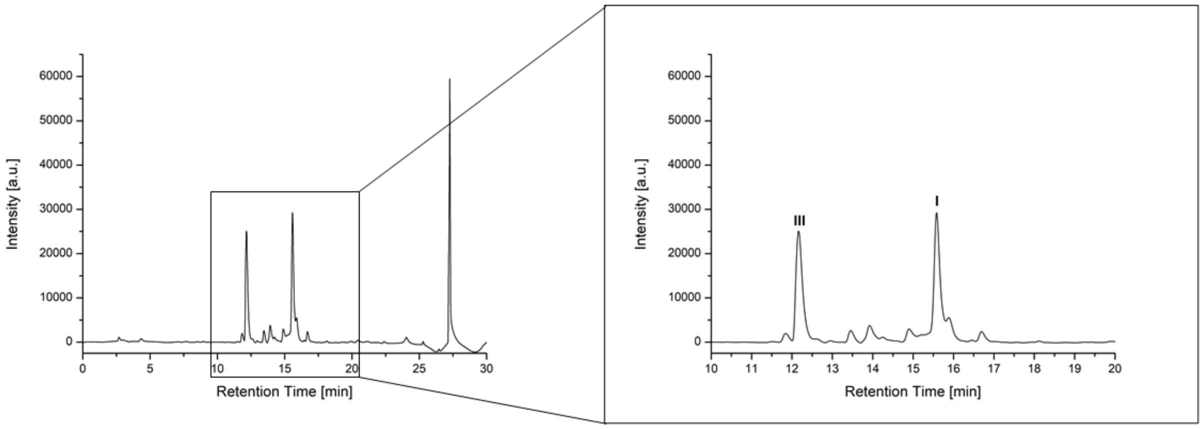

Figure 37: HPLC-trace and enlarged region of interest of D3 originated from Clt-resin. Crude product absorption at 214 nm. Peak (**I**): D3^{C}; Peak (**III**): SQINC.

After the purification via HPLC, the peptide D3^C did not show any impurities, which could be confirmed by MALDI-Tof MS (Figure 38) and LCMS (Figure 39).

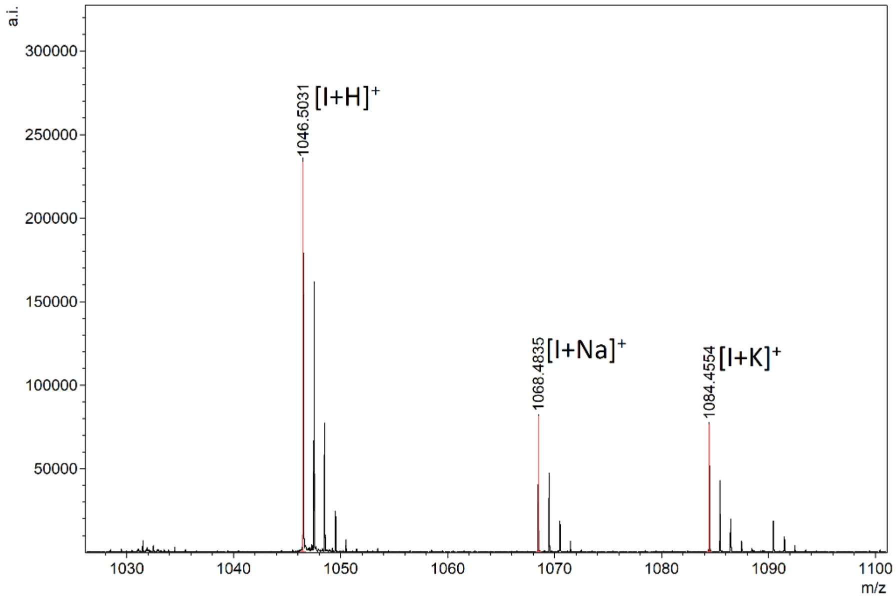

Figure 38: Enlarged region of interest of MALDI-ToF MS data of isolated D3^C (**I**). m/z: Calculated: [**I**+H]$^+$ = 1046.61, [**I**+Na]$^+$ = 1068.59, [**I**+K]$^+$ = 1084.56. Found: [**I**+H]$^+$ = 1046.50, [**I**+Na]$^+$ = 1068.48, [**I**+K]$^+$ = 1084.45.

As mentioned, the LCMS results reveal, that the isolated product D3^C (**I**) is free from impurities, because only one peak could be seen in the LC-trace, which had the same m/z value as the product D3 (Figure 39).

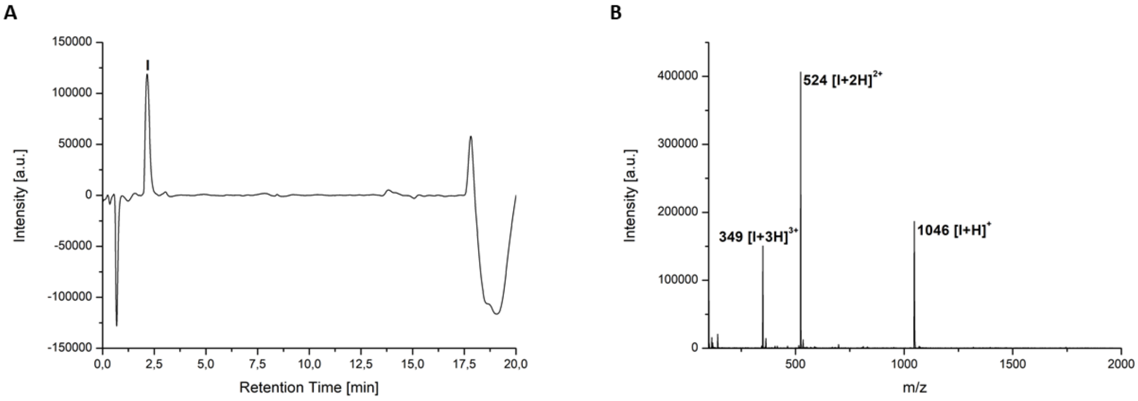

Figure 39: (**A**) LC-trace and (**B**) MS-spectrum of the product D3^C (**I**). m/z: Calculated: [**I**+H]$^+$ = 1046.61, [**I**+2H]$^{2+}$ =524.30, [**I**+3H]$^{3+}$ = 349.87. Found: [**I**+H]$^+$ = 1046, [**I**+2H]$^{2+}$ =524, [**I**+3H]$^{3+}$ = 349.

By optimization of the esterification step, the LC spectra is now dominated by the product peak with very few side-products visible. Unfortunately, the final yield of the product D3^C (**I**) remains low, with a minor improvement over the first reaction from 7.8% to 8.7%. To isolate the product peak better from side product peaks, the gradient must be optimized, which could increase the yield further. Also, the general work-up could be optimized by changing the cleavage cocktail or improve the precipitation step.

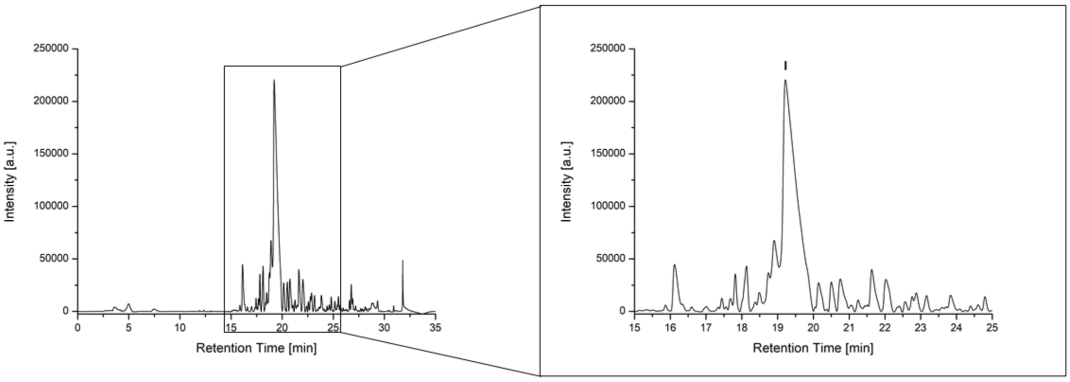

Figure 40: HPLC-trace and enlarged region of interest of D3^C (**I**) after optimized esterification. Crude product absorption at 214 nm.

Nevertheless, the product could be isolated without impurities, which was proven via LCMS (Figure 41). The LC-trace had only one peak, which contained only the product D3^C.

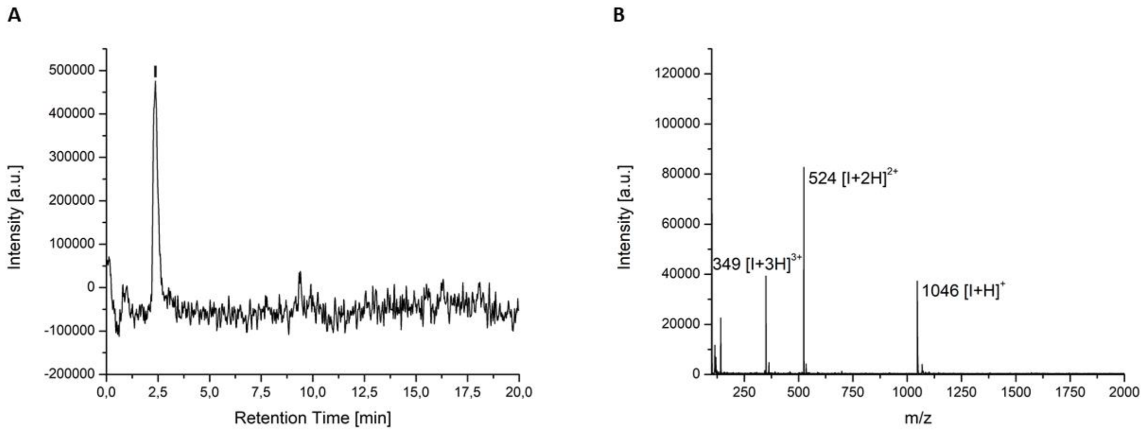

Figure 41: (**A**) LC-trace and (**B**) MS-spectrum of the product D3^C (**I**) after optimized esterification. m/z: Calculated: $[\mathbf{I}+H]^+$ = 1046.61, $[\mathbf{I}+2H]^{2+}$ =524.30, $[\mathbf{I}+3H]^{3+}$ = 349.87. Found: $[\mathbf{I}+H]^+$ = 1046, $[\mathbf{I}+2H]^{2+}$ =524, $[\mathbf{I}+3H]^{3+}$ = 349.

In summary, the depsi-peptide sequence KIKI(O-C(O))SQINC was initially synthesized on a Wang-resin. Due to different side reactions and purification problems, the resin was changed to a Clt-resin, which suppressed most of the side reactions and yielded a pure product D3^C. However, the change of the resin led to an increase of the side product SQINC. Since the amount of this fragment could be correlated with a worse esterification, this step was optimized by increasing the used amount of educts. However, the yield should have nearly doubled, instead of only increasing by 0.9%. Since the product peak in the HPLC trace was not completely isolated from other peaks, only a fraction of this peak could be collected to avoid impurities in the product fraction. Also, the used cleavage cocktail was suitable for Wang-resins but must be adapted for the Clt-resin. This step could increase the yield further. The depsi-peptides and its yields are listed in Table 1.

Table 1: Theoretical and experimental yields of the synthesized depsi-peptide D3 on Wang- ($D3^W$) or Clt-resin ($D3^C$) and on Clt-resin with optimized esterification step ($D3^C$ Esterification).

Peptide	Theoretical Yield [mg]	Experimental yield [mg]	Yield percentage
$D3^W$	104.6	6.1	5.8%
$D3^C$	522.8	40.5	7.8%
$D3^C$ Esterification	522.8	45.6	8.7%

3.2.2 Synthesis of polymer backbones

Synthesis of poly(phosphonate)

The poly(phosphonate)s were both synthesized by Timo Rheinberger (MPIP Mainz) according to the published procedure.[75]

The degradation rate and the possibility of degradation of poly(phosphonate)s in general is dependent on the type of end-group that the polymer carries. The initial polymer that was chosen as a backbone for hybrid synthesis did not carry an end-capping group, which was supposed to increase biodegradability. However, this particular polymer was so unstable, that it degraded already during the hybrid synthesis (Figure 53). Consequently, the synthesis was repeated with a polymer that carried end-capping groups (Figure 43). Since GPC analysis of the following polymers was not possible, NMR-spectroscopy was used to analyze length, ratio of the monomer units and purity of the poly(phosphonate)s.

The low molecular weight poly(phosphonate) without end-capping P(**VII**$_{90}$-co-**VIII**$_{27}$) (Phos1) (**IX**) was synthesized via anionic ring opening polymerization of 2-ethyl-2-1,3,2-dioxaphospholane 2-oxide (**VII**) and 2-allyl-2-oxo-1,3,2-dioxaphospholane 2-oxide (**VIII**) in DCM (Figure 42). The reaction was initiated by 2-methoxyethanole with the catalyst 1,8-

diazabicyclo-[5.4.0]undec-7-ene (DBU) at 0 °C. The polymerization was terminated by formic acid solved in DCM and the crude product was precipitated in cold diethyl ether. After dialysis against water, the product (**IX**) was lyophilized. The resulting dry product was characterized via ^{1}H- and ^{31}P-NMR to determine length, ratio of the monomer units and purity of the polymer in the master thesis of Luisa Wiechmann.[73] The determined length of the polymer was 117 monomer units with a ratio 10:3 in regard to the alkyl-functionalized monomer.

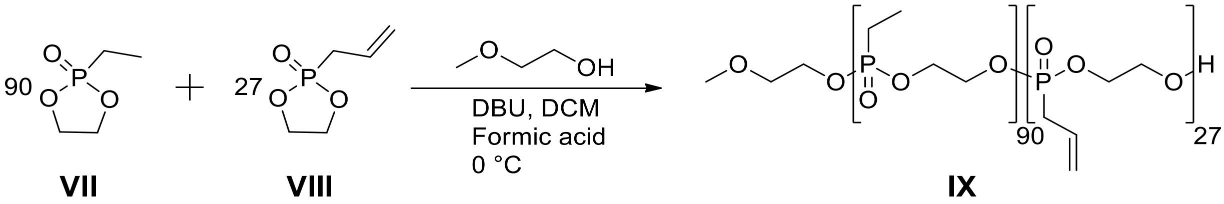

Figure 42: Synthesis scheme of the anionic ring opening polymerization of the monomers 2-ethyl-2-1,3,2-dioxaphospholane 2-oxide (**VII**) and 2-allyl-2-oxo-1,3,2-dioxaphospholane 2-oxide (**VIII**) in DCM with 2-methoxyethanole as initiator and DBU as catalyst at 0 °C to yield Phos1 (**IX**).

Due to the degradation of the polymer Phos1 (**IX**) during hybrid synthesis and fluid-like properties of the hybrid material (Figure 69), a polymer with higher molecular weight and end-capping was synthesized in order to increase the number of entanglements, prevent degradation and therefore increase general stability. The polymerization of high molecular weight poly(phosphonate) with end-capping P(**VII**$_{147}$-co-**VIII**$_{98}$) (Phos2) (**X**) was done analogue to the previous reaction, except for terminating the reaction with ethyl isocyanate instead of formic acid to obtain an end-capped polymer (Figure 43). NMR analysis after purification showed an overall longer polymer chain with a slightly different monomer composition, Phos2 (**X**).

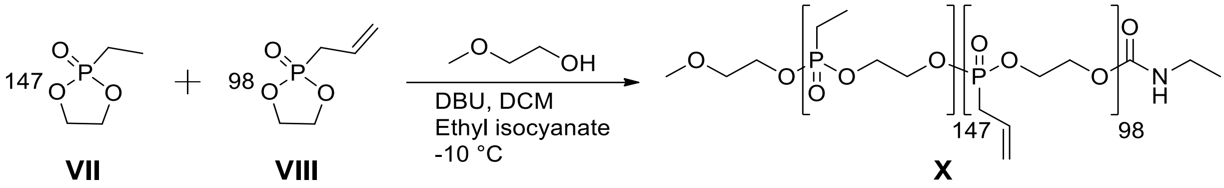

Figure 43: Synthesis scheme of the anionic ring opening polymerization of the monomers 2-ethyl-2-1,3,2-dioxaphospholane 2-oxide (**VII**) and 2-allyl-2-oxo-1,3,2-dioxaphospholane 2-oxide (**VIII**) in DCM with 2-methoxyethanole as initiator, DBU as catalyst at 0 °C and the termination reagent ethyl isocyanate to yield the poly(phosphonate) Phos2 (**X**).

Figure 44 depicts the ^{1}H-NMR-spectrum of Phos2 (**X**) with the molecular structure of the polymer. All hydrogen atoms could be assigned to their corresponding signals. The number of monomer units N_{M} can be calculated with the following formula,

$$N_{\mathrm{M}} = \frac{I_{\mathrm{Back}} - 2}{N_{\mathrm{H}}} \tag{23}$$

where $I_{\mathrm{Back}} - 2$ is the integral of the hydrogen atoms of the backbone minus the two hydrogen atoms of the initiator and N_{H} is the number of hydrogen atoms in the backbone per monomer unit. The integral of the initiator was adjusted to three hydrogen atoms, in order to get the total integral for the hydrogen atoms in the backbone $I_{\mathrm{Back}} \approx 980$. The number of monomer units N_{M} equals approximately 245.

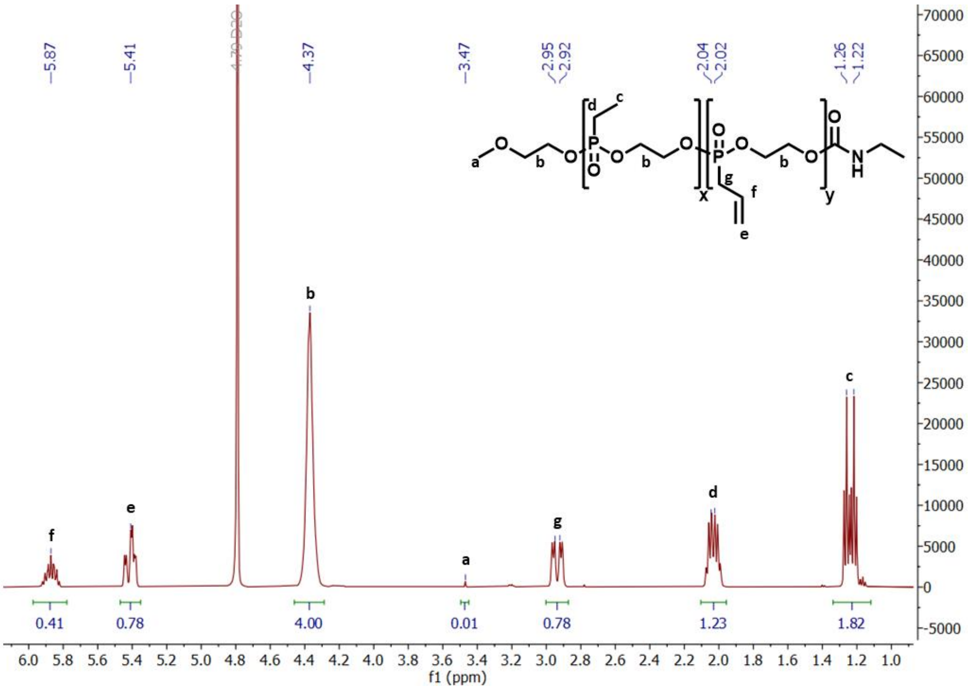

Figure 44: ^{1}H-NMR-spectrum of Phos2 (**X**) in D_2O (700 MHz) with the molecular structure and the assigned hydrogen atoms.

The relation between alkyl- and allyl-functionalized monomer units can be calculated via ^{31}P-NMR (Figure 45). For that, the ratio between the integral of the alkyl peak (38.34 ppm) and the allyl peak (31.30 ppm) was determined. The determined ratio is approximately 3:2 referred to the alkyl integral. Therefore, the number of alkyl-functionalized monomer units is 147 and the number of allyl-functionalized monomer units is 98. The aimed length of 250 monomer units was nearly reached and the calculated ratio of 3:2 achieved.

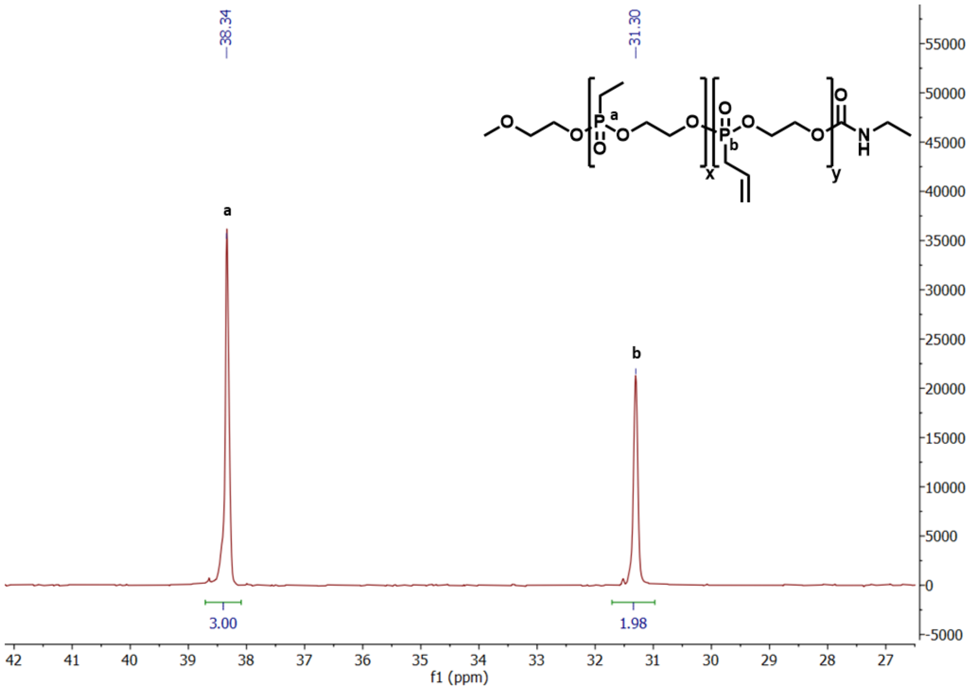

Figure 45: ^{31}P-NMR-spectrum of Phos2 (**X**) in D_2O (700 MHz) with the molecular structure and the assigned phosphorus atoms.

Both poly(phosphonate)s were successfully synthesized with the aimed length and alkyl-to-allyl ratio. The molecular weight, polymerization degree, alkyl-to-allyl ratio and end-group functionalization are listed in Table 2.

Table 2: Synthesized poly(phosphonate)s with molecular weight, alkyl-to-allyl ratio and end-group functionalization.

Polymer	M_n [g/mol] (NMR)	Polymerization degree	Alkyl-to-allyl ratio	End-group
Phos1 (**IX**)	16300	117	10:3	-OH
Phos2 (**X**)	35000	245	3:2	$-C(O)NHC_2H_5$

Synthesis of GMA functionalized dextran

Two glycidyl methacrylate (GMA)-functionalized dextran (DexGMA) polymers as backbones for hydrogel formation were synthesized according to a literature procedure.[43] The higher molecular weight GMA-functionalized dextran was synthesized after the rheological characterization of the low molecular weight dextran-peptide hybrid. Since the low molecular weight hybrid did not show the desired gel-strength (Figure 74A), a high molecular weight dextran was chosen, in order to increase entanglement of the polymer chains and thus increase the stability of the system. Further, dextran-based polymer backbones were chosen, because of fluid-like behavior of the poly(phosphonate) systems, which will be analyzed in the Chapter "Material Characterization".

To calculate the equivalents of GMA and DMAP for the reaction, the used dextran's were analyzed via H_2O-GPC to determine their number average molecular weight M_{n}. For that, the respective dextran was dissolved in MilliQ water and measured against a dextran standard by the polymer analytic department of the MPIP Mainz. The resulting GPC curves can be seen in Figure 46 and the molecular weights (M_{n}, M_{w}) and polydispersity's Đ are listed in Table 3. While the distribution of the low molecular weight dextran (Dex1) is monomodal, the high molecular weight dextran (Dex2) distribution has a shoulder in the higher molecular area. Additionally, the high molecular weight area of the Dex2 is outside of the calibration of the GPC device and therefore the value of the calculated molecular weight might be incorrect. Since the high molecular weight content is out of the bounds of the calibration curve, the determined molecular mass of the polymer should be too low. However, the data was used for the calculation of the equivalents for the condensation, since it can be used as an approximation. The number of glucose units N_{Gluc} can be calculated via the following formula,

$$N_{\mathrm{Gluc}} = \frac{M_{\mathrm{Dex}}}{M_{\mathrm{Gluc}}} \tag{24}$$

where M_{Dex} is the number average molecular weight of the dextran and $M_{\mathrm{Gluc}} = 162.14\ \mathrm{g/mol}$ the molecular mass of a glucose unit. Thus, the number of glucose units N_{Gluc} of the low molecular weight dextran equals approximately 116 monomer units and of Dex2 equals approximately 150 monomer units.

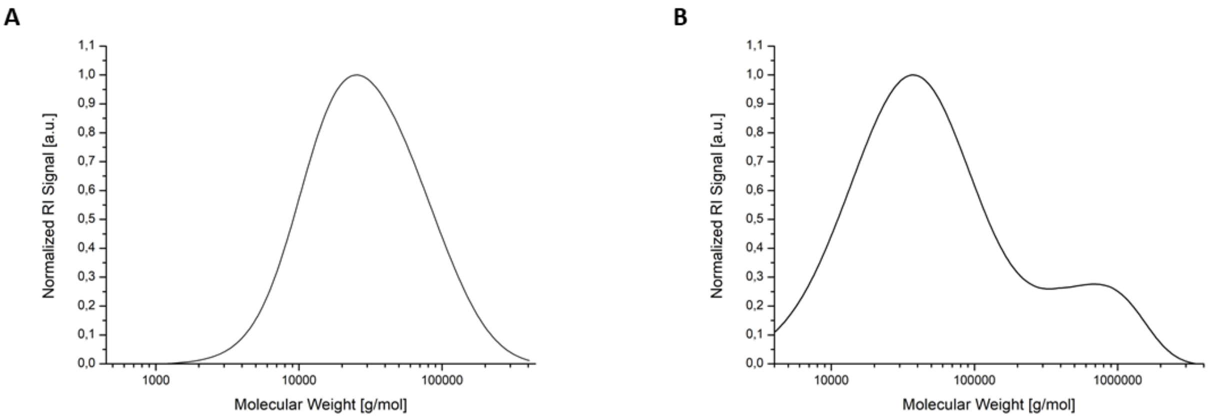

Figure 46: Normalized GPC curves of dextran with the low molecular weight (**A**) and high molecular weight (**B**).

The DexGMAs were synthesized via condensation of dextran and GMA (Figure 47). For that, Dex1 (**XI**) or Dex2 (**XII**) were dissolved in DMSO under nitrogen atmosphere and combined with DMAP and GMA. After heating for 12 h at 50 °C, the reaction mixture was neutralized with equimolar amount of hydrochloric acid (HCl), dialyzed against water and lyophilized. The resulting dry products (**XIII/XIV**) were analyzed via GPC and ^{1}H-NMR.

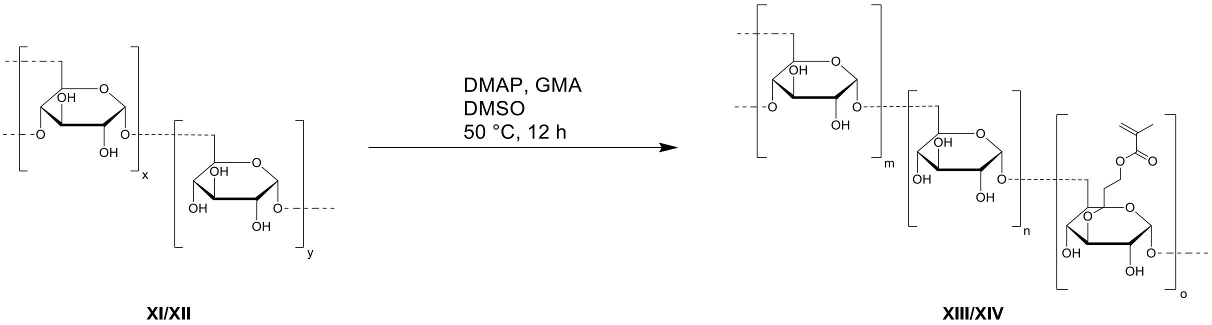

Figure 47: Synthesis scheme of the condensation of Dextran and GMA in DMSO with DMAP as catalyst at 50 °C for 12 h.

Figure 48 shows the ^{1}H-NMR-spectrum of DexGMA1 (**XIII**). All signals could be assigned to their relating hydrogen atoms. In the context of calculation of the functionalization degree with GMA, the peaks of the hydrogen atoms at the anomeric center (**c/d**) are relevant. The number of functionalized glucose units N_{GMA} can be calculated with the following formula,

$$N_{\mathrm{GMA}} = \frac{I_{\mathrm{GMA}}}{I_{\mathrm{GMA}} + I_{\mathrm{Gluc}}} \cdot N_{\mathrm{Gluc}} \qquad (25)$$

where I_{GMA} is the integral of the signal of the hydrogen atom at the anomeric center of GMA-functionalized glucose (**c**) and I_{Gluc} the integral of the signal of the hydrogen atom at the anomeric center of glucose (**d**). Since the solvent peak at 4.8 ppm has some tailing, the integral of peak (**d**) is overdetermined.

Figure 48 shows the ^{1}H-NMR-spectrum of DexGMA1 (**XIII**). The integrals of the peak at 5.02 ppm and 5.22 ppm were integrated and the values used with the equation (25) to calculate the number of functionalized glucose units N_{GMA}.

$$N_{\mathrm{GMA}} = \frac{I_{\mathrm{GMA}}}{I_{\mathrm{GMA}} + I_{\mathrm{Gluc}}} \cdot N_{\mathrm{Gluc}} = \frac{0.95}{0.95 + 2.07} \cdot 116 = 37$$

The results of the analysis are listed in Table 3.

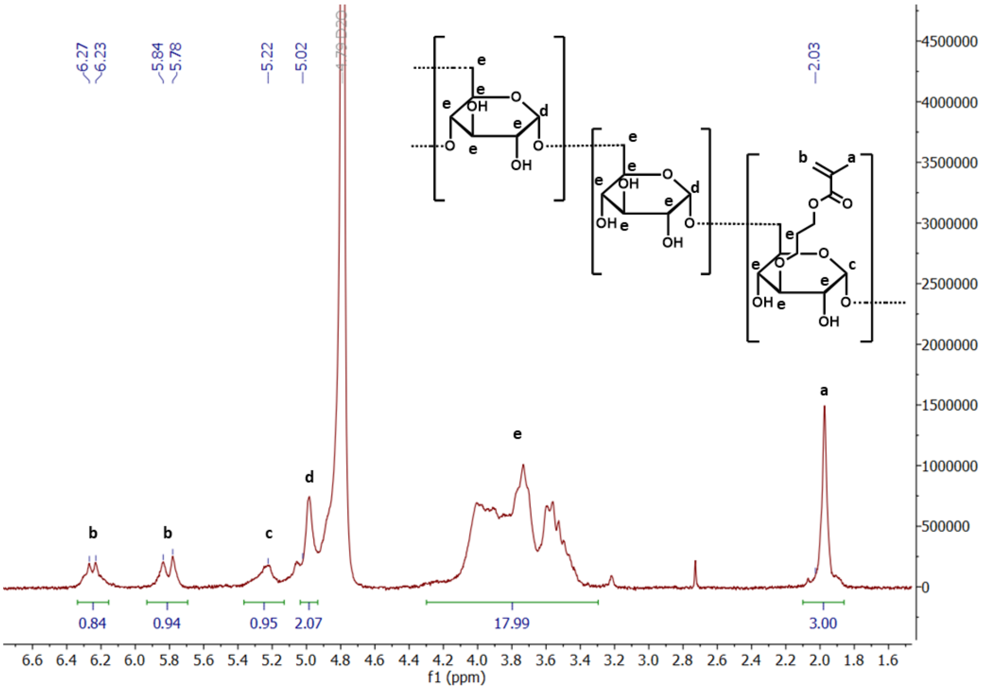

Figure 48: ^{1}H-NMR-spectrum of DexGMA1 (**XIII**) in D_2O (700 MHz) with the molecular structure and the assigned hydrogen atoms.

The functionalization degree of DexGMA2 was calculated similar to DexGMA1 yielding the results listed in Table 3. Although, the calculated number of glucose units could be incorrect, the value of the functionalization degree would hold true.

The purchased dextrans and the synthesized DexGMAs with their corresponding molecular weight, their degree of polymerization (DP) and functionalization degree are listed in Table 3. The molecular weight was either determined via GPC or NMR and the degree of polymerization via NMR.

Table 3: Dextran and the synthesized dextran backbones with molecular weight determined via GPC and/or NMR, polydispersity, degree of GMA-functionalization and DP. *A dextran standard was used.

Polymer	M_n [g/mol] (GPC)*	M_w [g/mol] (GPC)*	Đ	M_n [g/mol] (NMR)	GMA-functionalization	DP
Dex1 (**XI**)	18785	43851	2.33	-	0%	116
Dex2 (**XII**)	24283	175282	9.06	-	0%	150
DexGMA1 (**XIII**)	16530	37260	2.25	23400	31.9%	116
DexGMA2 (**XIV**)	-	-	-	28150	20.7%	150

Determination of the molecular weight by GPC was only suitable for the unfunctionalized dextran. Due to the change in chemical properties, the retention times of the DexGMA changed and result in an underestimation of the molecular weight. Therefore, the number average molecular weight calculated via NMR was used for further calculations. The aimed functionalization of 50% with GMA was not reached, however, the synthesized DexGMA could be used for polymer-peptide hybrid preparation.

3.3 Synthesis of polymer-peptide hybrids

The following Chapter describes the thiol-ene click reaction of the depsi-peptide D3 with the polymer backbones to form hybrids. At first, the functionalization of the poly(phosphonate)s is described and afterwards the functionalization of DexGMA.

Optimization of the functionalization of poly(phosphonate)

The following optimization of the functionalization of the poly(phosphonate) was carried out in cooperation with Timo Rheinberger (MPIP Mainz).

The synthesis of the polymer-peptide hybrid composed of a poly(phosphonate) and the depsi-peptide D3 (**I**) was carried out according to the established method by Timo Rheinberger and Luisa Wiechmann in her master thesis “Novel Responsive Peptide Crosslinker for Hydrogel Synthesis”. For that, Phos1 (**IX**), D3^{C}, tris(2-carboxyethyl)phosphine (TCEP) and

2,2-dimethoxy-2-phenylacetophenone (DMPAP) were combined and dissolved in DMF (0.2% H_2SO_4). The solution was degassed via freeze-pump-thaw cycles and irradiated with a wavelength of 366 nm for 2 h to couple polymer and depsi-peptide via photoinitiated thiol-ene click reaction (Figure 49).

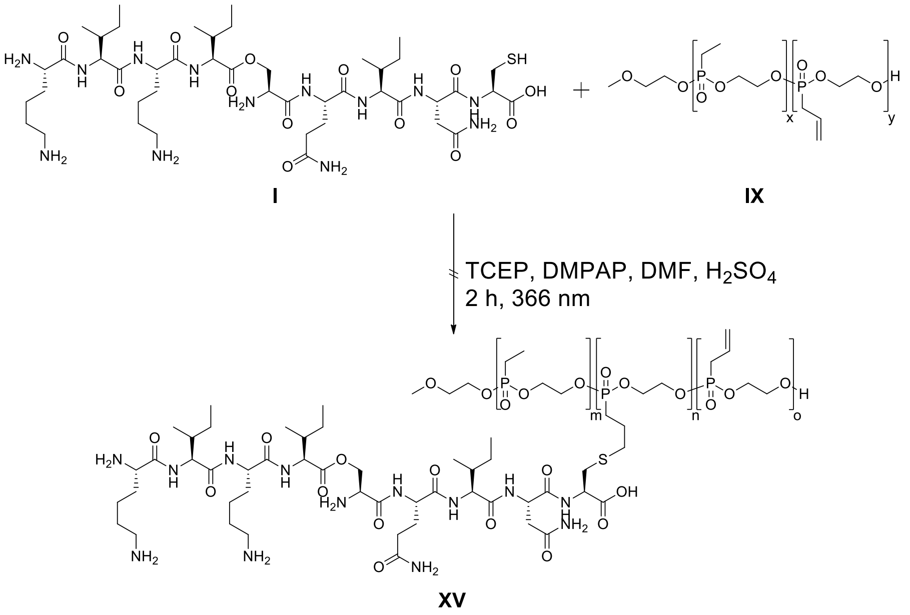

Figure 49: Synthesis scheme for the thiol-ene click reaction of D3 (**I**) and Phos1 (**IX**). The polymer, peptide and DMPAP were solved in 0.2% sulfuric acid DMF solution and irradiated for 2 h with the wavelength of 366 nm.

In contrast to previous works, the mixture turned cloudy within a few minutes after combining the educts and ultimately no reaction took place. In order to elicit the origin of the turbid species that appeared after a few minutes in the reaction mixture, all components were dissolved individually in 0.2% sulfuric acid DMF solution. As only the depsi-peptide solution showed turbidity, TEM of this solution ($D3^C$, 1 mg/mL, 0.2% H_2SO_4 DMF) was performed for better understanding. The results of TEM imaging are summarized in Figure 50 and indicate aggregate formation of $D3^C$ under these conditions. A possible explanation for this could be the sulfate ions, which are able to salt out the peptides, potentially yielding aggregates as depicted in Figure 50.[76] However, further experiments are necessary in order to prove this theory.

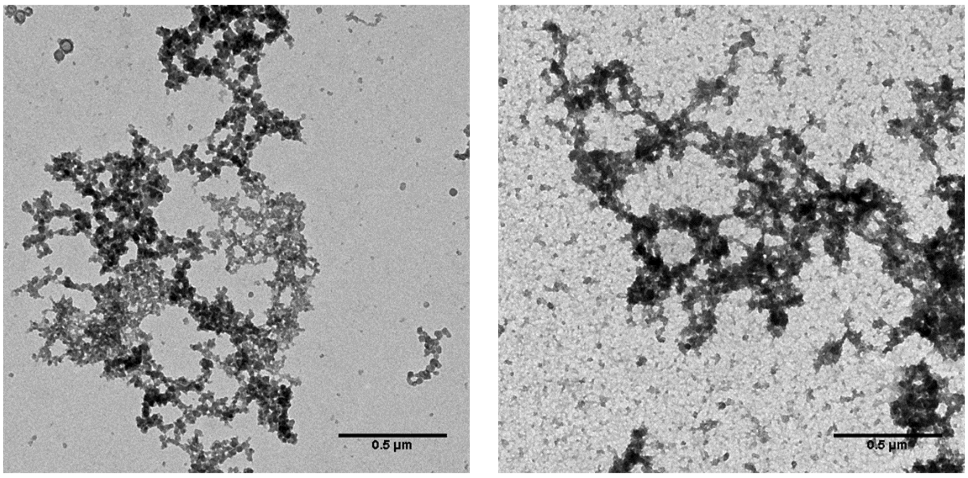

Figure 50: TEM images of D3^C incubated in 0.2% H_2SO_4 DMF (1 mg/mL, 16 h). Scalebars represent 50 µm.

To avoid the aggregation and optimize the reaction, by changing the solvent from DMF to water, the issue of turbidity could be resolved, however, a new photo-initiator, 1,2-bis(2-(4,5-dihydro-1*H*-imidazol-2-yl)propan-2-yl)diazene dihydrochloride (VA-044) (Figure 51), needed to be used, as the previously used DMPAP is not sufficiently soluble in aqueous solutions.

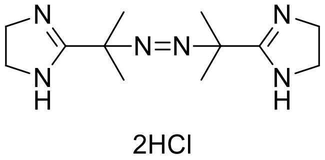

VA-044

Figure 51: Molecular structure of the thermo-initiator VA-044 ($t_{1/2}(44\ °\text{C}) = 10\ \text{h}$).

To test the new method, D3^W with minor impurities of side product (**VI**) (<5%) was used. For this purpose, D3^W (**I**), Phos1 (**IX**), TCEP and VA-044 were dissolved in 0.1% aqueous TFA and combined. To yield a highly functionalized poly(phosphonate), an excess of the peptide was used regarding the number of allyl groups. After combining the substances, the solution was heated to 37 °C for 19 h (Figure 52). The polymer-depsi hybrid PDH1 (**XV**) was purified via ultrafiltration (MWCO=10 kDa), subsequently lyophilized and characterized via ^{1}H- and ^{31}P-NMR.

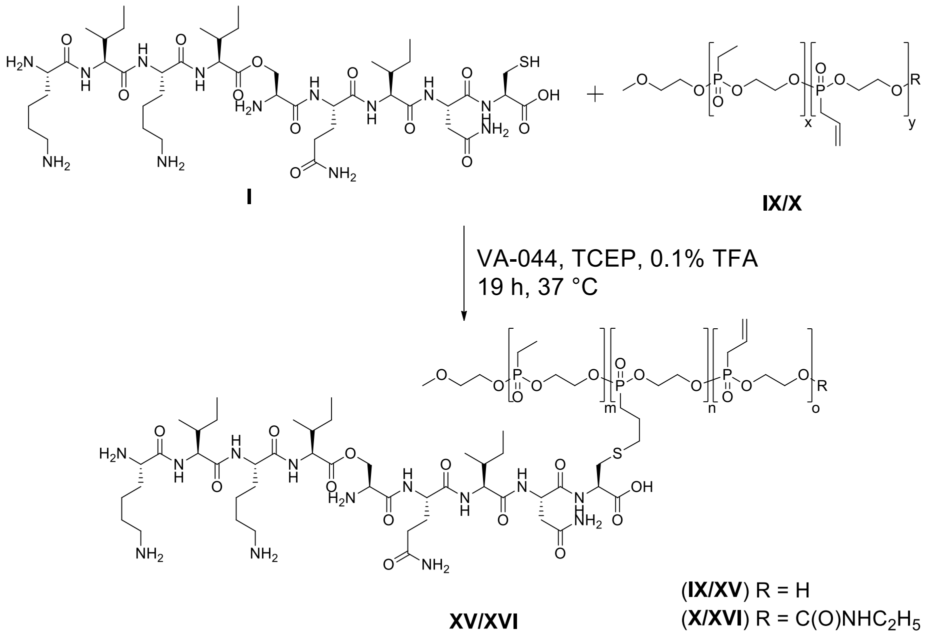

Figure 52: Synthesis scheme for (**XV/XVI**) via thiol-ene click reaction of D3 (**I**) and Phos1 (**IX**) or Phos2 (**X**). The polymer, peptide, TCEP and VA-044 were solved in 0.1% aqueous TFA and heated to 37 °C for 19 h.

Before purification, a ^{31}P-NMR was measured (Figure 53). This revealed besides the new signal at 35.30 ppm for the functionalized allyl group with the depsi-peptide, two other peaks at 56.59 ppm and 52.84 ppm. Those two signals could indicate the degradation of the polymer.

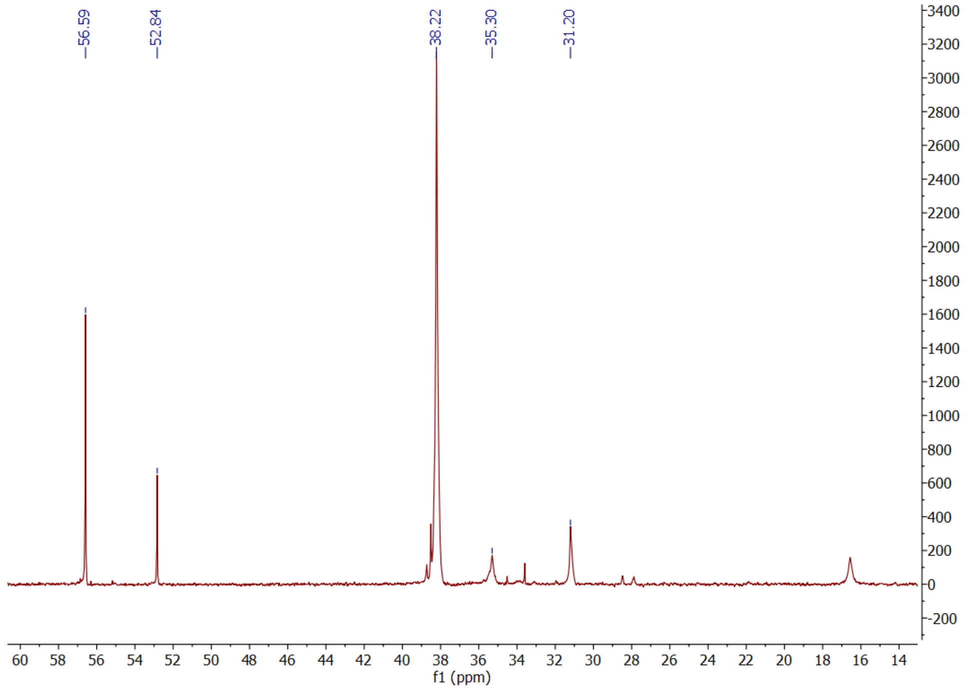

Figure 53: ^{31}P-NMR-spectrum of PDH1 (**XV**) in D_2O (700 MHz) before purification.

After purification NMR-spectra of PDH1 were measured. Signals of the allyl hydrogen atoms can be seen in the ^{1}H-NMR-spectrum (Figure 54) at 5.42 ppm, which indicates that around 50% functionalization of the allyl groups was reached. To calculate the ratio of functionalized to unfunctionalized allyl groups, the integrals of the allyl peak (5.42 ppm) I_{Allyl} and the S-CH$_2$ peak (2.41 ppm) I_{Cys} were used. The number of functionalized allyl groups N_{func} can be calculated with the following formula:

$$N_{\mathrm{func}} = \frac{I_{\mathrm{Cys}}}{I_{Cys} + I_{\mathrm{Allyl}}} \cdot N_{\mathrm{Allyl}} \tag{26}$$

where the number of allyl groups before functionalization is N_{Allyl}. The calculated values are listed in Table 4.

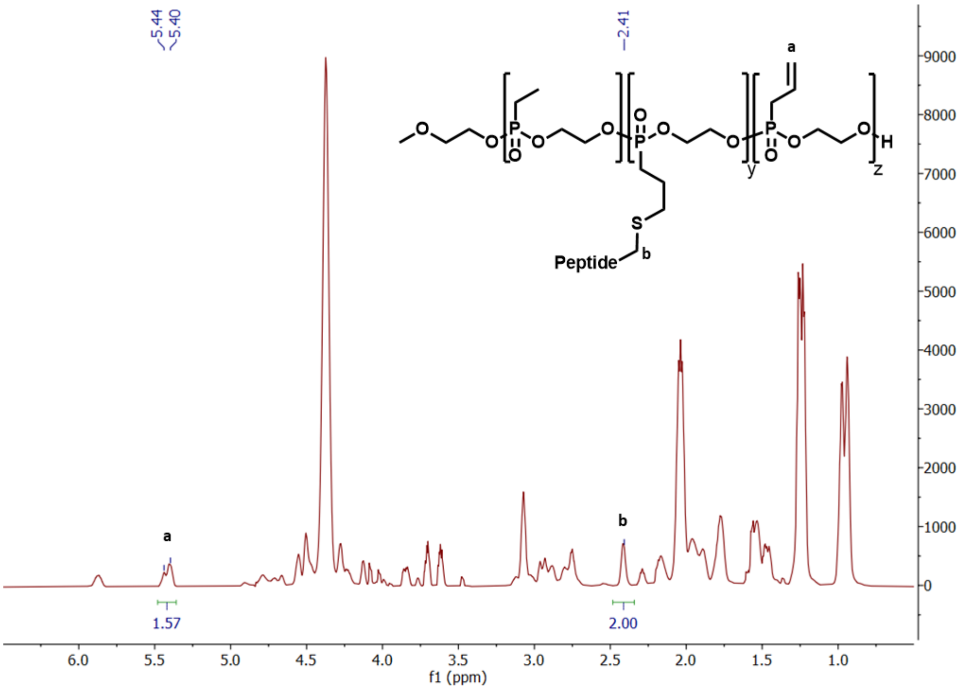

Figure 54: ^{1}H-NMR-spectrum of PDH1 (**XV**) in D$_2$O (700 MHz) with the molecular structure and the relevant assigned hydrogen atoms. The ^{1}H-NMR was measured with suppression of the water signal.

A new signal can be seen in the ^{31}P-NMR-spectrum (Figure 55) at 35.45 ppm in comparison with the poly(phosphonate) backbone (similar to Figure 45). This signal could be assigned to the new phosphorus species generated by the successful functionalization of the allyl group with D3. In theory, the number of functionalized allyl groups N_{func} can also be calculated via the ^{31}P-NMR signals. However, the baseline noise was too high in this specific case. Therefore, the ^{1}H-NMR signals were used for the calculation.

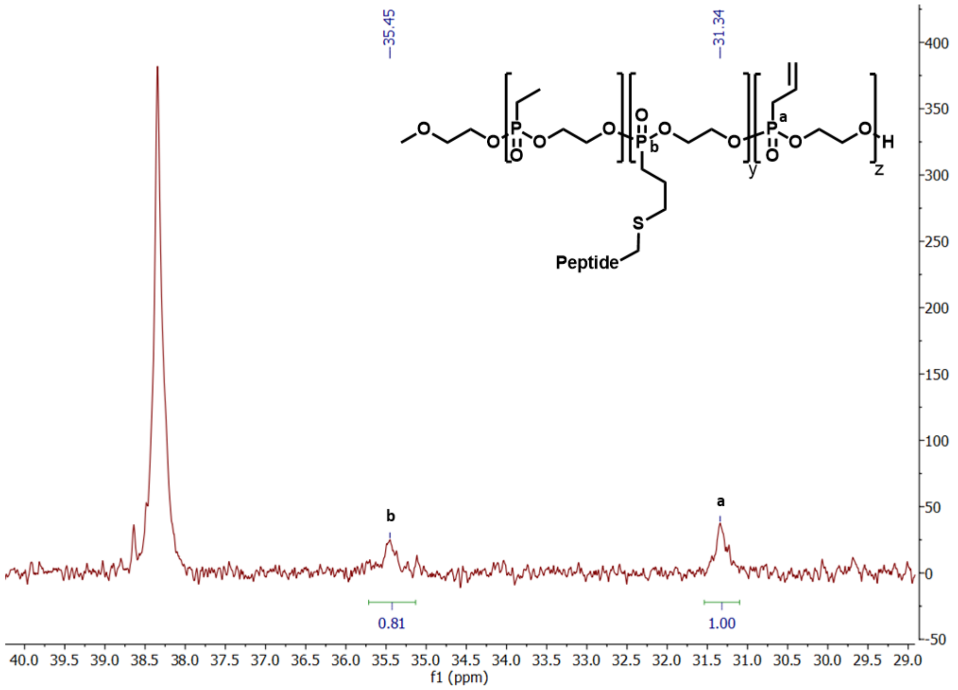

Figure 55: ^{31}P-NMR-spectrum of PDH1 (**XV**) in D_2O (700 MHz) with the molecular structure and the relevant assigned phosphorus atoms.

To determine, whether the analyzed material consists of one or two species with different diffusion coefficients, diffusion ordered spectroscopy (DOSY) was measured. Figure 56 illustrates the DOSY-spectrum of PDH1: The chemical shift is plotted against log(diffusion constant). If multiple species would be present, there would be several peaks on the y-axis. Therefore, the synthesized hybrid contains only one species with the same diffusion constant, indicating a successful coupling of peptide to the backbone.

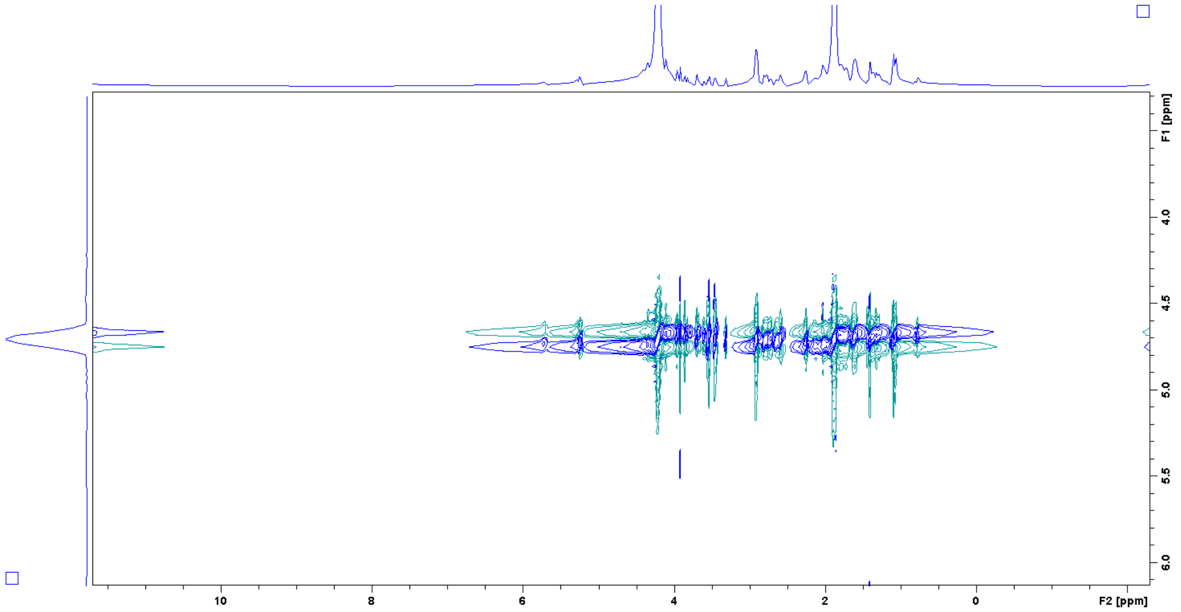

Figure 56: DOSY-spectrum of the hybrid PDH1 (**XV**) in D_2O (700 MHz).

Functionalization of end-capped poly(phosphonate)

Next, the end-capped polyphosphonate was also coupled with depsi peptide (D3^C) using the previously established reaction conditions in aqueous media. For that, D3^C (**I**), Phos2 (**X**), TCEP and VA-044 were dissolved in 0.1% aqueous TFA and combined To yield a highly functionalized poly(phosphonate), an excess of the peptide was used regarding the number of allyl groups. The remaining steps were carried out like the synthesis of PDH1 (Figure 52).

The functionalization degree, number average molecular weight of M_n and unfunctionalized allyl-to-peptide ratio was calculated via ^{1}H-NMR-spectroscopy like these values for PDH1 (Figure 94). The calculated values are listed in Table 4. The number of functionalized allyl groups N_func could also be calculated via the ^{31}P-NMR signals and are in good agreement with the results from the ^{1}H-NMR analysis (Figure 96).

Both poly(phosphonate)-peptide hybrids were successfully synthesized. However, their targeted functionalization degree was not reached. The number average molecular weight M_n, DP, functionalization degree regarding all monomer units and the unfunctionalized allyl-to-peptide ratio is listed in Table 4.

Table 4: Synthesized poly(phosphonate)-peptide hybrids with their number average molecular weight M_n, DP, functionalization degree regarding all monomer units and unfunctionalized allyl-to-peptide ratio.

Polymer	M_n [g/mol] (NMR)	DP	Functionalization degree	Allyl-to-peptide ratio
PDH1 (**XV**)	32000	117	12.8%	5:4
PDH2 (**XVI**)	83140	245	18.8%	10:9

Functionalization of GMA-functionalized dextran

In order to compare the synthesized poly(phosphonate)-peptide hybrids to hybrids with backbones of similar properties, dextran-based polymer-peptide hybrids were synthesized. The method to functionalize poly(phosphante)s via thiol-ene click reaction in 0.1% aqueous TFA with the thermo-initiator VA-044 was also used for the thiol-ene click reaction between the GMA-functionalized dextran and D3^C. In order to determine the influence of the functionalization degree and the polymer backbone on the stability of the potential hydrogel, three different dextran-peptide hybrids were synthesized: Two hybrids with high and low functionalization degree based on the polymer DexGMA1 and one hybrid based on the polymer DexGMA2 with a high functionalization degree.

For that, D3^{C} (**I**), DexGMA1/2 (**XIII/XIV**), TCEP and VA-044 were dissolved in 0.1% aqueous TFA and combined. To yield a high functionalization of the allyl groups, 1.5 eq. of the peptide were used regarding the number of allyl groups. Since the functionalization degree of the poly(phosphonate)s was quite low, a high excess of peptide was used in order to reach the desired functionalization. To yield a low functionalization of the allyl groups, 0.75 eq. of the peptide were used regarding the number of allyl groups. Like the high functionalized dextran, an excess of peptide was used. After combining the substances, the solution was heated to 37 °C for 19 h (Figure 57). The dextran-depsi hybrid DDH was purified via ultrafiltration (MWCO=10 kDa), subsequently lyophilized and characterized via ^{1}H-NMR.

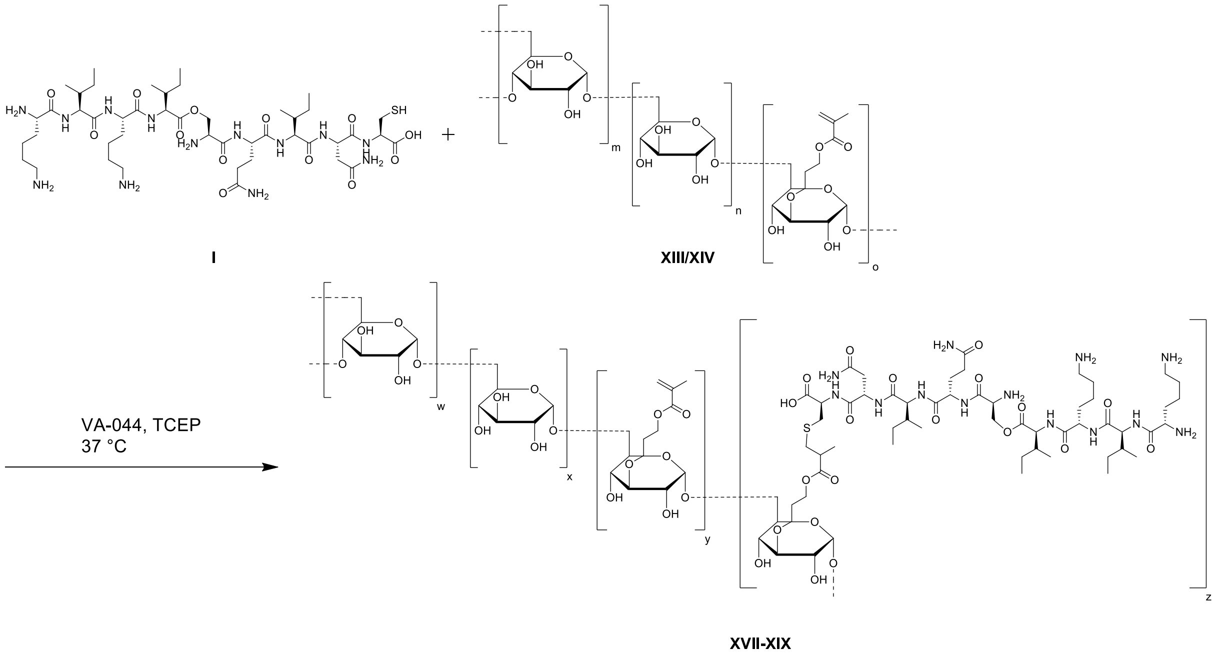

Figure 57: Synthesis scheme for the thiol-ene click reaction of D3 (**I**) and DexGMA1/2 (**XIII/XIV**). The polymer, peptide, TCEP and VA-044 were solved in 0.1% aqueous TFA and heated to 37 °C.

Figure 58 shows the ^{1}H-NMR-spectra of D3^{C} (**I**), DexGMA1 (**XIII**) and the product completely functionalized DexGMA1 with D3^{C} (DDH1) (**XVII**). The signals of the allyl group at 5.80 ppm and 6.25 ppm could not be seen in the spectrum of DDH1 and thus the dextran was functionalized quantitatively regarding the allyl groups. The resulting molecular weight and functionalization degree of the dextran-peptide hybrid is listed in Table 5.

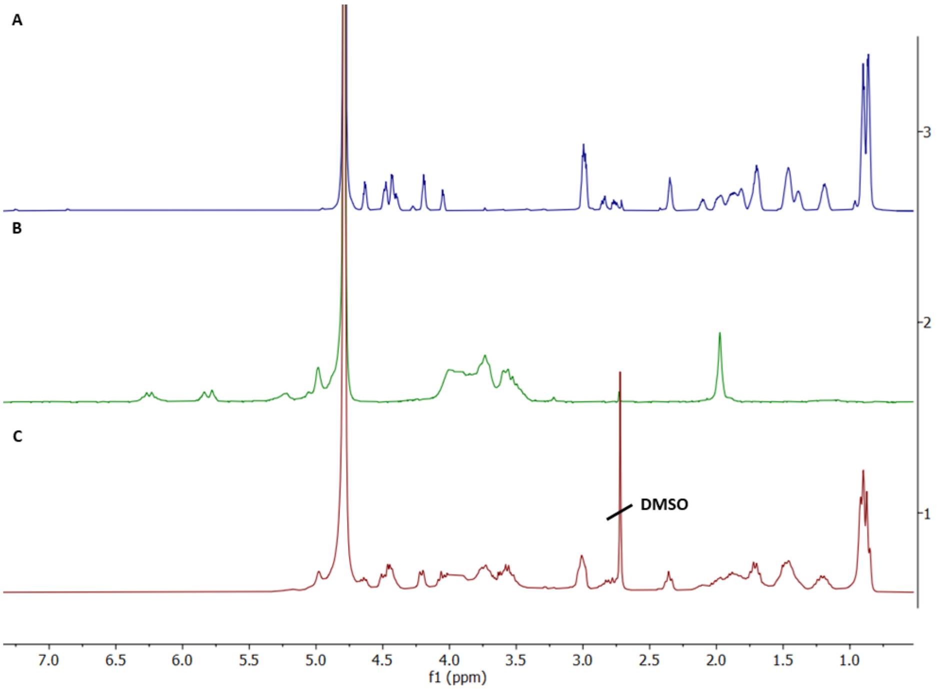

Figure 58: Comparison of ^{1}H-NMR-spectra of (**A**) D3^C, (**B**) DexGMA1 and (**C**) quantitatively functionalized DexGMA1 DDH1 (**XVII**) with D3^C in D_2O (700 MHz).

Figure 59 depicts the ^{1}H-NMR-spectrum of low functionalized DexGMA1 (DDH2) (**XVIII**). The number of functionalized allyl groups N_{func} can be calculated like the calculations of equation (25). Since the signals of the cysteine hydrogen atoms are under the signals of the dextran backbone, the signal of the CH_2-groups of isoleucine were used. Because of the ester bond two of the six signals are shifted, therefore, the integral of the isoleucine hydrogen atoms I_{Ile} at 1.20 ppm was set to four. Equation can be rewritten into the following formula:

$$N_{\mathrm{func}} = \frac{I_{\mathrm{Ile}}}{I_{\mathrm{Ile}} + I_{\mathrm{Allyl}}} \cdot N_{\mathrm{Allyl}} \qquad (27)$$

The calculated values are listed in Table 5. Since only 0.75 eq. were used, to synthesize the hybrid, the number of functionalized allyl groups was overestimated. The source of this error could be the baseline in the ^{1}H-NMR spectrum, which was not continuously at the y-value of zero. Therefore, the integral of the isoleucine hydrogen atoms was bigger than the actual value. It was assumed, that the actual value of the number of functionalized allyl groups is equal to the used D3 in this reaction.

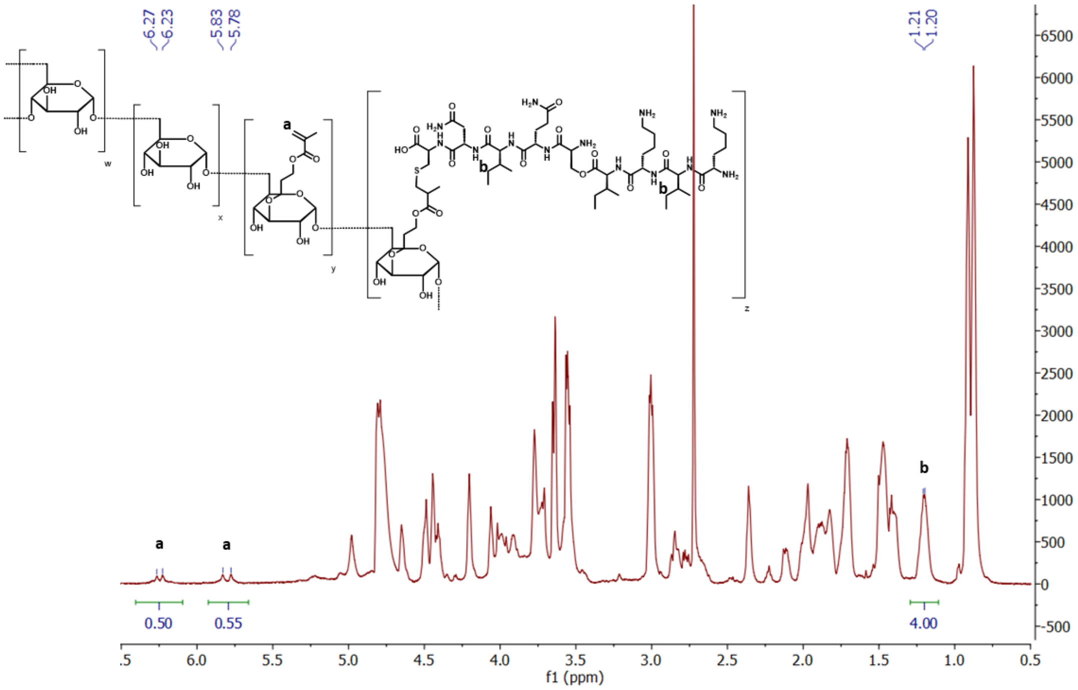

Figure 59: ^{1}H-NMR-spectrum of 75% functionalized DexGMA1 DDH2 (**XVIII**) with D3^C in D_2O with the suppression of water (700 MHz).

Since the signals of the alkene groups were missing in the ^{1}H-NMR spectrum of the high functionalized DexGMA2 (DDH3) (**XIX**), a complete functionalization regarding the alkene groups was determined. The calculated values of the molecular weight and functionalization degree are listed in Table 5.

All three dextran-peptide hybrids were successfully synthesized. However, the targeted low functionalization degree for the hybrid DDH2 exceeded because the used equivalents of depsi-peptide for the synthesis were too high. Since the targeted functionalization degree of the poly(phosphonate)s was not reached, a higher amount of reagents were used to functionalize the dextran. The functionalization of the dextran is quantitative and therefore an excess of educts is not necessary. The synthesized dextran-peptide hybrids with their number average molecular weight, functionalization degree regarding the glucose units and DP is listed in Table 5.

Table 5: Synthesized dextran-peptide hybrids with their number average molecular weight M_n, functionalization degree regarding allyl groups and DP.

Polymer	M_n $[\mathrm{g/mol}]$	Functionalization degree	DP
DDH1 (**XVII**)	62100	31.9%	116
DDH2 (**XVIII**)	53700	25%	116
DDH3 (**XIX**)	66300	20.7%	150

Concluding the section on the hybrid synthesis, while successful for both backbones, strong differences between the backbones in terms of depsi-peptide functionalization were observed. The synthesis of the poly(phosphonate)-peptide hybrids needs to be optimized in order to increase the peptide coupling efficiency. The reason for this low functionalization degree in comparison to the dextran backbones is unknown and needs further investigation. Also, the dextran-peptide hybrids were successfully synthesized. The functionalization with the depsi-peptide $D3^C$ was quantitative, which allows controllable functionalization degrees of the resulting hybrids via the equivalents of peptide used for this reaction. However, to increase the number of alkene functions on the polymer backbone and, thus, the number of possible cross-links, the GMA-functionalization needs to be optimized, since only 20-30% of the aimed 50% functionalization was achieved.

3.4 Material Characterization

After successful synthesis and molecular characterization, the properties of the depsi-peptide, the polymer backbones and the polymer-peptide hybrids were investigated, and the results are described in the following chapter.

3.4.1 Depsi-peptides

Since the synthesized peptide D3 should be used as potential cross-linker for hydrogel synthesis, the fibrillation of the peptide was investigated. For that, the product D3 and P3-Ctrl were incubated in either aqueous TFA (pH=2, 0.1 vol%, 16 h) or phosphate buffered saline (PBS) (pH=7.4, 1 mg/mL, 16 h) and prepared for TEM measurements. The results of the imaging process are depicted in Figure 60 (D3^{W}), Figure 61 (D3^{C}) and Figure 62 (P3^{C}-Ctrl). Similar to previous work, fibrillation of the peptide D3^{W} only occurred in PBS and the developed fibrils could be seen on the TEM grid (Figure 60A), while the TEM grid of the D3 under acidic conditions remained nearly empty (Figure 60C). However, a few aggregates could be seen, which could originate from the unknown side product (**VI**). The average length of fibril(fragment)s formed by D3^{W} due to shift to physiological pH was $329.2 \pm 67\ \mathrm{nm}$ and the average thickness was $16.3 \pm 6.4\ \mathrm{nm}$. Similar results were obtained by Luisa Wiechmann in her master thesis: Length $212.64 \pm 108.86\ \mathrm{nm}$ and thickness $15.26 \pm 3.54\ \mathrm{nm}$.[73]

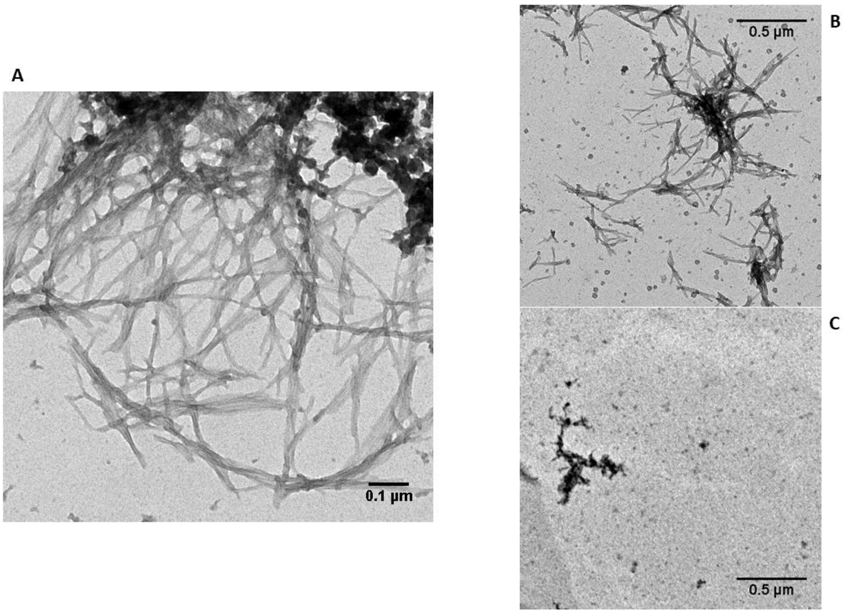

Figure 60: TEM images of D3^{W} and P3^{W}-Ctrl. (**A**) D3 incubated in PBS (after *O*,*N*-acyl shift). Scalebar 0.1 µm (**B**) P3^{W}-Ctrl incubated in PBS. Scalebar 0.5 µm. (**C**) D3^{W} incubated in 0.1% aqueous TFA. Scalebar 0.5 µm.

Figure 61 summarizes the results of TEM imaging of D3^{C} under acidic conditions and under physiological pH. The TEM grid of D3^{C} incubated in 0.1% aqueous TFA remained nearly empty indicating a missing aggregation of the peptide chains. After incubation in PBS, the peptides aggregated into fibrils, which can be seen in Figure 61B and C. The average length of a fibril(fragment) was $507 \pm 167\ \mathrm{nm}$ with a thickness of $24.9 \pm 11.4\ \mathrm{nm}$. These fibrils were significantly longer and thicker than the fibrils formed by D3^{W}. The less developed fibrils of D3^{W} could be caused by the impurities and a possible racemization induced by piperidine during the Fmoc-deprotection step. However, there were not any experiments providing evidence for the racemization.

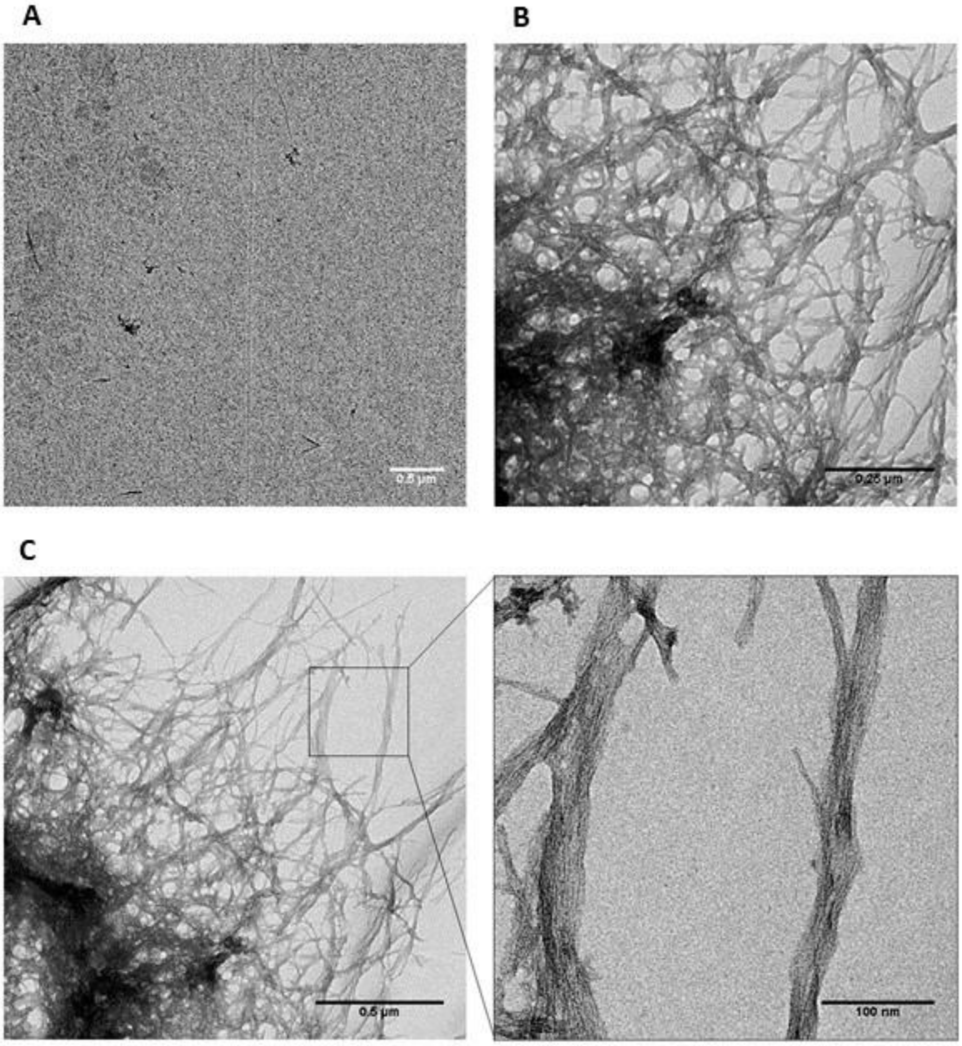

Figure 61: TEM images of D3^{C}. (**A**) D3 incubated in 0.1% aqueous TFA. Scalebar 0.5 µm. (**B**) D3^{C} incubated in PBS (after *O*,*N*-acyl shift). Scalebar 0.25 µm. (**C**) TEM images of D3^{C} with enlarged region of interest incubated in PBS (after *O*,*N*-acyl shift). Scalebar 0.5 µm/100 nm.

Figure 62 shows the TEM image of fibrils of P3^{C}-Ctrl. The formation of long and thick fibrils was also demonstrated by the peptide P3^{C}-Ctrl. The average length of the fibril(fragment)s was $844 \pm 278\,\mathrm{nm}$ with an average thickness of $33 \pm 10\,\mathrm{nm}$ and a cross-over distance of $233 \pm 27\,\mathrm{nm}$.

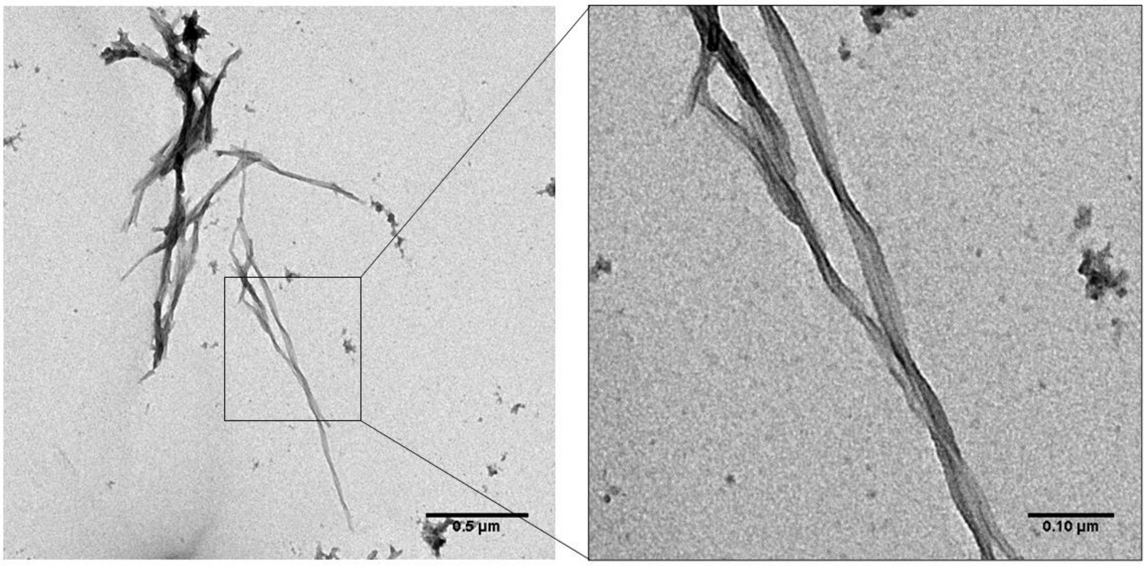

Figure 62: TEM images of P3^{C}-Ctrl with enlarged region of interest incubated in PBS. Scalebar 0.5 µm/ 0.1 µm.

The presence of β-sheets under physiological conditions (PBS) could be proven via a ThT-assay. For this experiment, the peptide D3 and P3-Ctrl were incubated in PBS (pH=7.4, 1 mg/mL, 16 h) and the fluorescent dye ThT added to the solution. After a short incubation time, the fluorescence intensity of ThT was measured at an emission wavelength of $\lambda_{\mathrm{em}} = 488\,\mathrm{nm}$ (Figure 63) by exciting the fluorescent dye with an excitation wavelength of $\lambda_{\mathrm{ex}} = 440\,\mathrm{nm}$. In this measurement, the fluorescence of the linear peptide was used as positive control and a solution of ThT in PBS as negative control. The results of the ThT-assay are shown in the bar chart in Figure 63. The measured fluorescence of ThT in the D3^{W} sample indicates the formation of β-sheets, however, only in low concentration, since the intensity was much smaller in comparison to the positive control P3^{W}-Ctrl. The impurities in D3^{W} could interfere with the fibril formation and thus reducing the signal intensity. Also, aggregates formed by the impurities could suppress the signal of ThT or the aggregation of the peptide was not complete. However, in agreement with the TEM images, the depsi-peptide forms fibrils under physiological pH.

D3^C showed higher fluorescence intensity than the positive control P3^C-Ctrl and also than D3^W. In contrast to D3^W, where minor impurities might have impaired fibril formation, here, the fibrillation of D3^C might not have been disturbed and the fluorescence of ThT not suppressed. This enabled optimal assembly to fibrils and/or interaction between the formed fibrils and ThT, resulting in a higher fluorescence intensity. The positive control P3^C-Ctrl should show similar intensities as the transformed peptide D3^C, yet the TEM images fewer fibrils on the grid than in case of D3^C. Therefore, it was assumed, that the lower intensity was caused by the overall lower concentration of fibrils of P3^C-Ctrl.

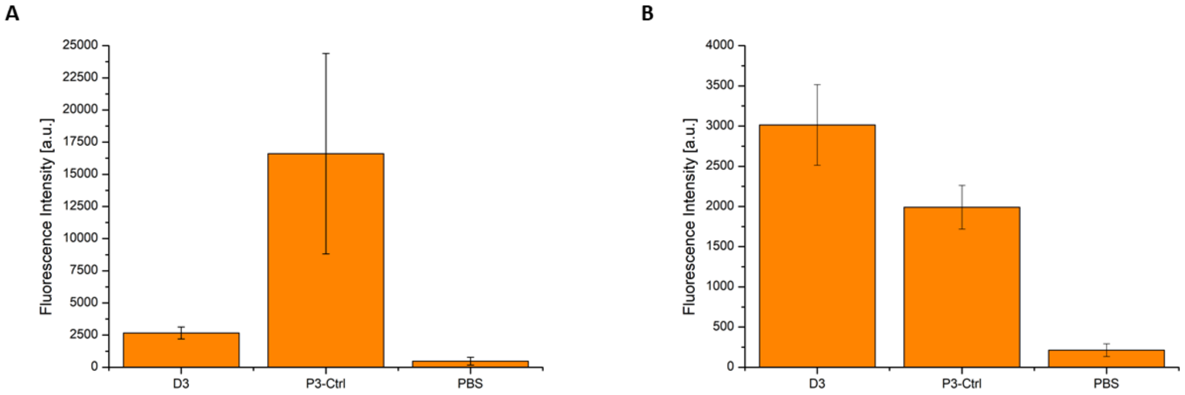

Figure 63: Fluorescence intensity of ThT with (**A**) D3^W and P3^W-Ctrl after incubation in PBS (after *O*,*N*-acyl shift of D3^W) and (**B**) D3^C and P3^C-Ctrl after incubation in PBS (after *O*,*N*-acyl shift of D3^C).

In order to analyze the secondary structure further, CD spectra of the incubated peptides D3^W and P3^W-Ctrl were measured. Both peptides were introduced in MilliQ water (1 mg/mL) and diluted to a concentration of 0.1 mg/mL using MilliQ water. After incubation (37 °C, 16 h), CD was measured. The resulting CD-spectra (Figure 64A) and the calculated percentual distribution (Figure 64B and C) of secondary structure elements did not fit the before observed properties of the peptides. While a high β-sheet content could be observed in the ThT-assay and fibrils could be seen in the TEM images, the calculated secondary structure elements in the CD-spectra were mainly unordered structures/random coils (47.9%). Since the pH was not adjusted to neutral by introducing sodium hydroxide solution, differences in the ionic strength of the solution or changes to the pH due to the missing buffering capacity of the solution could be a reason for the large discrepancy. Also, the incubation time of 1 h could be too short for complete fibril formation.

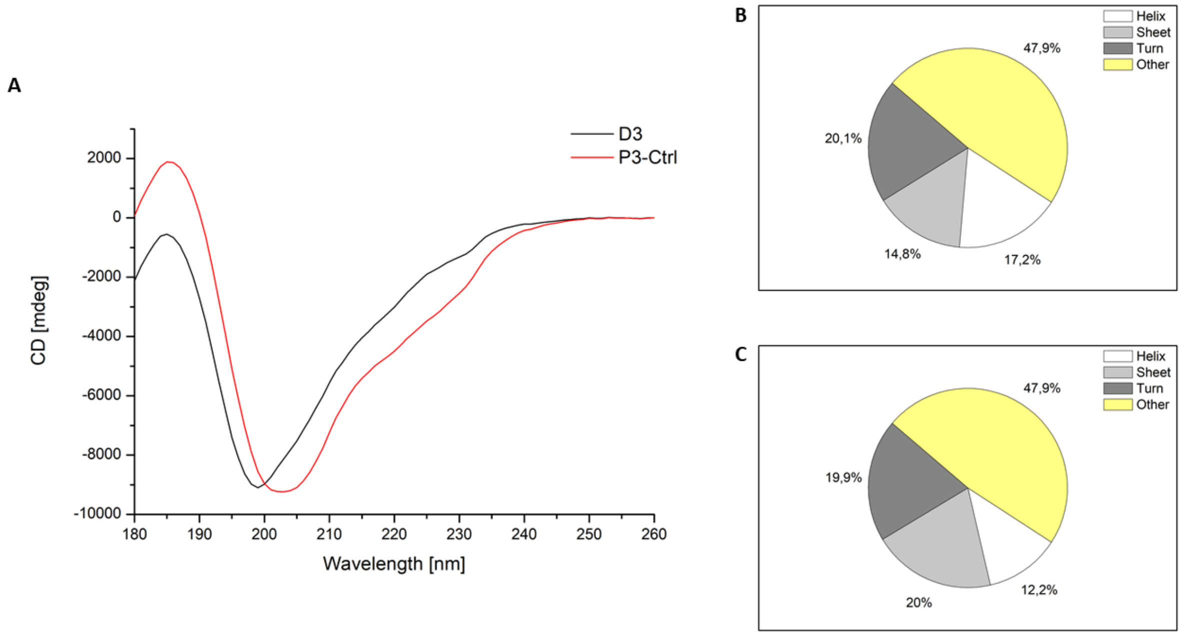

Figure 64: (**A**) CD-spectrum of D3^{W} and P3^{W}-Ctrl at neutral pH in H_2O. (**B**) Percentual distribution of secondary structure elements of D3^{W} calculated from the CD-spectrum. (**C**) Percentual distribution of secondary structure elements of P3^{W}-Ctrl calculated from the CD-spectrum.

In order to determine the ratio of peptides that participate in aggregate formation versus being present as molecularly dissolved species, a conversion-assay[8] was performed. For that, D3^{W} and P3^{W}-Ctrl were incubated in aqueous TFA (pH=2, 0.1 vol%, 16 h) and PBS (pH=7.4, 1 mg/mL, 16 h) respectively. One half of the respective solution was filtered in order to remove fibrillary structures and aggregates. After lyophilization of both solutions, the obtained peptide powder were dissolved in DMSO and incubated with fluorescamine, which reacts with primary amines like the N-terminus and the amine groups of the lysins. Due to the reaction with primary amines fluorescamine was able to exhibit fluorescence. The fluorescence intensity of fluorescamine was measured at an emission wavelength of $\lambda_{\text{em}} = 470\text{ nm}$ ($\lambda_{\text{ex}} = 365\text{ nm}$). The conversion rates were determined via calculations with equation (1)

$$CR = 100 - \frac{100 * I_{\text{Filtrate}}}{I_{\text{Original}}}\ [\%]$$ (1)[8]

and the error of the conversion rate ΔCR was calculated via Gaussian propagation of uncertainty with the following formula,

$$\Delta CR = \sqrt{\left(\frac{100}{I_{\text{O}}} \cdot \Delta I_{\text{F}}\right)^2 + \left(\frac{50 \cdot I_{\text{F}}}{{I_{\text{O}}}^2} \cdot \Delta I_{\text{O}}\right)^2} \tag{28}$$

where I_O is the intensity of the original solution with the error ΔI_O and I_F the intensity of the filtered solution with the error ΔI_F. The conversion rate of D3$^\mathrm{W}$ and P3$^\mathrm{W}$-Ctrl in 0.1% aqueous TFA or PBS respectively are depicted in Figure 65A. Similar behavior of D3$^\mathrm{W}$ in PBS and P3$^\mathrm{W}$-Ctrl in both media could be seen, while there was approximately no conversion of D3$^\mathrm{W}$ under acidic conditions. Since the error of the conversion rate of D3$^\mathrm{W}$ under acidic conditions was higher than the value itself and the conversion rate took on a negative value, this result was not trustworthy. Yet, a trend could be seen, where the value tends to zero conversion rate, which matches the theory and the previous results.

The conversion rate of D3$^\mathrm{C}$ and P3$^\mathrm{C}$-Ctrl are depicted in Figure 65B. P3$^\mathrm{C}$-Ctrl incubated in both 0.1% aqueous TFA and PBS had similar conversion rates as well as the rate of D3$^\mathrm{C}$ in PBS. However, surprisingly also D3$^\mathrm{C}$ in TFA showed a conversion rate of around 50%. Since there were no fibrils or aggregates on the TEM grid of D3$^\mathrm{C}$ incubated in TFA, there must be another reason, why this peptide shows conversion. The molecular weight cut-off of the spin filter was 3000 Da and therefore small enough to prevent a dipeptide of D3$^\mathrm{C}$ to pass through. The dipeptide of D3$^\mathrm{C}$ could be formed through oxidation of the thiol-group to form a disulfide bridge between two D3$^\mathrm{C}$ sequences. This might have led to a false result for the conversion rate of the peptide D3$^\mathrm{C}$ in acidic media. This phenomenon only occurred in the case of D3$^\mathrm{C}$ because it was measured weeks later after storing it in the freezer, while D3$^\mathrm{W}$ was measured only several days after synthesis.

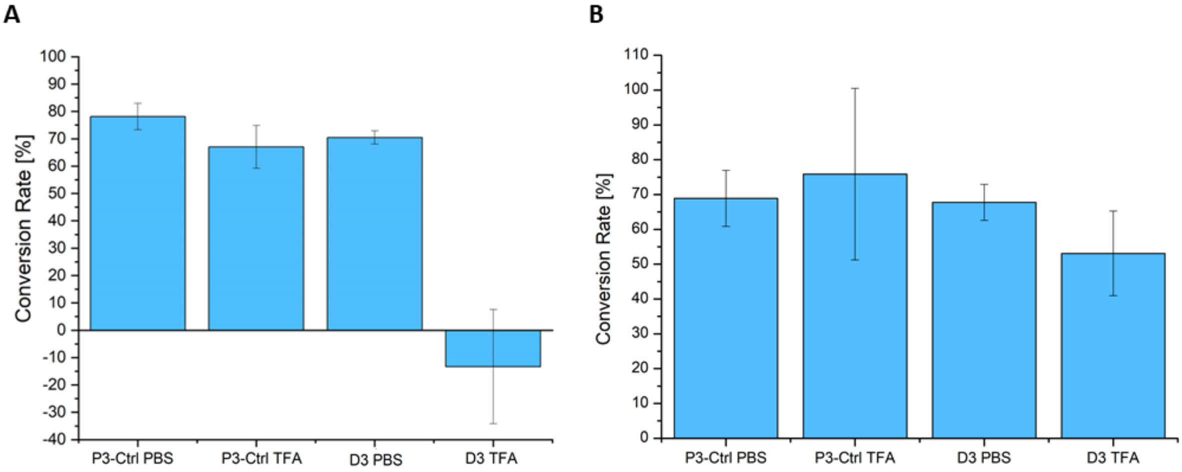

Figure 65: Conversion rate of (**A**) D3$^\mathrm{W}$ and P3$^\mathrm{W}$-Ctrl after incubation in 0.1% aqueous TFA and PBS (after *O*,*N*-acyl shift of D3$^\mathrm{W}$) respectively and (**B**) D3$^\mathrm{C}$ and P3$^\mathrm{C}$-Ctrl after incubation in 0.1% aqueous TFA and PBS (after *O*,*N*-acyl shift of D3$^\mathrm{W}$) respectively.

The calculated conversion rates and their errors are listed in Table 6.

Table 6: Conversion rates and errors of D3^{W} and P3^{W}-Ctrl incubated in 0.1% aqueous TFA and PBS, respectively.

	Conversion Rate [%]	Error [%]
P3^{W}-Ctrl PBS	78.1	4.8
P3^{W}-Ctrl TFA	67.0	7.8
D3^{W} PBS	70.5	2.4
D3^{W} TFA	-13.3	20.9
P3C-Ctrl PBS	68.9	8.0
P3C-Ctrl TFA	75.9	24.6
D3C PBS	67.8	5.2
D3C TFA	53.1	12.1

Via ATR-FTIR-spectroscopy, measured by Jasmina Gačanin, the secondary structure elements of the fibrils from D3^{C} and P3^{C}-Ctrl were examined. The region between 1850-1450 cm^{-1} was recorded and the amide I band region analyzed, which indicates the presence of secondary structure elements like α-helices, β-sheets or unordered structure. In order to observe pH-responsiveness, the peptides D3^{C} and P3^{C}-Ctrl were incubated in aqueous TFA (pH=2, 0.1 vol%, 16 h) and PBS (pH=7.4, 1 mg/mL, 16 h) respectively. D3^{C} incubated under acidic conditions showed a maximum at 1639 cm^{-1}, which could be assigned to unordered structures.[65] This indicates that D3^{C} was present as depsi-peptide at acidic pH, which is in good agreement with the previous characterizations. D3^{c} incubated under physiological pH shows a maximum at 1630 cm^{-1}, which is in the β-sheet region.[65] These results further confirm the pH-induced formation of cross-β-sheet fibrils in PBS. P3^{C}-Ctrl incubated in either 0.1% aqueous TFA or PBS showed both similar behaviors, because there was no pH-responsiveness of the peptide. P3^{C}-Ctrl showed a maximum at 1628 cm^{-1} and at 1674 cm^{-1}.[65] The first peak could be clearly assigned to a β-sheet region, while the second one could be either assigned to β-sheet or β-turn.[65] Since, the peptide is too short to contain β-turns, this maximum was also assigned to β-sheet. These results confirm that P3^{C}-Ctrl is not pH-responsive and forms fibrils under acidic and physiological pH.

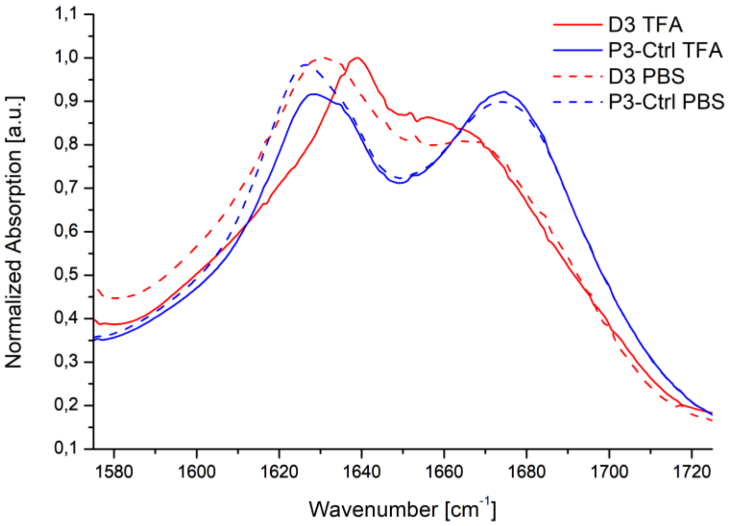

Figure 66: ATR-FTIR-spectra of D3^{C} and P3^{C}-Ctrl incubated in 0.1% aqueous TFA and in PBS (after *O*,*N*-acyl shift of D3^{C}).

Both peptides D3^{W} and D3^{C} were analyzed in respect to their pH-responsiveness and aggregation/fibrillation behavior. D3^{W} formed slightly smaller and thinner fibril(fragment)s and the ThT fluorescence intensity was relatively low in comparison to the positive control P3^{W}-Ctrl. These results could be caused by the minor impurity of the side product (**VI**) in D3^{W}, which led to less developed fibrils and less β-sheet formation in general. However, the pH-responsiveness of both peptides was proven via TEM imaging, conversion assay (D3^{W}) and ATR-FTIR (D3^{C}). The formation of cross-β-sheet fibrils of D3^{C} was proven via TEM imaging, ATR-FTIR and ThT-assay. Since D3^{C} was free from impurities, an undisturbed formation of fibrils was possible leading to well-developed long and thick fibrils in comparison to the less developed fibrils of D3^{W}.

3.4.2 Polymer-peptide hybrids and their polymer backbones

In order to characterize the synthesized polymer-peptide hybrids, TEM images, a ThT-assay and ATR-FTIR spectra were measured for secondary structure element and morphology analysis of the hybrid and their corresponding polymer backbones. Also, rheological characterization of the hybrids, including oscillatory time sweeps and if reasonable amplitude and amplitude/time sweeps were measured to analyze their mechanical properties. The characterized polymers with their number average molecular weight, DP and the functionalization degree regarding the number of monomer units are listed in Table 7.

Table 7: Synthesized polymer-peptide hybrids and their backbones with the corresponding number average molecular mass (M_n), DP and the functionalization degree with D3 regarding the number of monomer units.

Polymer	M_n [g/mol]	DP	Functionalization degree
Phos1	16300	117	-
Phos2	35000	245	-
DexGMA1	23400	116	-
PDH1	32000	117	12.8%
PDH2	83140	245	20.0%
DDH1	62100	116	31.9%

At first, the poly(phosphonate)-peptide hybrids are discussed. Due to their different chemical and physical properties they are separated from the discussion of the dextran-peptide hybrids. The ATR-FTIR and TEM imaging of PDH1 have not been measured yet, as well as the TEM imaging of PDH2.

Figure 67 depicts the results of the ThT-assay of PDH2 and its corresponding polymer backbone. For the ThT-assay preparation, PDH2 and the high molecular weight poly(phosphonate) were incubated in PBS (pH=7.4, 1 mg/mL, 16 h) and ThT added to the solutions and PBS as negative control. Both PDH2 and the polymer backbone solutions showed at an emission wavelength $\lambda_\mathrm{em} = 488\ \mathrm{nm}$ ($\lambda_\mathrm{ex} = 440\ \mathrm{nm}$) similar fluorescence of ThT as the negative control PBS. For the polymer backbone, those results were expected, because it is missing β-sheet-like structure due to missing peptides. However, PDH2 should show fluorescence at the emission wavelength due to the possible β-sheet formation, caused by the peptides between polymer backbones. The missing fluorescence of ThT could be explained by the missing interactions between peptide chains in the material.

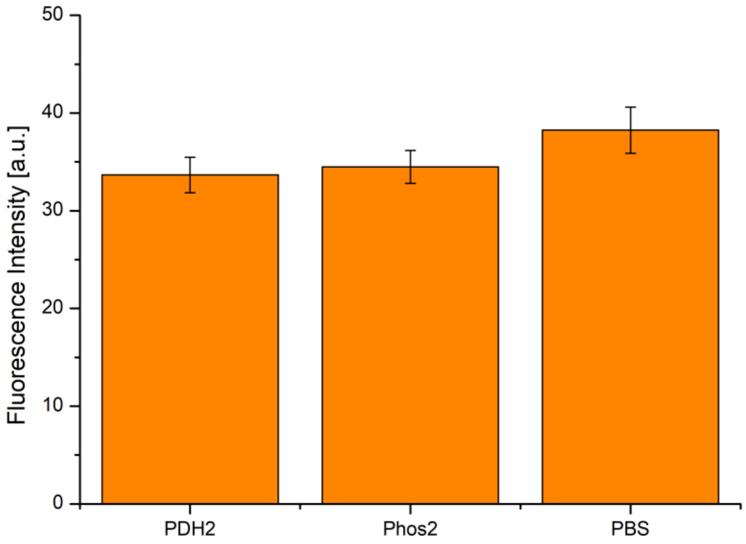

Figure 67: Fluorescence intensity of ThT with PDH2 and Phos2 after incubation in PBS (after *O*,*N*-acyl shift of the depsi-peptide) and PBS.

Via ATR-FTIR-spectroscopy, the secondary structure elements of the hybrid and the high molecular weight poly(phosphonate) were examined. After preparation of the samples, the vials of the 0.1% aqueous TFA incubated species did not contain enough substance to measure ATR-FTIR spectra with good signal-to-noise ratio. Therefore, only the spectra of the PBS incubated species are shown. The region between 1850-1450 cm^{-1} was recorded and the amide I and II band region analyzed. Signals in the amide II region were analyzed in order to prove reliably the presence of coupled peptide on the polymer backbone and could only be seen in the spectrum of PDH2 caused by the peptides covalently attached to the polymer backbone. The maximum of 1635 cm^{-1} in the amide I region of the PH2 spectrum could be assigned to β-sheets.[65] The maximum of 1640 cm^{-1} of the polymer backbone could be assigned to the valence vibration of the C=C-bond.[77] The maximum of both materials at 1680 cm^{-1} could be assigned to the valence vibration of the C=C-bond.[77]

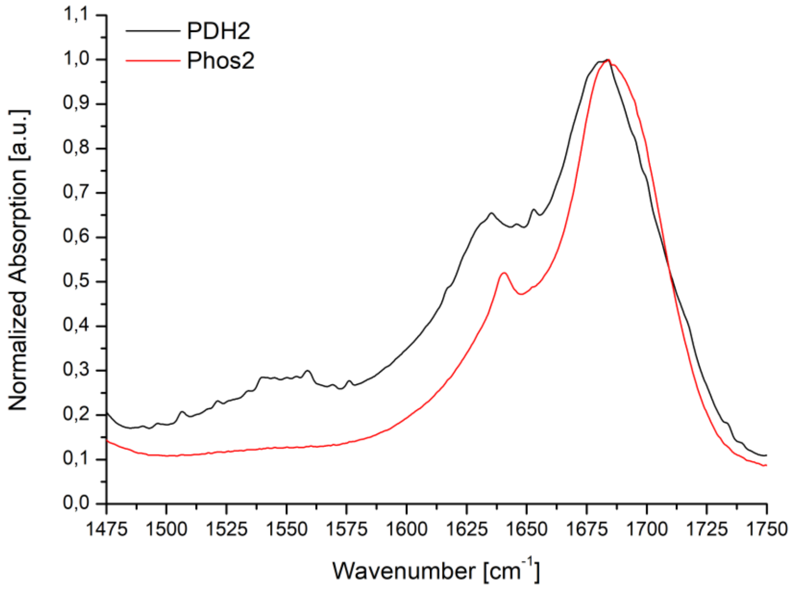

Figure 68: ATR-FTIR of PDH2 and Phos2 incubated in PBS (after *O*,*N*-acyl shift of the depsi-peptide). The spectrum of PDH2 was smoothed to make the comparison clearer.

In order to determine the mechanical properties of PDH1 and PDH2, an oscillatory time sweep with fixed oscillatory strain (0.1%) and fixed frequency (1 Hz) was measured for each potential hydrogel composed of the respective depsi-polymer hybrid (4 wt%, 30 µL 100mM PB, pH=7.4). PDH1 showed values of G' between 17.5-28 Pa and G'' between -4.5-4.5 Pa (Figure 69A). The negative values of G'' originated from the inability of the rheometer to measure the data correctly. Because of the low values of G', G'', and the complex viscosity ($J_{\mathrm{PDH1}} \approx 4\ \mathrm{Pa \cdot s}$), the material was classified as fluid-like. PDH2 showed a linear stable region with G' values of 23.5-25 Pa and G'' values of 0.75-2.25 Pa (Figure 69B). Nevertheless, PH2 was classified as fluid-like because of the low values of G', G'', and $J_{\mathrm{PDH2}} \approx\ 4\ \mathrm{Pa \cdot s}$.

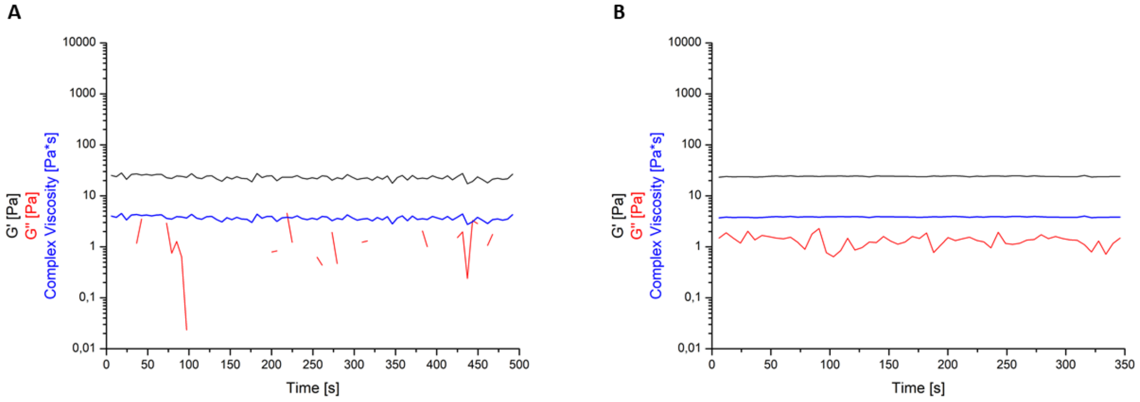

Figure 69: Oscillatory time sweep of (**A**) PDH1 and (**B**) PDH2.

Similar results were obtained from the oscillatory time sweeps of the corresponding polymer backbones. In order to compare the polymer backbones Phos1 and Phos2 with their corresponding polymer-peptide hybrid, an oscillatory time sweep with fixed strain (0.1%) and fixed frequency (1 Hz) of the polymer backbones (4 wt%, 30 µL 100mM PB, pH=7.4) was measured. The polymer backbones showed values for G' between 4-6 Pa for the low molecular weight polymer Phos1 and between 18.5-21.5 Pa for the high molecular weight polymer Phos2. The higher value of G' of the high molecular polymer in comparison to the low molecular polymer can be explained by the higher number of entanglements of the longer polymer chains. G'' was similar in both cases and around 1-2 Pa. Theoretically both polymers show viscoelastic properties, because G' was higher than G'', yet the difference in G' and G'' was too marginal and the complex viscosity too low ($J_{\mathrm{A}} \approx 1\ \mathrm{Pa \cdot s}$ and $J_{\mathrm{B}} \approx 3.3\ \mathrm{Pa \cdot s}$) to classify them as gels. Since there are no cross-links between the polymer chains except for their entanglements, these properties were expected.

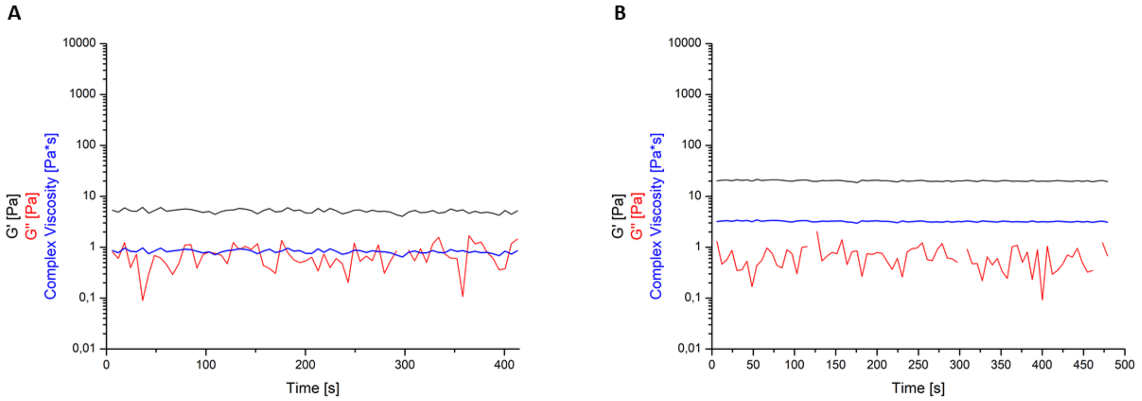

Figure 70: Oscillatory time sweep of (**A**) Phos1 and (**B**) Phos2.

Since both hybrid materials show similar rheological properties to their corresponding polymer backbone material and the ThT-assay suggested missing interactions between peptide chains for PDH2, it was assumed, that the hybrid materials are not cross-linked. TEM imaging could have revealed, whether the hybrid materials aggregate/cross-link or not.

In the following section the characterization of the dextran-based polymer-peptide hybrid is discussed. In order to determine the morphology of the hybrid material TEM images were measured. DDH1 was incubated in aqueous TFA (pH=2, 0.1 vol%, 16 h) and respectively and PBS (pH=7.4, 1 mg/mL, 16 h) prepared for TEM imaging, in order to show pH-responsiveness of the polymer-peptide hybrid (Figure 71). The hybrid showed no aggregation behavior under acidic conditions, while it formed aggregates under physiological conditions. This indicates that the aggregation was caused by the *O*,*N*-acyl shift of the depsi-peptide leading to cross-links of the dextran backbones.

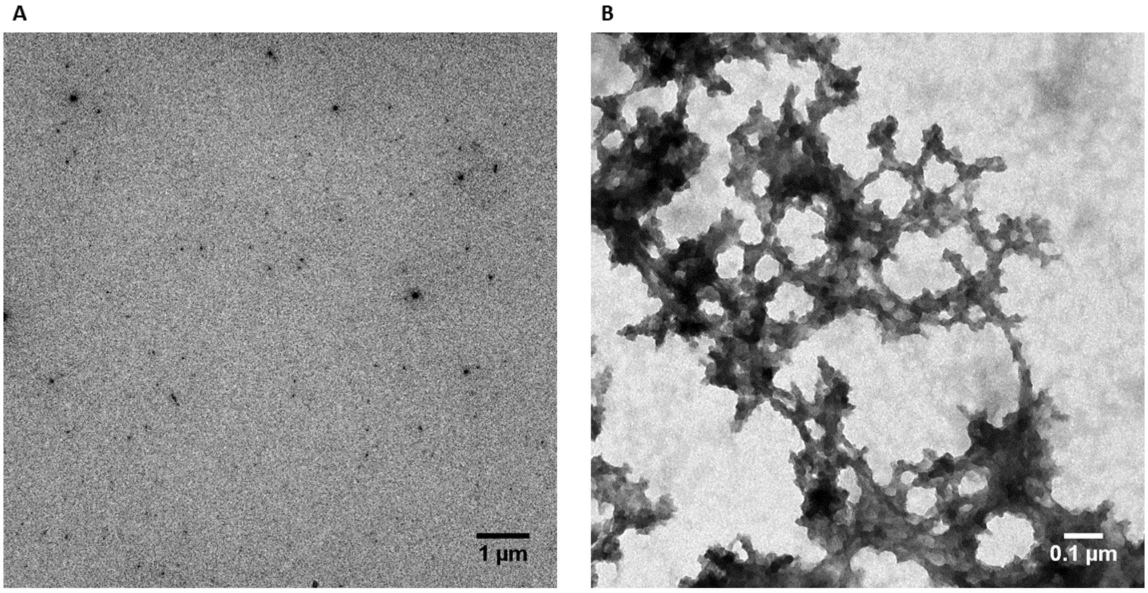

Figure 71: TEM images of DDH1. (**A**) DDH1 incubated in 0.1% aqueous TFA. Scalebar 1 µm (**B**) DDH1 incubated in PBS (after *O*,*N*-acyl shift). Scalebar 0.1 µm.

For comparison, DexGMA1 was incubated in aqueous TFA (pH=2, 0.1 vol%, 16 h) and PBS (pH=7.4, 1 mg/mL, 16 h) respectively and prepared for TEM imaging, in order to show missing pH-responsiveness of the polymer backbone. Figure 72 shows the TEM images of the polymer backbone incubated in either 0.1% aqueous TFA or PBS. DexGMA1 showed missing aggregation behavior in both media and therefore the TEM grids remained nearly empty, which was expected.

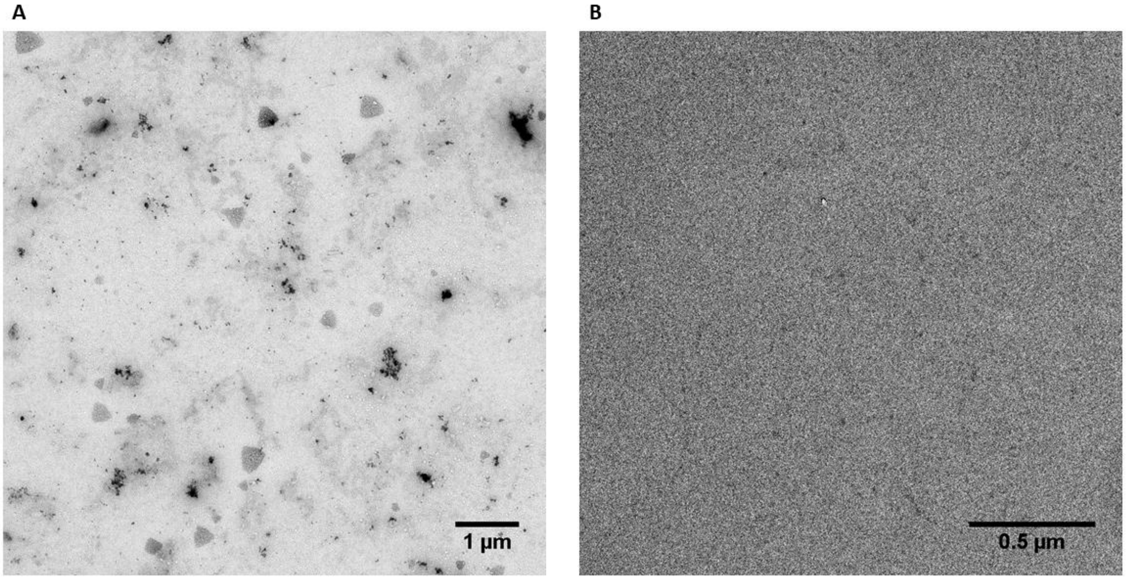

Figure 72: TEM images of DexGMA1. (**A**) DexGMA1 incubated in PBS. Scalebar 1 µm. (**B**) DexGMA1 incubated in 0.1% aqueous TFA. Scalebar 0.5 µm.

Figure 73A shows the results of the ThT-assay of DDH1. To determine, whether the fluorescence of ThT is caused by the backbone or the formed β-sheets, DDH1 and the corresponding polymer backbone DexGMA1 were incubated in PBS (pH=7.4, 1 mg/mL, 16 h). The C-C rotation of ThT can also be suppressed by dextran and its derivatives and therefore ThT showed fluorescence with the polymer backbone and a false positive result.[78] However, the fluorescence intensity of DDH1 was even higher, which was probably caused by embedding ThT into the formed β-sheets.

Via ATR-FTIR-spectroscopy, measured by Jasmina Gačanin, the secondary structure elements of DDH1 and DexGMA1 were examined. The region between 1850-1450 cm^{-1} was recorded and the amide I band region analyzed, which indicates the presence of secondary structure elements. Figure 73B shows the FTIR-spectra of DDH1 incubated in aqueous TFA (pH=2, 0.1 vol%, 16 h) or PBS (pH=7.4, 1 mg/mL, 16 h) and DexGMA1 incubated in PBS (pH=7.4, 1 mg/mL, 16 h). DDH1 incubated in 0.1% aqueous TFA showed a maximum between 1630-1640 cm^{-1}, which indicates unordered structures with a small β-sheet proportion,[65] and a shoulder between 1640-1666 cm^{-1}, which could be assigned to the carbonyl vibrations of the acrylate.[77] DDH1 incubated in PBS had a maximum at 1629 cm^{-1} and 1674 cm^{-1}, which was assigned to a high β-sheet content.[65] These signals were missing in the DDH1 TFA spectrum, because the depsi-peptides could not interact with each other due to the ester bond, which suppresses β-sheet formation. DexGMA1 incubated in PBS had a maximum at 1676 cm^{-1}, which could be assigned to the alkene valence and carbonyl vibrations.[77]

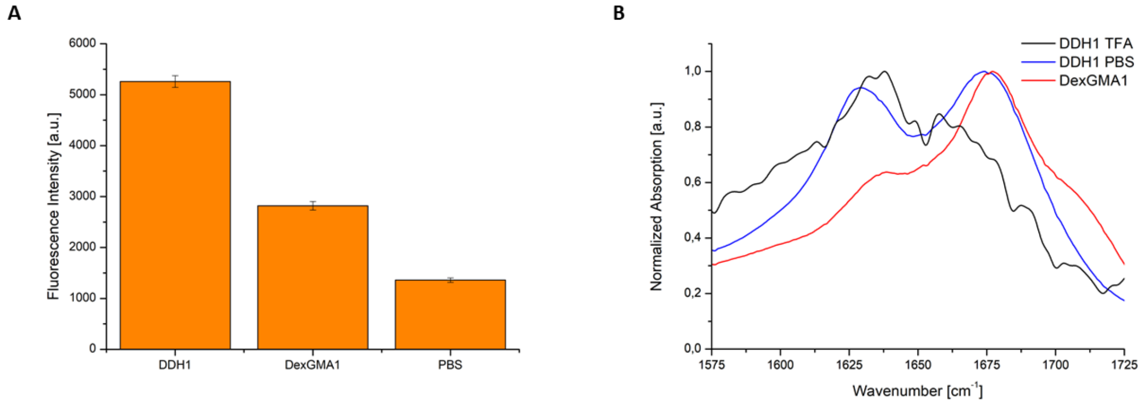

Figure 73: (**A**) Fluorescence intensity of ThT with DDH1 and DexGMA1 after incubation in PBS (after *O*,*N*-acyl shift of the depsi-peptide) and PBS. (**B**) ATR-FTIR of DDH1 and DexGMA1 incubated in PBS (after *O*,*N*-acyl shift of the depsi-peptide) and DDH1 in 0.1% aqueous TFA. The spectrum of DDH1 TFA was smoothed to make the comparison clearer.

In order to determine the mechanical properties of the synthesized polymer-peptide hybrid, an oscillatory time sweep was measured. The gelation of the hybrid (4 wt%, 30 µL 100mM PB, pH=7.4) happened instantaneously. The formed hydrogel H1 had a storage modulus $G' = 1100$ Pa and a loss modulus $G'' = 130$ Pa, both were constant over time (400 s) at a oscillatory strain of 0.1% (Figure 74A). Furthermore, an amplitude sweep with a fixed frequency (1 Hz) and increasing oscillatory strain (0.01-1000%) was measured. G' and G'' remained constant until an oscillatory strain of 0.15%. Higher oscillatory strain led to a steady decrease of G' and a slow increase of G'' until a strain of 0.64%, where G'' also started to decrease. At an oscillatory strain 3.8% G' and G'' crossed and the gel-to-sol transition occurred, which led to characteristics of a fluid of the material (Figure 74B).

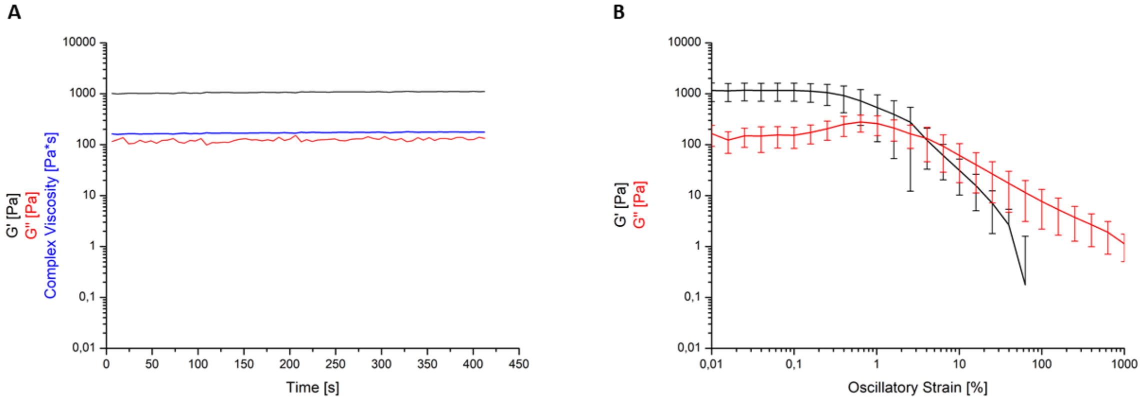

Figure 74: (**A**) Oscillatory time sweep of DDH1. (**B**) Amplitude sweep of DDH1.

For comparison, an oscillatory time sweep measurement with fixed oscillatory strain (0.1%) and fixed frequency (1 Hz) of the polymer backbone DexGMA1 (4 wt%, 30 µL 100mM PB, pH=7.4) was measured (Figure 75). The values of G' were between 3-5 Pa and of G'' between 0.5-2 Pa. Also, in this case like the poly(phosphonate) backbones, the difference in G' and G'' was too marginal and the complex viscosity too low ($J = 0.75\ \mathrm{Pa \cdot s}$). Thus, the polymer backbone was too unstable to classify it as gel, which can be also explained by the missing cross-links between polymer chains.

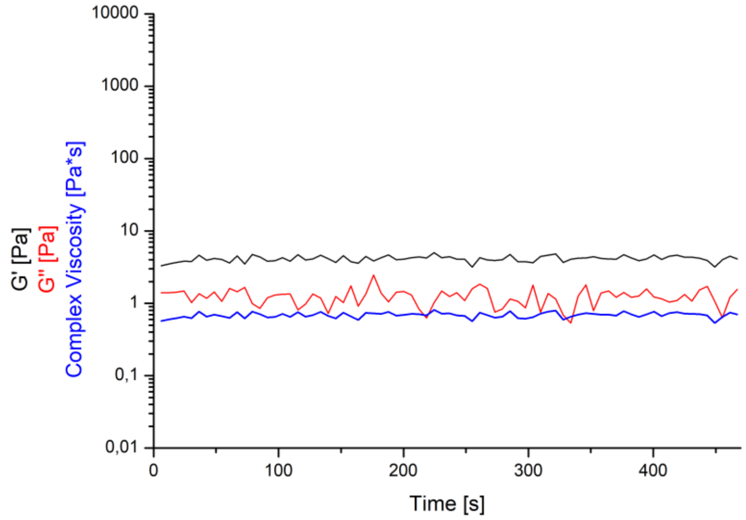

Figure 75: Oscillatory time sweep of DexGMA1.

The self-healing capability of the hydrogel was tested, by application of increasing oscillatory strain (amplitude sweep) followed by a recovery time with low fixed oscillatory strain (time sweep) (Figure 76). After fissure of the gel by high oscillatory strain (up to 1000%), the gel recovered immediately to 58.9% of its original stability and managed to recover further after 866 s to 89.3% of its original storage modulus G'. After a second gel-to-sol transition by high oscillatory strain, the gel recovered immediately to 69.8% of its stability before the second fissure and recovered further to 98.9% of its stability before the second fissure after 866 s. After the third fissure the gel recovered itself immediately to 73% of its stability before the third fissure and recovered further to 101.8% of its stability before the third fissure after 866 s. The original stability of the hydrogel could be caused by high amount of entanglements of the backbones coupled with the cross-linking via the peptides. After the first fissure, most of the entanglements were untied, leading to a general lower stability. However, this stability could be recovered after enough recovery time. Therefore, the hydrogel exhibited near thixotropic to thixotropic properties.

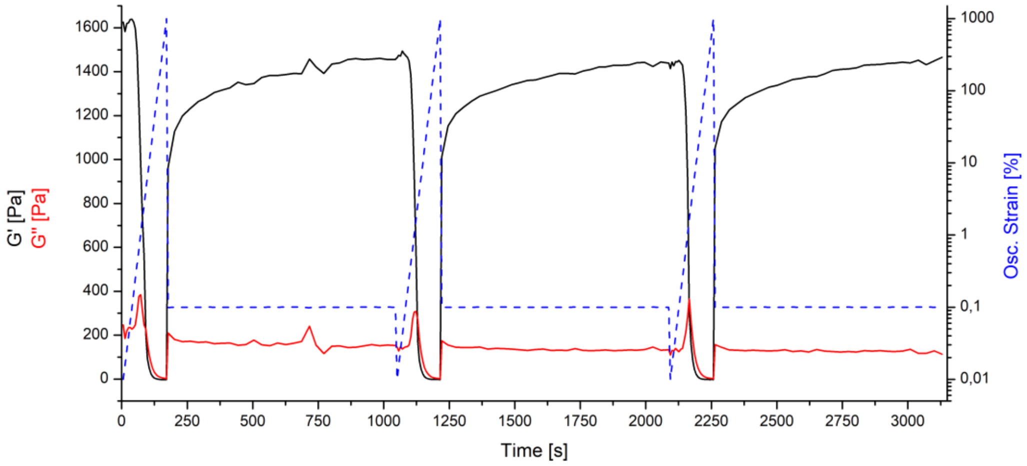

Figure 76: Three amplitude and time sweeps in a row, to show near thixotropic properties of DDH1.

The polymer-peptide hybrid DDH2 and DDH3 were not measured yet.

The synthesized polymer-peptide hybrids PDH1, PDH2 and DDH1 were analyzed regarding their pH-responsiveness and secondary structure elements. Rheological properties of the corresponding materials were determined via oscillatory time sweep and amplitude/time sweep measurements. The results of the characterizations are listed in Table 8. Unfortunately, PDH1 and PDH2 were not able to form a hydrogel in combination with PB (30 µL, 100 mM, pH=7.4) at 4 wt%. However, DDH1 was able to form a very soft hydrogel under these conditions and exhibited near thixotropic properties.

Table 8: Synthesized polymer-peptide hybrids and HSA-hydrogel H1 with their number average molecular mass M_n, DP and functionalization degree regarding their monomer units; ThT activity and gelation of the material (1.2 mg) in PB (30 µL, 100 mM, pH=7.4).

Polymer	M_n [g/mol]	DP	Functionalization degree	ThT activity?	Gelation?
PDH1	32000	117	12.8%	-	No
PDH2	83140	245	20.0%	No	No
DDH1	62100	116	31.9%	Yes	Yes
DDH2	53700	116	25.0%	-	-
DDH3	66300	150	20.7%	-	-
H1[8]	145000	585	3.4%	Yes	Yes

The poly(phosphonate)-peptide hybrid materials seemed to lack of stability due to unknown interference of the peptide-peptide interactions. Even a higher molecular weight had nearly no influence on the stability of this system. Therefore, the poly(phosphonate)s are not suitable as backbones for these specific hydrogels. However, by adapting the peptide sequence to this specific polymer backbones, cross-linking could be possible.

The dextran-based hydrogel DDH1 showed a linear domain of $G' = 1100\,\mathrm{Pa}$ at 0.1% oscillatory strain, which suggests a very soft hydrogel. Also, the hydrogel exhibited thixotropic-like properties, which could be seen in the amplitude/time sweep measurements. After orientating the polymer chains and cross-links due to rupture, the hydrogel lost some stability, which could be caused by reduction of the number of entanglements of the polymer chains. However, after the second and third rupture, the hydrogel managed to recover to nearly the same G' value. This behavior indicates that the hydrogel exhibits thixotropic properties after orientation of the polymer chains and cross-links. To prove this theory, further experiments with this hydrogel are necessary. Comparing the properties of the hybrid DDH1 with the established hydrogel by Jasmina Gačanin, a lot of improvement is required in order to reach similar stability, thixotropic properties and ultrafast self-healing.[8] Higher molecular weight dextran-peptide hybrids like DDH3 could exhibits improved stability due to their higher number of entanglements, since H1 has nearly three times more molecular weight than DDH1. Also, the number of cross-links could improve the stability of the hydrogel, which is dependent on a higher functionalization degree with GMA. The thixotropic properties could only be possible after the first rupture of the hydrogel and the resulting reorientation. However, if this system would find any applications in the biomedical fields, the first rupture could be intentionally induced in order to achieve thixotropic properties. The ultrafast self-healing properties could be achieved by adapting the cross-linking peptides for this individual polymer backbone.

Concluding, the poly(phosphonate) backbones were difficult to functionalize and their corresponding hybrid materials lacked stability. Therefore, these poly(phosphonate)s are not suitable as polymer backbones in combination with the peptide sequence KIKISQINC.

The dextran backbones could be functionalized quantitively with the depsi-peptide D3 and the low molecular weight hybrid material exhibited properties of a soft hydrogel. Improving this system could yield hydrogels with similar properties of the HSA-based hydrogel H1.

4. Summary and Outlook

The pH-responsive depsi-sequence KIKI(O-C(O))SQINC (D3) was successfully synthesized via Merrifield SPPS on a Wang-resin. Purification of D3^{W} via HPLC was difficult due to similar elution times of the product and a side product, leading to an impure depsi-peptide. MALDI-ToF MS and LCMS revealed that the purified product could contain huge quantities of side products in the product fraction of the HPLC purification. However, pH-responsiveness and the formation of β-sheet containing fibrils could be proven via ThT-assay and TEM imaging. The results of the conversion-assay suggested that approximately 70% of the depsi-peptides can aggregate under physiological conditions.

Due to the high amount of side reactions occurring during peptide synthesis and purification, which influenced the yield and purity of the product, the resin for the SPPS was changed to a Clt-resin, which provided sterical protection of the cysteine and thus suppressed most of the side reactions occurring on the Wang-resin. Additionally, the side reaction with the degradation product of the Wang-resin during TFA-cleavage was not possible and reduced the number of possible side reactions further. However, due to the change of the resin, the esterification step was less successful but could be optimized by increasing the amount of educts for the reaction. Overall, the yields might be increased from 5.8% to 8.7% regarding the theoretical yield. Further improvement of the yields could be reached, by optimizing the precipitation protocol as well as the HPLC gradient, to isolate the product peak completely from the side product peaks. The purity of the synthesized depsi-peptide D3^{C} was demonstrated via MALDI-ToF MS and LCMS. Improved fibrillation of D3^{C} due to missing impurities and pH-responsiveness was shown via TEM imaging, ATR-FTIR spectroscopy and ThT-assay.

Four different polymer backbones were successfully synthesized for the polymer-peptide hybrid synthesis, thereof the poly(phosphonate)s by the cooperation partner, and could be characterized by NMR-spectroscopy, ATR-FTIR, TEM imaging and ThT-assay. The first poly(phosphonate) Phos1 had been developed in earlier work as a model polymer backbone, which exhibits biodegradability and -compatibility and could be coupled with the synthesized depsi-peptide D3 via thiol-ene click reaction due to its allyl-functionality. However, the polymer degraded during the click reaction and the rheological measurements revealed that the hybrid material was not able to form a gel. For these reasons, a new polymer Phos2 was prepared, which was not able to degrade during thiol-ene click reaction due to its end-capping with ethyl isocyanate. Also, the longer chain should increase the number of entanglements leading to a more stable material after functionalization. Unfortunately, the functionalized poly(phosphonate) material did not gelate under given circumstances. The ThT-assay showed that the polymer-peptide hybrid had similar ThT fluorescence intensities as the negative control PBS, suggesting that this material is not able to cross-link via efficient β-sheet formation of the peptide grafts. The coupling of β-sheet fibril forming peptides to polar polymers was found to potentially result in the prevention of β -sheet formation under certain circumstances. [79] Optimization regarding the polymer-to-peptide ratio therefore is important and could explain missing efficiency in assembly of D3 coupled to the poly(phosphonate)s. As a result, a further optimization regarding the functionalization degree with D3 in respect to polymer length might be required for this kind of polymer to enable better cross-linking. In order to determine, whether these materials form efficient cross-links or lack them, further experiments are necessary. Since already a relatively high number of grafts has been introduced, another reason for missing aggregation could be the high solubility of the hybrids PDH1/2 in water at the given temperature (25 °C) and pH (7.4). Temperature and pH dependency might have an influence with these polymers and could be analyzed via temperature dependent rheological measurements.[75] Therefore, an increase in the functionalization degree with D3 would not lead to better cross-linking. The suppression of aggregation of β-sheet forming peptides coupled to polar polymers was reported and could indicate missing assembly of D3 coupled to the poly(phosphonate)s.[79] In order to determine, whether these materials form cross-links or lack of them, further experiments are necessary. Another reason for missing aggregation could be the high solubility of the hybrids PDH1/2 in water at the given temperature (25 °C) and pH (7.4). Temperature and pH dependency could be analyzed via temperature dependent rheological measurements.

Besides the two poly(phosphonate)s, two different GMA-functionalized dextran backbones were synthesized. In order to determine the influence of molecular weight/polymer chain length on the hybrid material, a dextran with the high molecular weight and low molecular weight were functionalized. The functionalization degree and the molecular weight of both backbones was determined via GPC and NMR-spectroscopy. Also, the functionalization degree of the polymer backbone was analyzed by functionalizing 100% and 75% of the GMA groups of the low molecular weight dextran. The functionalization of alkene carrying, water-soluble polymer backbones with cysteine containing peptides via thiol-ene click reaction was successful and enabled quantitative functionalization of DexGMA with the depsi-peptide D3. The synthesized polymer-peptide hybrids were characterized by NMR-spectroscopy regarding their molecular weight and functionalization degree and the hybrid DDH1 via ATR-FTIR, TEM imaging and ThT-assay regarding its pH-responsiveness and secondary structure elements. The polymer-peptide hybrid DDH1 was able to gelate upon pH-shift from acidic to physiological pH due to the β-sheet formation of the peptides. Rheological measurements of the hybrid material showed that the gel was stable under an oscillatory strain of 0.1% and exhibited thixotropic-like behavior after rupture with relatively short regeneration times. Since this hybrid material was soft ($G' \approx 1000\,\mathrm{Pa}$ at 0.1% oscillatory strain), the not yet measured high molecular weight dextran-peptide hybrid could reach higher stability due to its higher number of entanglements.

In order to prove the aimed biodegradability and -compatibility of the synthesized polymer-peptide hybrids, suitable durability/degradation and cell tests are necessary. Due to the effective functionalization of the dextran system, defined copolymeric systems could be synthesized, which carry peptides as cross-linker (KIKISQINC) and bioactive peptide sequences to enable the manipulation of living matter.

Concluding, the synthesis of the depsi-peptide sequence KIKI(O-C(O))SQINC could be improved by changing the used resin for the SPPS and increasing the equivalents used for the esterification step. The peptide could be coupled to four different biocompatible and -degradable polymer backbones via an optimized thiol-ene click reaction, generating a potential biocompatible and -degradable polymer-peptide hybrid. One of those hybrids DDH1 was able to gelate under given conditions (4 wt%, PB, pH=7.4) and could be a model for future, more stable hybrid materials. The novel polymer-peptide hybrid is expected to exhibit biocompatibility and -degradability and could be suitable in the medical fields for tissue engineering. A wide variety of different dextran biopolymers varying in length and branching are accessible, therefore these systems can be further adapted and upscaled at a low cost. Due to its efficient functionalization, these dextran hybrids could be easily adapted to their intended fields of application.

5. Materials

Table 9: Materials – Apparatuses and equipment

Apparatuses and equipment	**Appliance brand**
385 well-plate	Flat bottom black polystyrene small volume, Greiner Bio-One
3k MWCO; IVSS VIVASPIN 500 Centrifugal Concentrat	Sigma-Aldrich
ATR-FTIR	Bruker TENSOR II with PLATINUM ATR single reflection diamond ATR accessory
Chromafil® Xtra RC-20/13 syringe filter	Macherey-Nagel GmbH & Co. KG
Circular Dichroism	JASCO J-1500
Freeze Dryer	CHRIST Alpha 2-4 LSCbasic
HPLC	Shimadzu with Kinetex 5 µm EVO C18 100 Phenomenex column
LCMS	Shimadzu with Kinetex 2.6 µm EVO C18 100 Å LC 50x2.1 mm column
MALDI-TOF MS apparatus	Waters MALDI SYNAPT G2-Si HDMS
NMR	Bruker Avance II 300 MHz Bruker Avance III 700 MHz
Rheometer	DHR3 Rheometer TA Instruments
Scales	Sartorius AG
Shaker	Eppendorf
SPPS	CEM Liberty Blue Automated Peptide Synthesizer
Tecan	Spark 20 M microplate reader
TEM	JEOL 1400
TEM Grids	Plano GmbH
Vortexer	Heidolph Reax top

Table 10: Materials – Chemicals

Chemicals	**Brand**
α-cyano-4-hydroxycinnamic acid	Sigma-Aldrich
Acetonitrile	VWR
Boc-Ser-OH	Sigma-Aldrich
Diethyl ether	VWR
N,N-Dimethylpyridin-4-amine	VWR
Dimethylsulfoxid	Sigma-Aldrich
Dulbecco's Phosphate Buffered Saline	Sigma-Aldrich
Fluorescamin	Sigma-Aldrich
Fmoc-L-Cys(Trt)-Wang-resin	Bachem
Fmoc-L-Ile-OH	Merck Novabiochem
Fmoc-L-Asn(Trt)-OH	Merck Novabiochem
Fmoc-L-Gln(Trt)-OH	Merck Novabiochem
Fmoc-L-Lys(Boc)-OH	Merck Novabiochem
Fmoc-L-Ser(^{t}Bu)-OH	Merck Novabiochem
H-Cys(Trt)-2-chlorotrityl-resin	Bachem
N,N'-Diisopropylcarbodiimid	VWR
N,N-Dimethylformamide	VWR
Piperidine	Roth
Oxyma	CEM
Sulfuric acid	Fisher Scientific
TCEP	Acros Organics
Triisopropyl silane	Sigma-Aldrich
Tris(2-carboxyethyl)phosphin	Sigma-Aldrich
Thioflavin T	Sigma-Aldrich
Trifluoroacetic acid	Roth
Uranyl acetate dihydrate	Merck

6. Methods

6.1 Synthesis of depsi-peptides and peptide-polymer hybrids

6.1.1 Merrifield solid-phase peptide synthesis of depsi-peptides

Clt-resin (0.5 mmol), to which a N-terminal Trityl-protected Cysteine is already attached, was swollen in 5 mL DMF (RT, 1 h, 800 rpm). The following steps were performed to synthesize the depsi-peptide KIKISQINC. The swollen resin was transferred into the reaction vessel. After draining the vessel, it was filled with 20 mL DMF and a short swelling process (20 s) was performed. The reaction vessel was drained and the resin washed three times. After the last washing step, a coupling step with a Fmoc-protected AA (lysine, isoleucine, glutamine or asparagine) was performed. The Fmoc-protecting group was removed via deprotection step. This cycle was repeated until the position in the amino acid sequence, where the ester was intended to be introduced (serine). Here, the Boc-protected serine was introduced to the growing peptide chain in order to continue peptide synthesis at the hydroxyl group of serine. Therefore, after serine coupling the resin was transferred to a 40 mL vial with DCM. DCM was evaporated and 5 mL DMF, isoleucine in DMF (0.35 g/mL, 2 mL), 0.773 mL DIC and 0.06 g DMAP solved 1 mL DMF were added. The reaction mixture was shaken (800 rpm) at room temperature for 2 h. Then, the resin was washed with DMF (1x, 20 mL) and the coupling step was repeated for 16 h followed by washing the resin with DMF (3x, 20 mL). Afterwards, the resin was transferred back to the reaction vessel of the SPPS and the remaining AA were coupled as described.

The Wang-resin based peptide was synthesized in the same way, except for an additional deprotection step at the beginning in order to remove Fmoc from the first AA.

Table 11: Synthesis steps at the SPPS.

Peptide synthesis step	Program
Deprotection	Fill with 20% piperidine in DMF (10 mL) Heat to 70 °C for 25 s Heat to 90 °C for 65 s Drain
Wash	Fill with DMF (7 mL) Drain for 7 s
Coupling	Fill with AA solution (0.2 M in DMF, 10 mL), DIC solution (0.5 M in DMF, 4 mL) and oxyma solution (1.0 M in DMF, 2 mL) Heat to 70 °C for 30 s Heat to 90 °C for 120 s Drain

6.1.2 Cleavage of the peptide from the resin

A mixture of TFA/TIPS/MilliQ water (20 mL, 95%/2.5%/2.5%) was added to the resin for the cleavage from the resin and of the protecting groups and shaken (800 rpm) at room temperature for 2 h. The peptide was precipitated in ice cold diethyl ether (80 mL), centrifuged (4000 rpm, 10 min, 4 °C) and the excess diethyl ether removed. The precipitate was dispersed in ice cold diethyl ether (80 mL), centrifuged (4000 rpm, 10 min, 4 °C) and the excess diethyl ether removed. The peptide was fully dried by evaporating remaining diethyl ether, solved in 0.1% aqueous TFA (20 mL) and lyophilized (48 h) yielding a colorless powder.

6.1.3 High performance liquid chromatography

The lyophilized crude peptide was solved in 0.1% aqueous TFA (pH≤2, 0.5 mg/mL) and filtered through regenerated cellulose filters (0.20 µm). The filtered solution was applied into the reversed phase HPLC with a gradient composed of Milli-Q water (0.1% TFA) and acetonitrile (0.1% TFA). The gradient in Table 12 was used for the C18 100 Phenomenex column. The collected fraction containing the depsi-peptide were collected and lyophilized (48 h) yielding a colorless dry powder.

Table 12: HPLC program.

Flow Rate $\left[\frac{\mathrm{mL}}{\mathrm{min}}\right]$	Injection volume $[\mathrm{mL}]$	Duration $[\mathrm{min}]$	Acetonitrile $[\%]$	Milli-Q water $[\%]$
25	20	0.01	0	100
		6.00	0	100
		25.00	40	60
		27.00	100	0
		28.00	100	0
		30.00	0	100
		35.00	0	100

6.1.4 Synthesis of polymer backbones

Polyphosphonate: Representative procedure for the ring-opening polymerization catalyzed with DBU

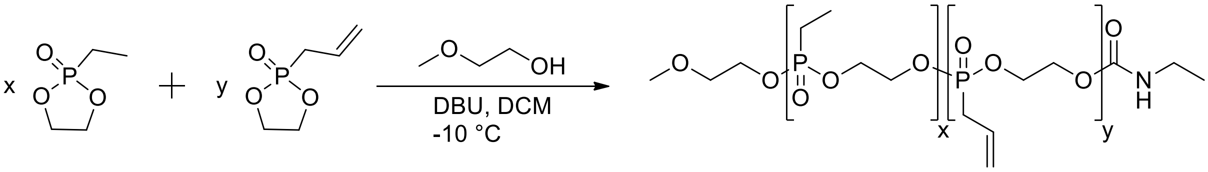

Polymerization was performed according to a modified literature protocol.[75] The particular monomers were weighed in a flame-dried Schlenk-tube, dissolved in dry benzene and dried by three times lyophilization. The monomer was dissolved in dry dichloromethane to a total concentration of 4 mol/L. A stock solution of initiator 2-methoxyethanol in dry dichloromethane was prepared with a concentration of 0.2 mol/L and the calculated amount was added to the monomer solution via Hamilton syringe. A stock solution of DBU in dry dichloromethane was prepared with a concentration of 0.2 mol/L. The monomer solution and the catalyst solution were set to the respective reaction temperature (-10 °C).

The polymerization was initiated by the addition of the calculated volume of catalyst solution containing 3.0 equivalents of DBU in respect to the initiator. Polymerization was terminated by the rapid addition of an excess of ethyl isocyanate (3 eq). The colorless, amorphous polymers were purified by precipitation in cold diethyl ether, followed by dialysis against water for three days (MWCO=10 kDa) and lyophilization yielding a yellow oil. The weighed in compounds are listed in Table 13. The product was analyzed via NMR-spectroscopy (Figure 77).

Table 13: Batch of the synthesis of Phos2.

	M $[\frac{\mathrm{g}}{\mathrm{mol}}]$	m [g]	n [mmol]	Eq.
2-Ethyl-1,3,2-dioxaphospholane 2-oxide	136.09	0.58	4,25	150
2-Allyl-1,3,2-dioxaphospholane 2-oxide	148.10	0.42	2,84	100
2-Methoxyethanol	76.09	2.15	0,03	1
DBU	152.24	12.93	0,09	3
Ethyl isocyanate	71.08	6.038	0,09	3

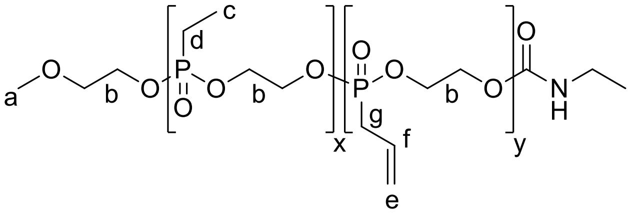

Figure 77: Phos2.

^{1}H-NMR: (700 MHz, D_2O) δ [ppm]= 5.87 (1H, m, H_f), 5.41 (2H, dd, H_e), 4.37 (4H, br, H_b), 3.47 (3H, s, H_a), 2.95 (1H, d, H_g), 2.92 (1H, d, H_g), 2.03 (2H, m, H_d), 1.24 (3H, m, H_c).

^{31}P-NMR: (700 MHz, D_2O) δ [ppm]= 38.34 (1P, s, P-CH_2-CH_3), 31.30 (1P, s, P-CH_2-CH-).

GMA-functionalized dextran

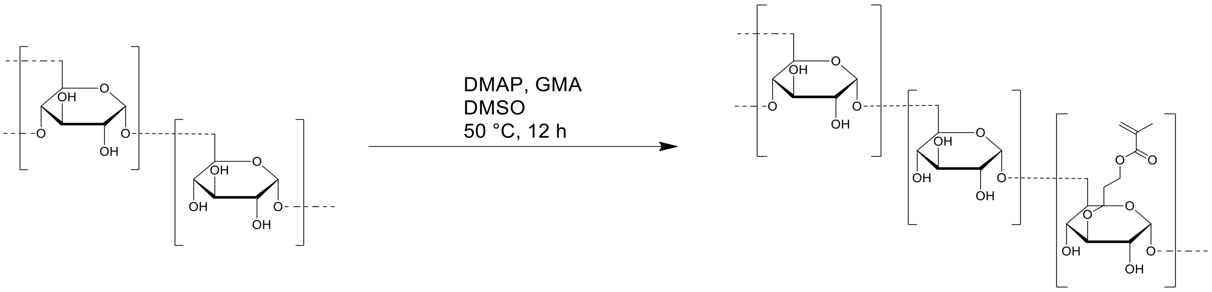

Dextran was dissolved in DMSO and the solution was stirred under nitrogen atmosphere until dextran was completely dissolved. After the solution became transparent DMAP and GMA were added. Then the solution was stirred under nitrogen atmosphere for 12 h and after that, equimolar amount of HCl was added to the solution to neutralize DMAP. The reaction mixture was added to a dialysis cassette (MWCO=10 kDa) and dialyzed against water for four days and lyophilized yielding a white powder.[43] The weighed in compounds are listed in Table 14 and Table 15. The product was analyzed via NMR-spectroscopy (Figure 78).

Table 14: Batch of the synthesis of DexGMA1. Equivalents in respect to the glucopyranosyl rings.

	$M\ [\frac{g}{mol}]$	m [g]	n [mmol]	Eq.
Dextran	18785	0.25	0.08	4
DMSO	78.13	1.1	-	-
DMAP	122.17	0.38	3.08	2
GMA	142.15	0.22	6.16	1

Table 15: Batch of the synthesis of DexGMA2. Equivalents in respect to the glucopyranosyl rings.

	$M\ [\frac{g}{mol}]$	m [g]	n [mmol]	Eq.
Dextran	24280	2.00	0.08	2
DMSO	78.13	16.50	-	-
DMAP	122.17	0.38	3.08	0.5
GMA	142.15	0.88	6.16	1

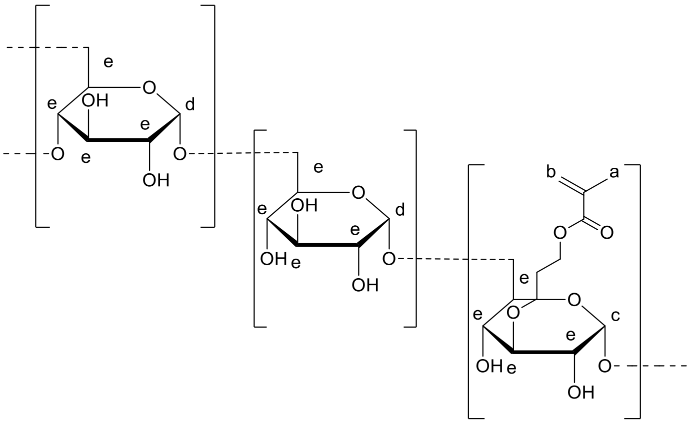

Figure 78: DexGMA.

^{1}H-NMR: (700 MHz, D_2O) δ [ppm]= 6.25 (1H, d, H_b), 5.80 (1H, d, H_b), 5.22 (1H, br, H_c), 5.02 (1H, br, H_d), 4.30-3.30 (6H/12H, br, H_e), 2.03 (3H, s, H_a).

6.1.5 Synthesis of polymer-peptide hybrids

Representative procedure to functionalize alkene carrying polymers with D3 via thiol-ene click reaction

Polymer, D3, TCEP and VA-044 were each solved in 0.1% aqueous TFA and combined. The solution was degassed with argon for 10 min and heated (37 °C, 800 rpm, 19 h). After heating, the reaction mixture was spin filtered (MWCO=5000 kDa, 3000 rpm) with 0.1% aqueous TFA (15 ml) and lyophilized yielding a colorless powder. The batches for the polymer-peptide hybrid synthesis are listed in Table 16 to Table 20. The products were analyzed via NMR-spectroscopy (Figure 79/Figure 80).

Table 16: Batch of the synthesis of PDH1. Equivalents in respect to the allyl-functionalized monomer units.

	$M\ [\frac{g}{mol}]$	m [mg]	n [µmol]	Eq.	V [µL]
Phos1	16300	11.548	0.7	1	
D3[W]	1045.60	30.000	28.7	1.5	
TCEP	250.19	6.221	24.9	1.3	
VA-044	323.27	8.039	24.9	1.3	
0.1% TFA					500

Table 17: Batch of the synthesis of PDH2. Equivalents in respect to the allyl-functionalized monomer units.

	$M\ [\frac{g}{mol}]$	m [mg]	n [µmol]	Eq.	V [µL]
Phos2	35000	7.000	0.2	1	
D3[C]	1045.60	22.543	21.6	1.1	
TCEP	250.19	4.904	19.6	1	
VA-044	323.27	6.336	19.6	1	
0.1% TFA					400

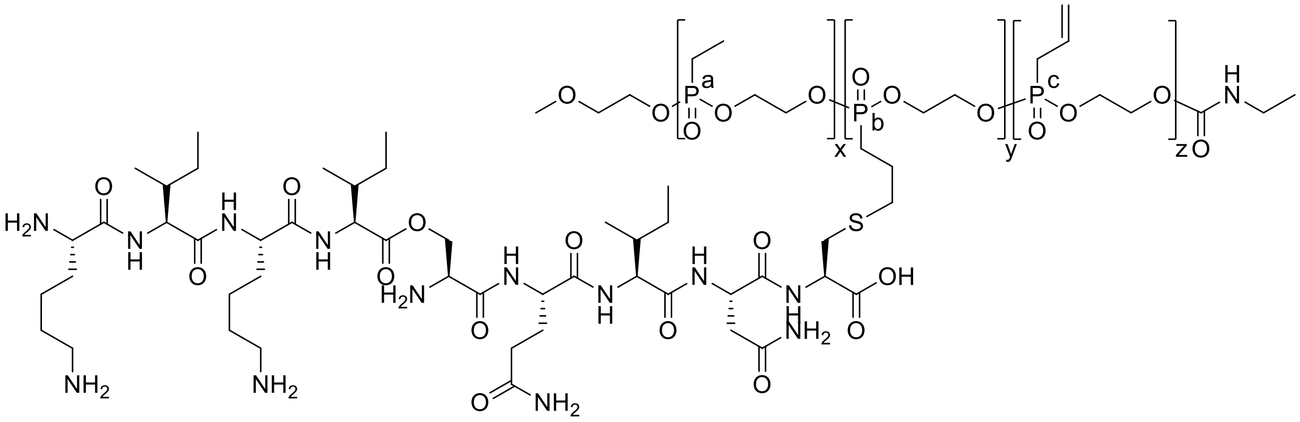

Figure 79: PDH2

^{31}P-NMR: (700 MHz, D_2O) δ [ppm]= 38.31 (1P, s, P_a), 35.37 (1P, s, P_b), 31.23 (1P, s, P_c).

Table 18: Batch of the synthesis of DDH1. Equivalents in respect to the alkene-functionalized monomer units.

	$M\ [\frac{g}{mol}]$	m [mg]	n [µmol]	Eq.	V [µL]
DexGMA1	23400	3.757	0.2	1	
D3^{C}	1045.60	11.962	11.4	1.5	
TCEP	250.19	2.602	10.4	1.3	
VA-044	323.27	3.362	10.4	1.3	
0.1% TFA					400

Table 19: Batch of the synthesis of DDH2. Equivalents in respect to the alkene-functionalized monomer units.

	$M\ [\frac{g}{mol}]$	m [mg]	n [µmol]	Eq.	V [µL]
DexGMA1	23400	3.757	0.2	1	
D3^{C}	1045.60	5.981	5.7	0.75	
TCEP	250.19	1.301	5.2	0.65	
VA-044	323.27	0.841	5.2	0.65	
0.1% TFA					200

Table 20: Batch of the synthesis of DDH3. Equivalents in respect to the alkene-functionalized monomer units.

	$M\ [\frac{g}{mol}]$	m [mg]	n [µmol]	Eq.	V [µL]
DexGMA2	28150	12.000	0.4	1	
D3^C	1045.60	17.482	16.7	1.3	
TCEP	250.19	3.803	15.2	1.3	
VA-044	323.27	4.914	15.2	1.3	
0.1% TFA					800

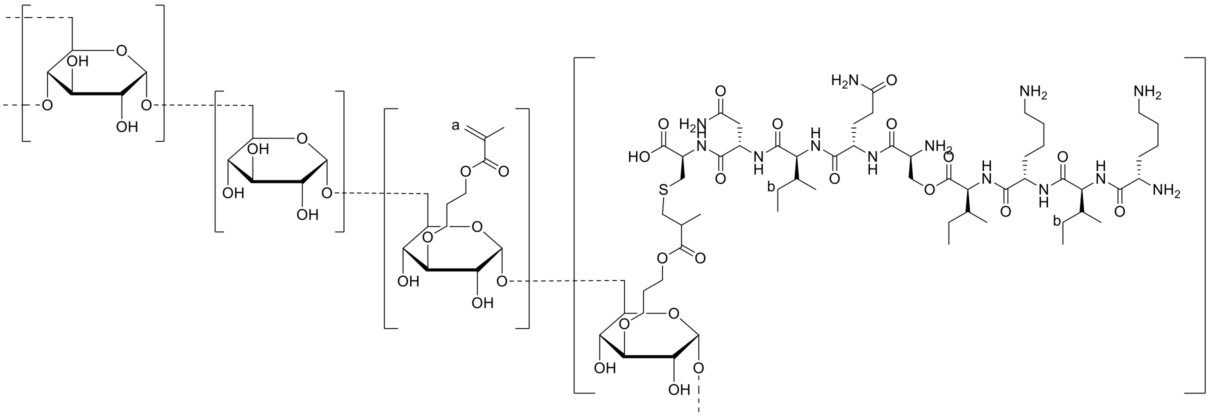

Figure 80: DDH3

^{1}H-NMR: (700 MHz, D_2O) δ [ppm]= 6.25 (1H, d, H_a), 1.20 (4H, br, H_b)

6.2 Characterization of the depsi-peptide

The following chapter contains the characterization of the synthesized depsi-peptides.

6.2.1 Matrix-assisted laser desorption/ionization-time of flight mass spectroscopy

Samples were prepared by mixing the matrix, a saturated α-cyano-4-hydroxycinnamic acid (CHCA)solution in Milli-Q water/ACN 1/1 + 0.1% aqueous TFA with the respective sample solved in 0.1% aqueous TFA (1 µg/ml).

6.2.2 Liquid chromatography mass spectroscopy

A peptide solution was prepared using 0.1% aqueous TFA (50 µg/mL) and injected into the HPLC-ESI-MS. The solvents were Milli-Q water + 0.1% formic acid and ACN. The solvent gradient started at 5% ACN content, which was increased to 95% over 12 min.

6.2.3 Thioflavin T-Assay

Stock solutions of the depsi-peptide D3 or the linear peptide P3^{C}-Ctrl in DMSO (10 mg/mL) were prepared and introduced to filtered (0.2 µm filter unit) PBS yielding a sample solution (1 mg/mL). The sample solutions were incubated on a shaker (600 rpm) at 37 °C for 16 h. An aliquot (2 µL) of the respective solution was taken and introduced to a ThT solution in PBS (50 µM, 10 µL), which was placed in a 384 well-plate (flat bottom black polystyrol small volume, Greiner bio-one). As a reference, the sample was substituted by PBS (2 µL) and introduced to the ThT solution (50 µM, 10 µL). The ThT mixtures were mixed and incubated at room temperature for 5 min to allow interactions between ThT and potential fibrillary structures. Before the fluorescence read-out the mixtures were shaken for 5 s and the fluorescence emission was recorded at $\lambda_{\text{em}} = 488\ \text{nm}$ upon excitation at $\lambda_{\text{ex}} = 440\ \text{nm}$ with 10 nm bandwidths and multiple reads per well (3x3) (Tecan). A total of three measurements per sample were performed.[8]

6.2.4 Conversion-Assay

To quantify the assembled linear peptides P3^{C} into fibrils, conversion rates of the depsi-peptide D3 and the linear peptide P3^{C}-Ctrl were determined. Therefore, the respective peptide DMSO stock solutions (10 mg/mL, 20 µL) were introduced into sterile filtered (0.2 µm filter unit) 0.1% aqueous TFA or PBS (180 µL), respectively, and incubated on a shaker (600 rpm) at 37 °C for 16 h. After incubation, the solutions were split and one half of the solution (100 µL) was centrifuged (13.2 krpm, 99 min, 4 °C) using Vivaspin 500 tubes (MWCO=3000 Da) to remove peptide aggregates from the solution. The filtrate and the original solutions were lyophilized for 16 h to obtain solid compounds. The resulting solids were dissolved in 25 µL DMSO. To determine the amount of free amino groups via fluorescent read-out, 10 µL of the respective DMSO sample solution were placed into a black 384 well-plate (flat bottom black polystyrol small volume, Greiner bio-one) and fluorescamine solution (3 mg/mL in DMSO, 3 µL) was added. The mixture was incubated at room temperature in the dark for 30 min. After incubation the samples were shaken for 5 s and the fluorescence intensities detected with an excitation wavelength of $\lambda_{\mathrm{ex}} = 365\ \mathrm{nm}$ and emission wavelength of $\lambda_{\mathrm{em}} = 470\ \mathrm{nm}$ with 10 nm bandwidths and multiple reads (3x3) per well. A total of three measurements per sample were performed. Thereby, the n-fold fluorescence intensity enhancements (DMSO=1) was calculated and defined the conversion rate (CR) according to Equation 1.[8]

6.2.5 Transmission electron microscopy

A DMSO stock solution (10 mg/mL) of the depsi-peptide D3 and the linear peptide P3^{C}-Ctrl were introduced into a sterile filtered (0.2 µm filter unit) solvent (0.1% aqueous TFA or PBS) to yield 10 µL sample solutions (1 mg/mL). All samples were incubated on a shaker (600 rpm) at 37 °C for 16 h. The copper grids coated with a thin electron-transparent Formvar-layer were plasma etched with 20% oxygen plasma for 30 s for the measurements. A 3 µL droplet of the sample was deposited on the copper grid and incubated for 5 min. After incubation the sample solution was removed by using filter paper, 7 µL of an aqueous 4% uranyl acetate solution were placed on a parafilm and the copper grid deposited on top of the droplet (top with deposited sample facing downwards). The sample was incubated for 2.5 min to enhance sample contrast via staining, washed three times with Milli-Q water and the excess water was removed with filter paper. After air drying the imaging was performed in high vacuum at an acceleration voltage of 120 kV.

6.2.6 Attenuated total reflection-Fourier transformation infrared spectroscopy

For the analysis of the secondary structure elements of the peptide, ATR-FTIR measurements were performed. A DMSO stock solution (10 mg/mL) of the depsi-peptide and the control peptide were introduced into a sterile filtered (0.2 µm filter unit) solvent (0.1% aqueous TFA or PBS) to yield 40 µL sample solutions (1 mg/mL). All samples were incubated on a shaker (600 rpm) at 37 °C for 16 h and lyophilized. The spectra were recorded with a spectral resolution of 2 cm^{-1}, each spectrum with an average of 20 scans.[8]

6.2.7 Circular dichroism spectroscopy

For the analysis of the secondary structure elements of the peptides, CD measurements were performed. An aqueous stock solution (1 mg/mL) of the depsi-peptide and the control peptide were introduced into sterile filtered (0.2 µm filter unit) Milli-Q water to yield 300 µL sample solution (0.1 mg/mL). All samples were incubated on a shaker (600 rpm) at 37 °C for 16 h. The sample was measured at 25 °C from 260 nm to 180 nm with a data pitch of 0.2 nm, a bandwidth of 1.00 nm and a scanning speed of 20 nm/min. The data was recorded by 5 times data accumulation and edited with the “JASCO Spectra Manager II”.

6.3 Characterization of the polymer backbones

The following chapter contains the characterization of the synthesized polymer backbones.

6.3.1 Transmission electron microscopy

A DMSO stock solution (10 mg/mL) of the poly(phosphonate) and dextran were introduced into a sterile filtered (0.2 µm filter unit) solvent (0.1% aqueous TFA or PBS) to yield 10 µL sample solutions (1 mg/mL). All samples were incubated on a shaker (600 rpm) at 37 °C for 16 h. The copper grids coated with a thin electron-transparent Formvar-layer were plasma etched with 20% oxygen plasma for 30 s for the measurements. A 3 µL droplet of the sample was deposited on the copper grid and incubated for 5 min. After incubation the sample solution was removed by using filter paper, 7 µL of an aqueous 4% uranyl acetate solution were placed on a parafilm and the copper grid deposited on top of the droplet (top with deposited sample facing downwards). The sample was incubated for 2.5 min to enhance sample contrast via staining, washed three times with Milli-Q water and the excess water was removed with filter paper. After air drying the imaging was performed in high vacuum at an acceleration voltage of 120 kV.

6.3.2 Attenuated total reflection-Fourier transformation infrared spectroscopy

For the analysis of the secondary structure elements of the poly(phosphonate) and dextran, ATR-FTIR measurements were performed. A DMSO stock solution (10 mg/mL) of the polymer backbones were introduced into a sterile filtered (0.2 µm filter unit) solvent (0.1% aqueous TFA or PBS) to yield 40 µL sample solutions (1 mg/mL). All samples were incubated on a shaker (600 rpm) at 37 °C for 16 h and subsequently lyophilized. The spectra were recorded with a spectral resolution of 2 cm^{-1}, each spectrum with an average of 20 scans.

6.3.3 Rheology

Rheological characterization of the polymer backbones was performed using a rheometer equipped with a solvent reservoir in order to prevent drying. The experiments were conducted by using an 8 mm parallel-plate geometry with hydrogels/solutions of 30 µL volume resulting in a gap size of 0.50 mm at 25 °C. For the characterization, the polymer backbone (1.2 mg) was prepared using phosphate buffer (pH=7.4, 100 mM, 30 µL).

Time sweep: In order to determine the mechanical properties of the hydrogels/solutions as a control experiment, time sweeps were conducted at a fixed oscillatory strain (0.1%) and fixed frequency (1 Hz). The time sweep was performed until the storage (G') and loss (G'') were constant.

6.4 Characterization of the polymer-peptide hybrid

The following chapter contains the characterization of the synthesized polymer-peptide hybrids.

6.4.1 Transmission electron microscopy

A DMSO stock solution (10 mg/mL) of the poly(phosphonate)-peptide hybrid and dextran-peptide hybrid were introduced into a sterile filtered (0.2 µm filter unit) solvent (0.1% aqueous TFA or PBS) to yield 100 µL sample solutions (1 mg/mL). All samples were incubated on a shaker (600 rpm) at 37 °C for 16 h. The copper grids coated with a thin electron-transparent Formvar-layer were plasma etched with 20% oxygen plasma for 30 s for the measurements. A 3 µL droplet of the sample was deposited on the copper grid and incubated for 5 min. After incubation the sample solution was removed by using filter paper, 7 µL of an aqueous 4% uranyl acetate solution were placed on a parafilm and the copper grid deposited on top of the droplet (top with deposited sample facing downwards). The sample was incubated for 2.5 min to enhance sample contrast via staining, washed three times with Milli-Q water and the excess water was removed with filter paper. After air drying the imaging was performed in high vacuum at an acceleration voltage of 120 kV.

6.4.2 Attenuated total reflection-Fourier transformation infrared spectroscopy

For the analysis of the secondary structure elements of the poly(phosphonate)-peptide hybrid and dextran-peptide hybrid, ATR-FTIR measurements were performed. A DMSO stock solution (10 mg/mL) of the polymer-peptide hybrid were introduced into a sterile filtered (0.2 µm filter unit) solvent (0.1% aqueous TFA or PBS) to yield 40 µL sample solutions (1 mg/mL). All samples were incubated on a shaker (600 rpm) at 37 °C for 16 h and subsequently lyophilized. The spectra were recorded with a spectral resolution of 2 cm^{-1}, each spectrum with an average of 20 scans.

6.4.3 Thioflavin T-Assay

A stock solution of the polymer-peptide hybrid or the polymer backbone in DMSO (10 mg/mL) were prepared and introduced to filtered (0.2 µm filter unit) PBS yielding a sample solution

(1 mg/mL). The sample solutions were incubated on a shaker (600 rpm) at 37 °C for 16 h. An aliquot (2 µL) of the respective solution was taken and introduced to a ThT solution in PBS (50 µM, 10 µL), which was placed in a 384 well-plate (flat bottom black polystyrol small volume, Greiner bio-one). As a reference, the sample was substituted by PBS (2 µL) and introduced to the ThT solution (50 µM, 10 µL). The ThT mixtures were mixed and incubated at room temperature for 5 min to allow interactions between ThT and potential fibrillary structures. Before the fluorescence read-out the mixtures were shaken for 5 s and the fluorescence emission was recorded at $\lambda_{\mathrm{em}} = 488\ \mathrm{nm}$ upon excitation at $\lambda_{\mathrm{ex}} = 440\ \mathrm{nm}$ with 10 nm bandwidths and multiple reads per well (3x3) (Tecan). A total of three measurements per sample were performed.

6.4.4 Rheology

Rheological characterization of the polymer-peptide hybrids was performed using a rheometer equipped with a solvent reservoir in order to prevent drying. The experiments were conducted by using an 8 mm parallel-plate geometry with hydrogels/solutions of 30 µL volume resulting in a gap size of 0.50 mm at 25 °C. For the characterization, the hybrids hydrogels (4 wt%, 1.2 mg hybrid brush) were prepared using phosphate buffer (pH=7.4, 100 mM, 30 µL).

1. Time sweep: In order to determine the mechanical properties of the hydrogels/solutions, time sweeps were conducted at a fixed oscillatory strain (0.1%) and fixed frequency (1 Hz). The time sweep was performed until the storage (G') and loss (G'') were constant.

2. Amplitude sweep: Oscillatory strain sweeps (0.01-1000%) were performed with a fixed frequency (1 Hz) to determine the mechanical properties of the gels in dependency of increasing strain, eliciting the strain needed for gel-to-sol transition.

3. Amplitude time sweeps: Cycles of oscillatory strain sweeps (0.01-1000%) at a fixed frequency (1 Hz) followed by a 866 s time sweep with fixed low oscillatory strain (0.1%) and fixed frequency (1 Hz) were performed three times in a row, in order to analyze the self-healing of the hydrogel after disruption due to shear stress.

7. Acknowledgement

First of all, I thank Prof. Dr. T. Weil for the fantastic opportunity to work in her research group at the Max Planck Institute for Polymer Research in Mainz on my master thesis and gain insight in her interesting research in the fields of synthesis of macromolecules and the work in the department.

I also want to thank Prof. Dr. H. Frey for taking his time to read my master thesis as a second corrector.

Further, I thank Dr. Christopher Synatschke for the possibility to work in his subgroup at the MPIP Mainz. Also, I want to thank him for always taking his time to discuss preliminary results and share his knowledge during the working days and in the subgroup meetings. Additionally, I want to thank him for encouraging me to do my PhD studies.

Special thanks goes to Jasmina Gačanin, who supervised the work performed in this project and had always time to discuss with me my preliminary results and problems occurring during the works on the subject. Even though the work was hard and the motivation low sometimes, she found some uplifting words to keep me going.

I want to thank the cooperation partner Dr. F. Wurm and especially Timo Rheinberger for the synthesized poly(phosphonate)s and the assistance in developing a thiol-ene click reaction in aqueous media.

A huge thank you goes to the entire working group for the friendly environment and any support. I enjoyed the work and daily life with all the people in the group. Especially, I want to thank Luisa Wiechmann for the synthesis of DexGMA1 and the TEM analysis of $P3^{W}$, Adriana Sobota and Michaela Pieszka for helping me with the peptide synthesis, Adriana Sobota and Yingke Wu for measuring TEM images, Astrid Heck for measuring fluorescence intensities with the TECAN, Maksymilian Zegota for helping me with HPLC and LCMS related problems and Ali Rouhanipour for the LCMS service.

I thank Christoph Sieber for the TEM service.

Last but not least, I want to thank my girlfriend, Johanna, my parents, Birgit and Jürgen, my brother, Christian, and all of my friends, who supported me all these years and helped me through rough times of my studies. A very special thank you goes to my parents for the financial support, the encouragement, and the possibility to fulfill my dreams.

8. Annex

8.1 Supplementary Data

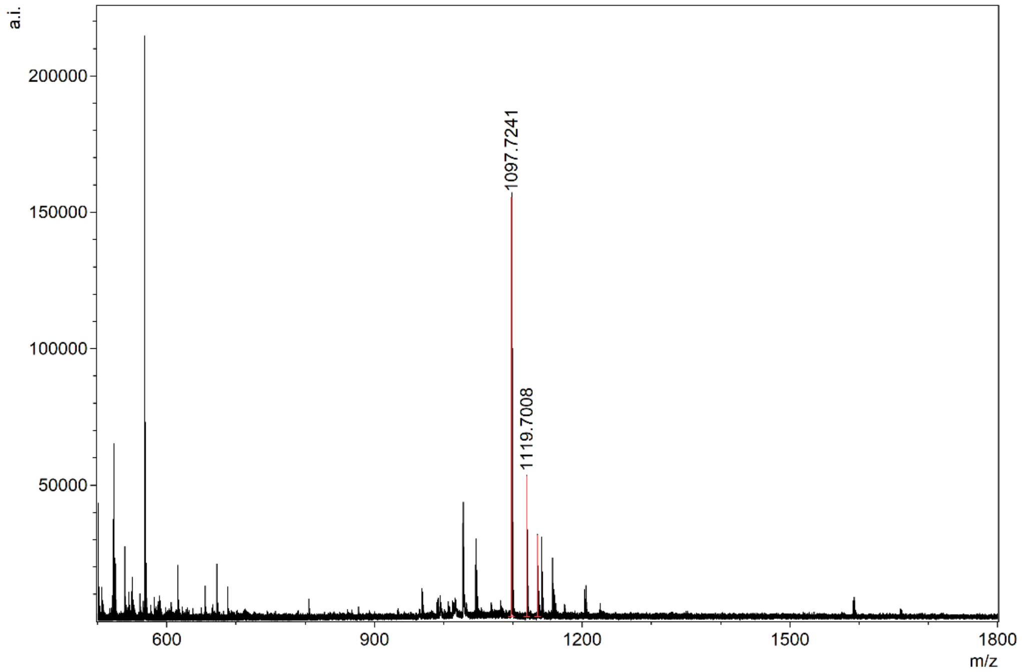

Figure 81: MALDI-ToF MS data of isolated side product KIKI(O-C(O))SQINA^{Pip} (**IV**). m/z: Calculated: [**IV**+H]$^+$ = 1097.71, [**IV**+Na]$^+$ = 1119.69, [**IV**+K]$^+$ = 1135.66. Found: [**IV**+H]$^+$ = 1097.72, [**IV**+Na]$^+$ = 1119.70, [**IV**+K]$^+$ = 1135.68.

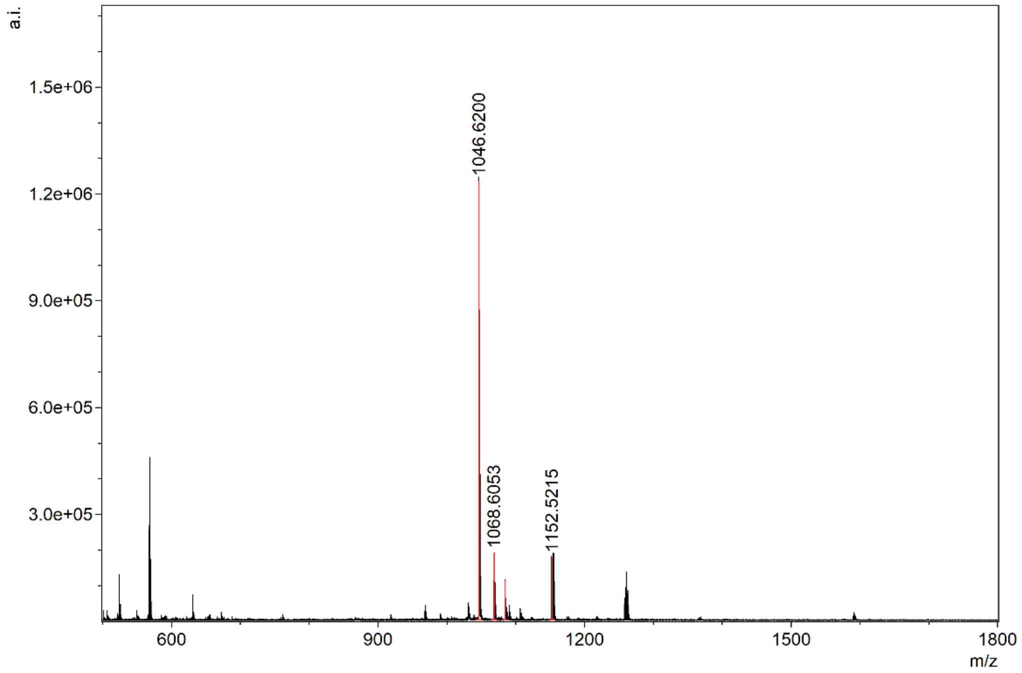

Figure 82: MALDI-ToF MS data of isolated side product P3^W (**II**) with side product (**V**). m/z: Calculated: [**II**+H]$^+$ = 1046.61, [**II**+Na]$^+$ = 1068.59, [**II**+K]$^+$ = 1084.56, [**V**+H]$^+$ = 1152.64. Found: [**II**+H]$^+$ = 1046.62, [**II**+Na]$^+$ = 1068.61, [**II**+K]$^+$ = 1084.58, [**V**+H]$^+$ = 1152.52.

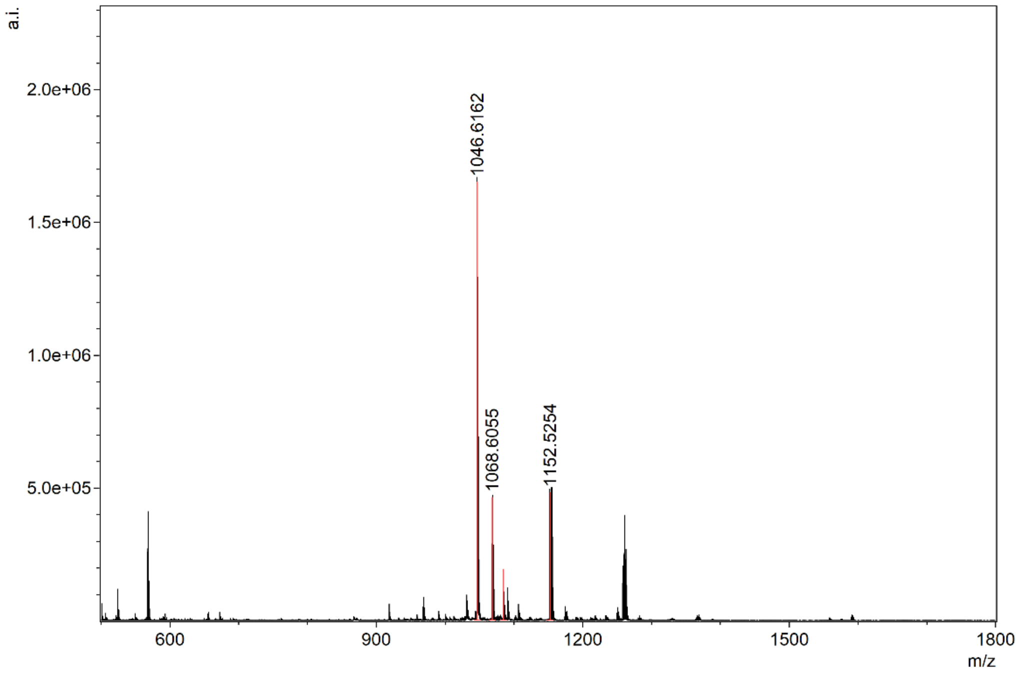

Figure 83: MALDI-ToF MS data of isolated D3^{W} (**I**) with side product (**V**). m/z: Calculated: [**I**+H]$^{+}$ = 1046.61, [**I**+Na]$^{+}$ = 1068.59, [**I**+K]$^{+}$ = 1084.56, [**V**+H]$^{+}$ = 1152.64. Found: [**I**+H]$^{+}$ = 1046.62, [**I**+Na]$^{+}$ = 1068.61, [**I**+K]$^{+}$ = 1084.58, [**V**+H]$^{+}$ = 1152.52.

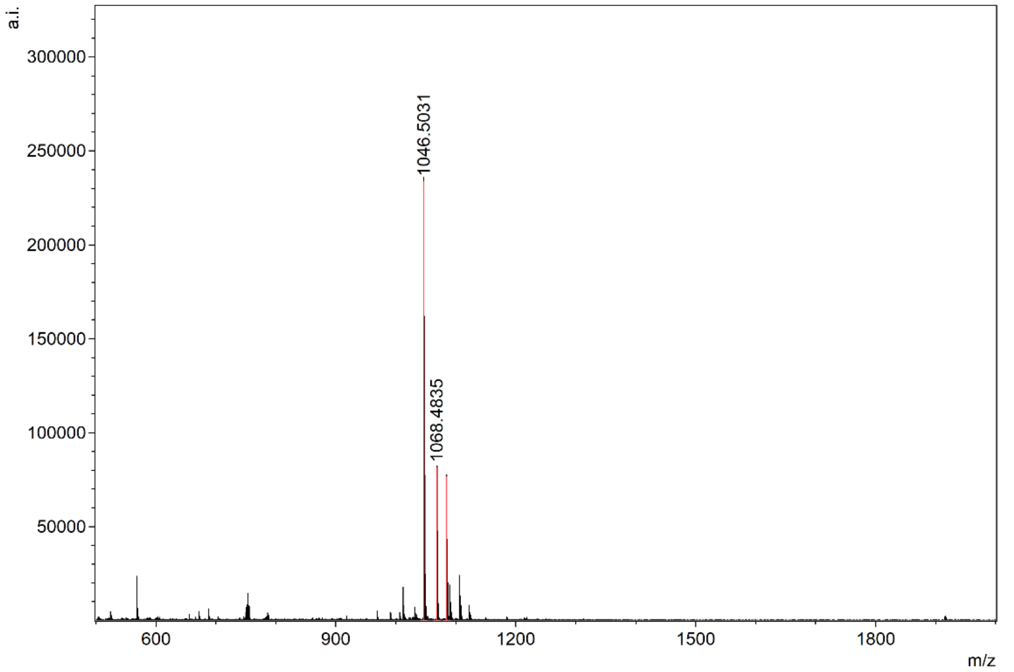

Figure 84: MALDI-ToF MS data of isolated D3^{C} (**I**). m/z: Calculated: [**I**+H]$^{+}$ = 1046.61, [**I**+Na]$^{+}$ = 1068.59, [**I**+K]$^{+}$ = 1084.56. Found: [**I**+H]$^{+}$ = 1046.50, [**I**+Na]$^{+}$ = 1068.48, [**I**+K]$^{+}$ = 1084.45.

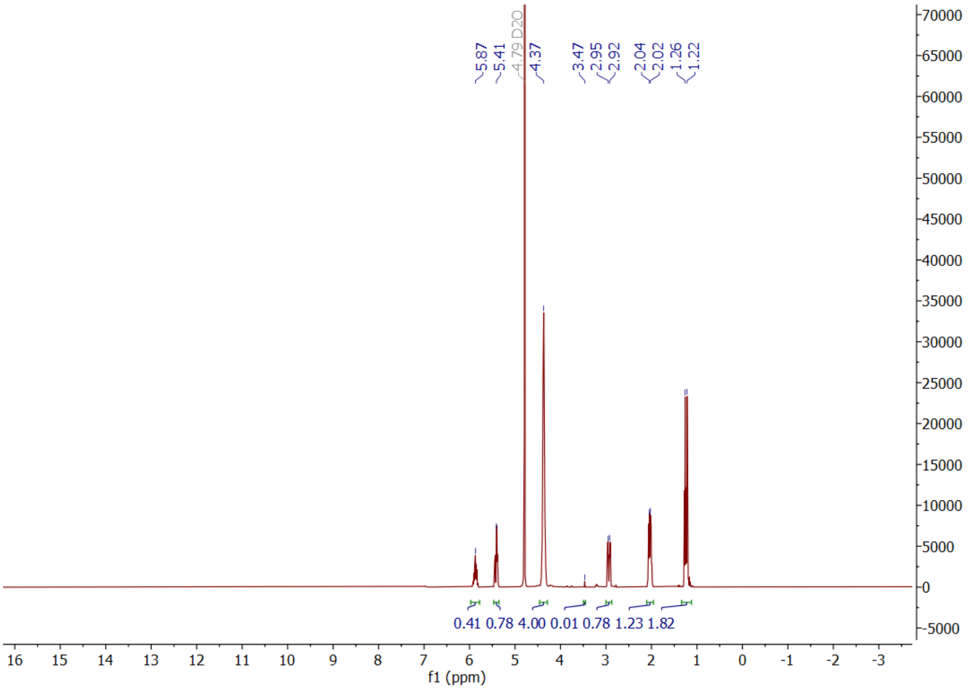

Figure 85: ^{1}H-NMR-spectrum of Phos2 (**X**) in D_2O (700 MHz).

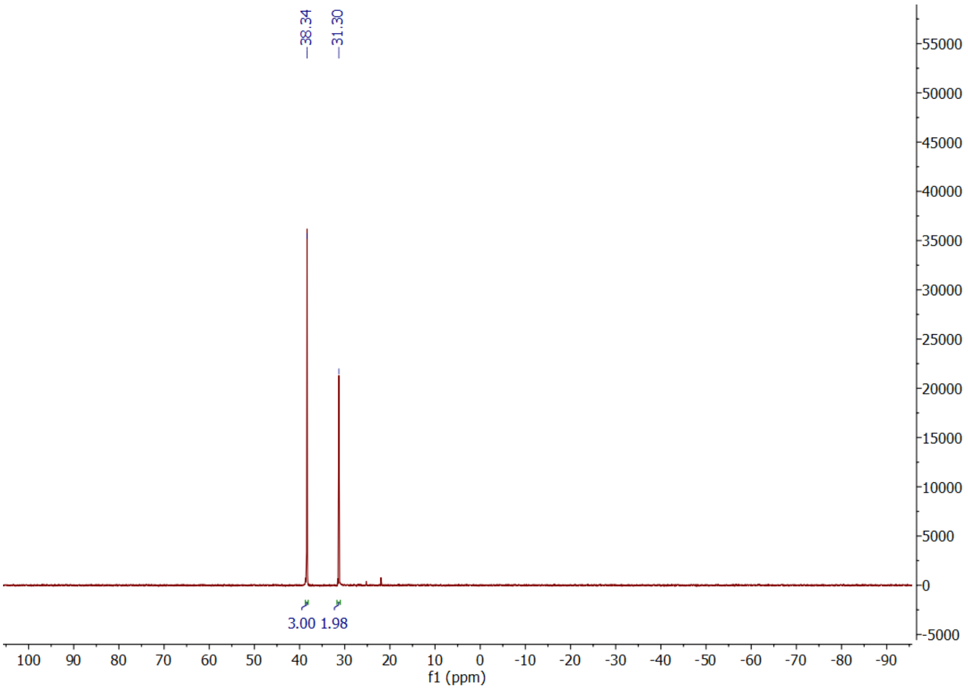

Figure 86: ^{31}P-NMR-spectrum of Phos2 (**X**) in D_2O (700 MHz).

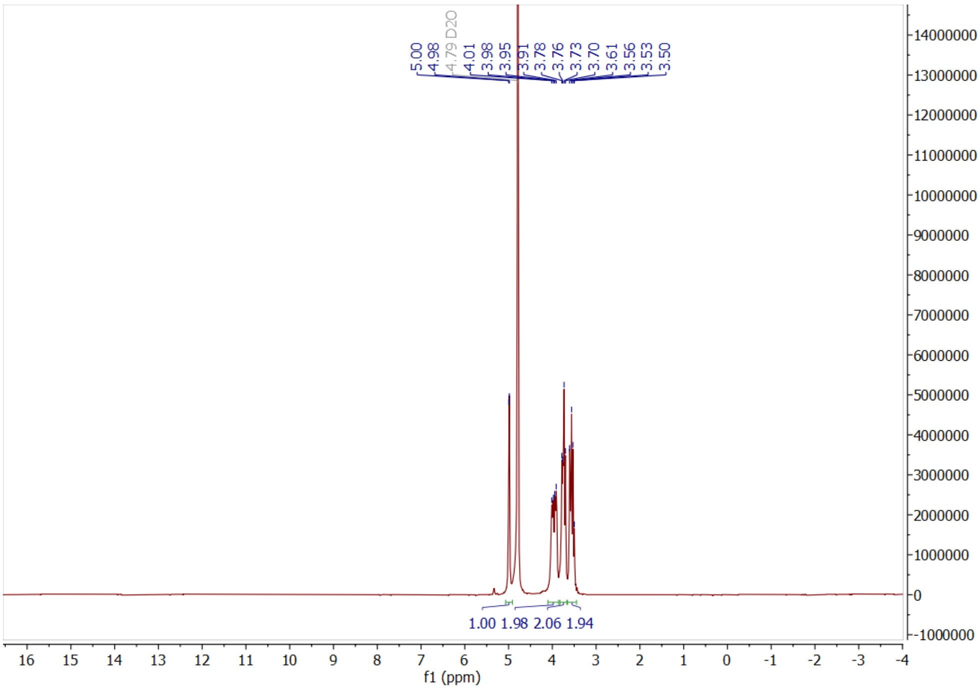

Figure 87: ^{1}H-NMR-spectrum of Dex1 in D_2O (700 MHz).

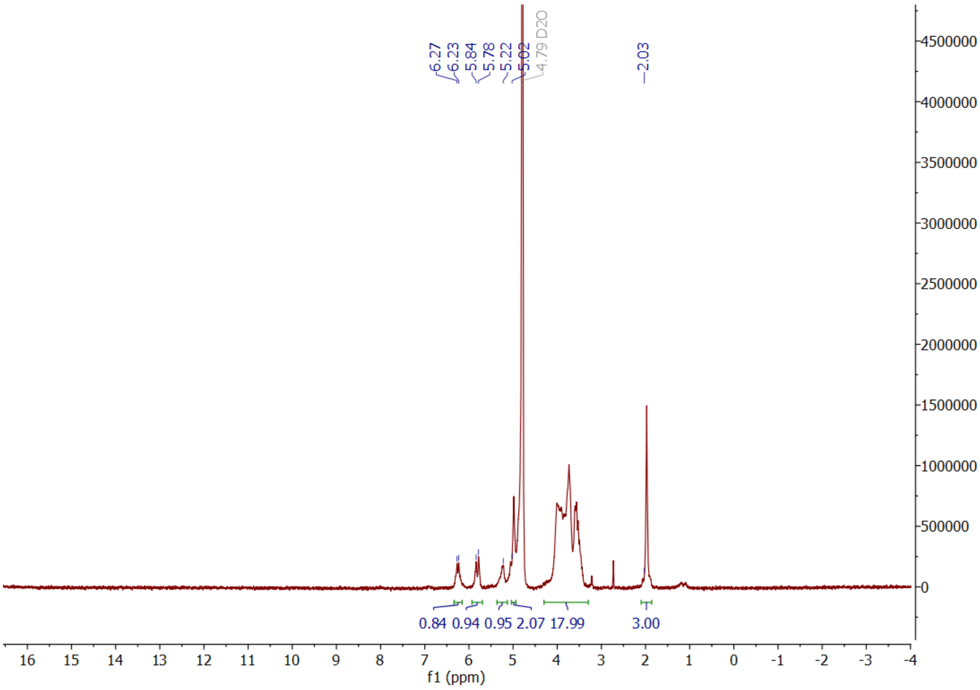

Figure 88: ^{1}H-NMR-spectrum of DexGMA1 (**XIII**) in D_2O (700 MHz).

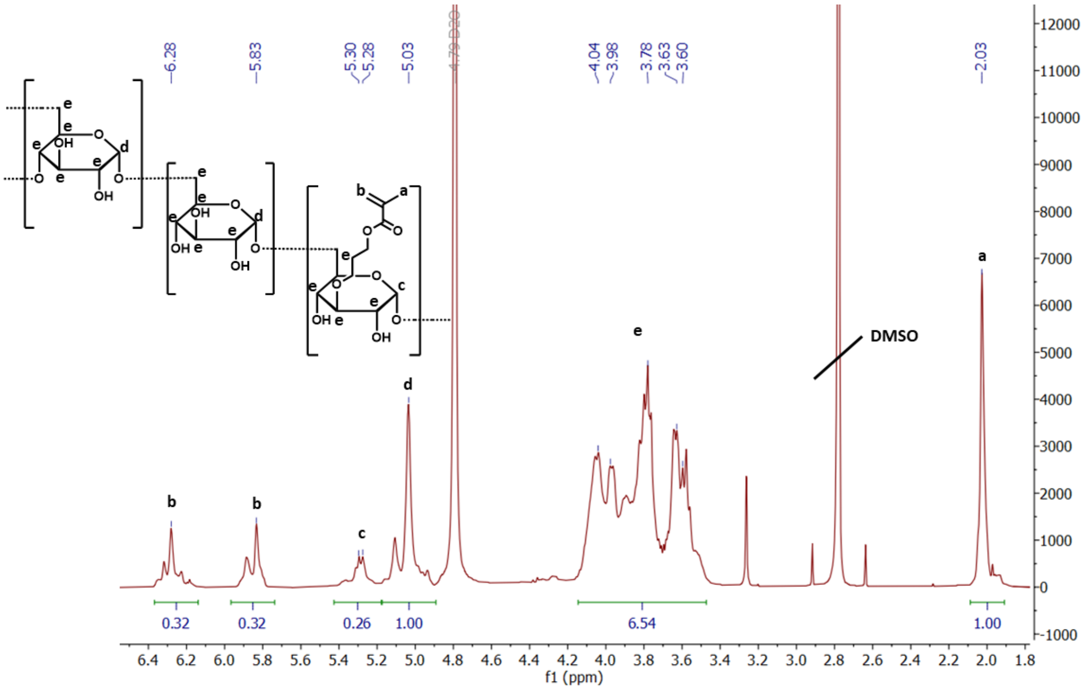

Figure 89: ^{1}H-NMR-spectrum of DexGMA2 (**XIV**) in D_2O (700 MHz) with the molecular structure and the assigned hydrogen atoms.

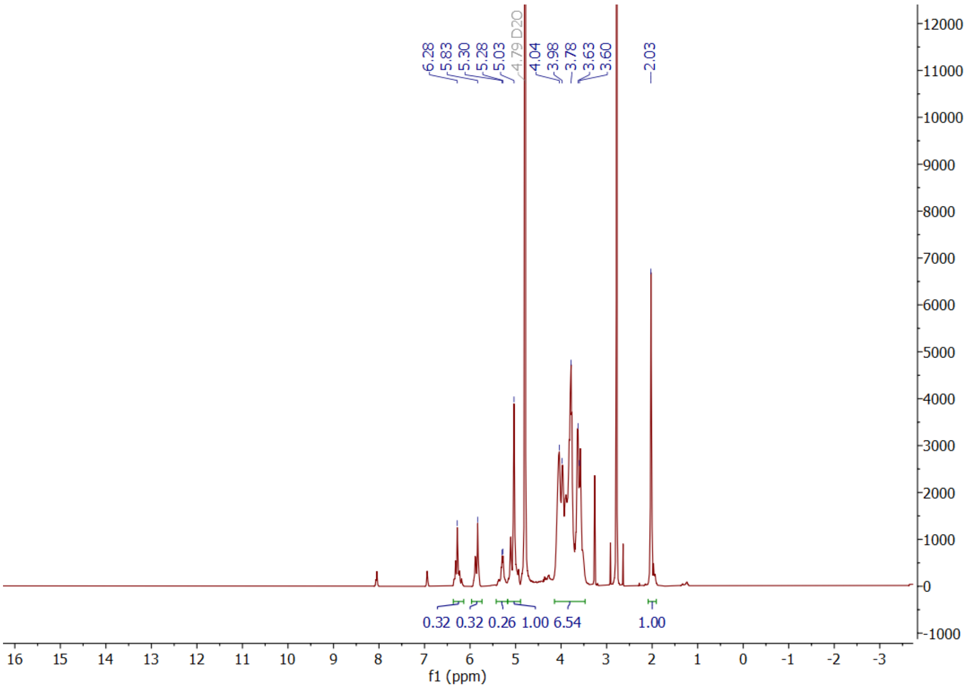

Figure 90: ^{1}H-NMR-spectrum of DexGMA2 (**XIX**) in D_2O (700 MHz).

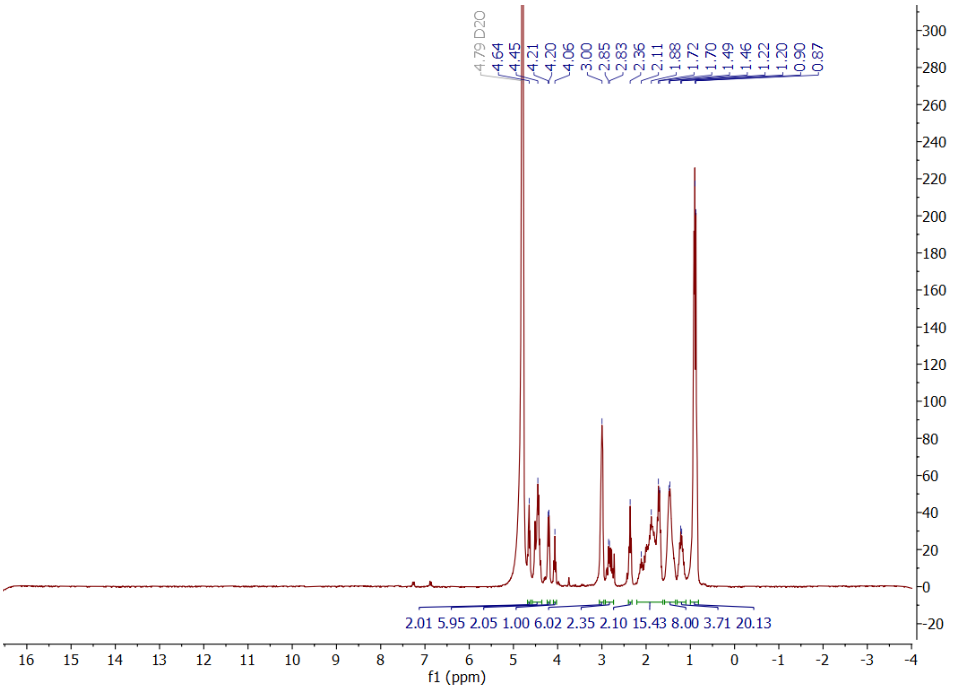

Figure 91: ^{1}H-NMR-spectrum of D3^C in D$_2$O (700 MHz).

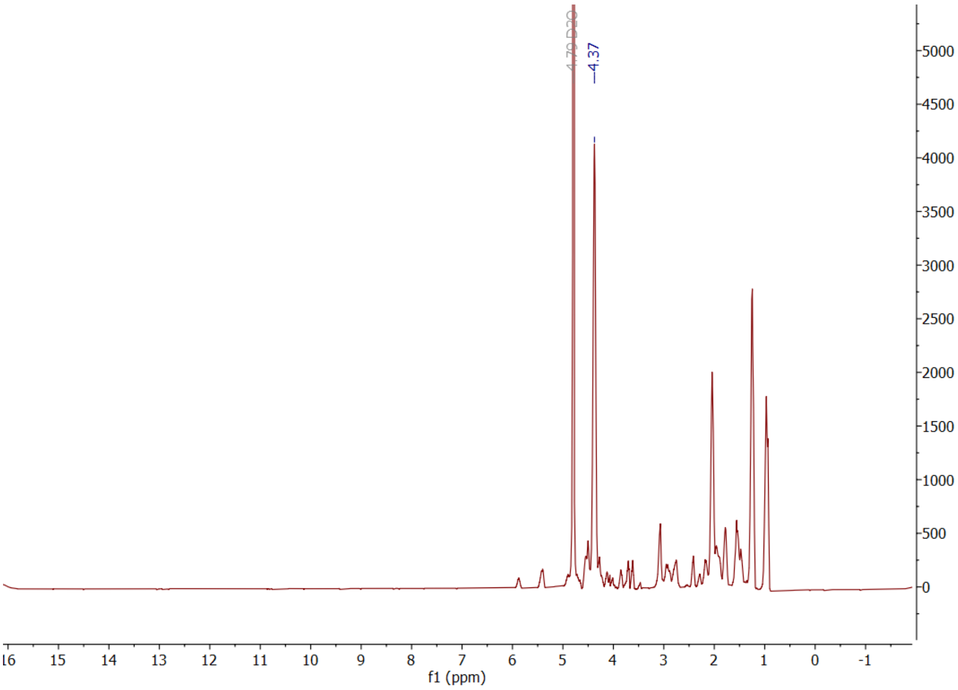

Figure 92: ^{1}H-NMR-spectrum of PDH1 (**XV**) in D$_2$O (700 MHz).

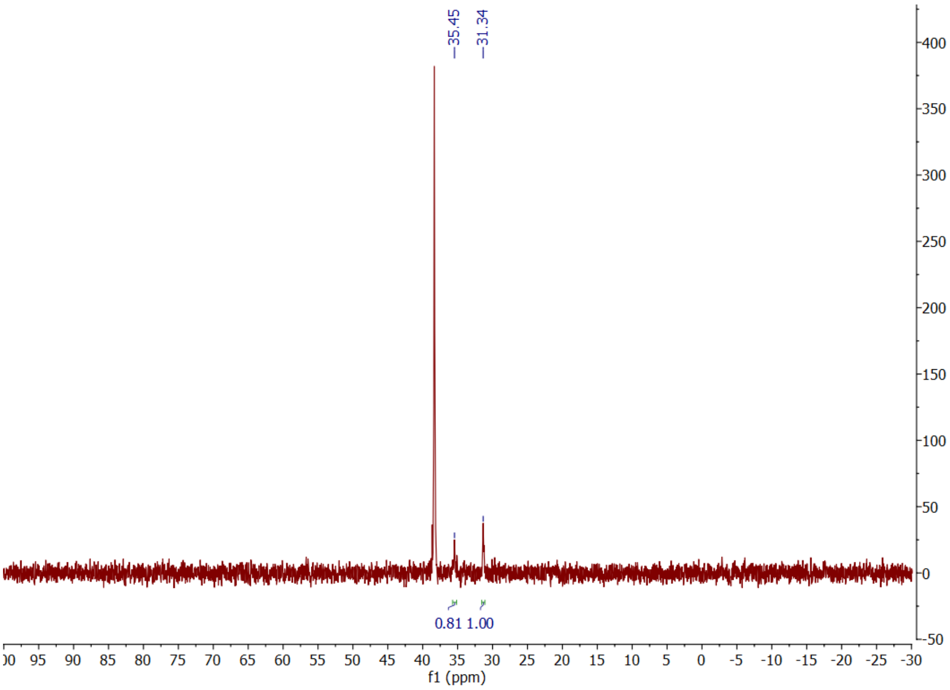

Figure 93: ^{31}P-NMR-spectrum of PDH1 (**XV**) in D_2O (700 MHz).

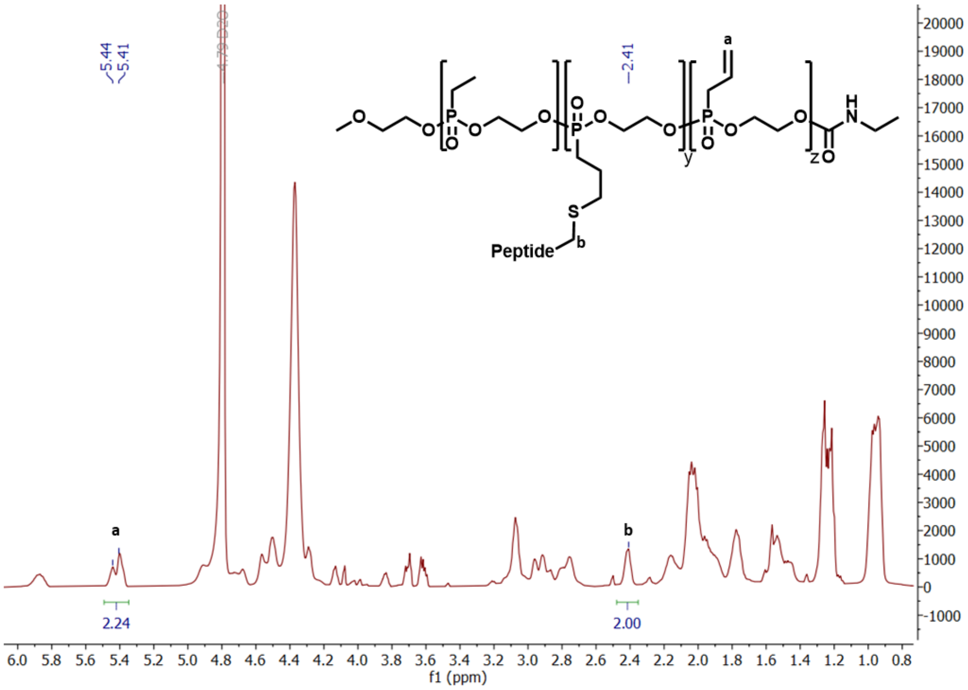

Figure 94: ^{1}H-NMR-spectrum of PDH2 (**XVI**) in D_2O (700 MHz) with the molecular structure and the relevant assigned hydrogen atoms

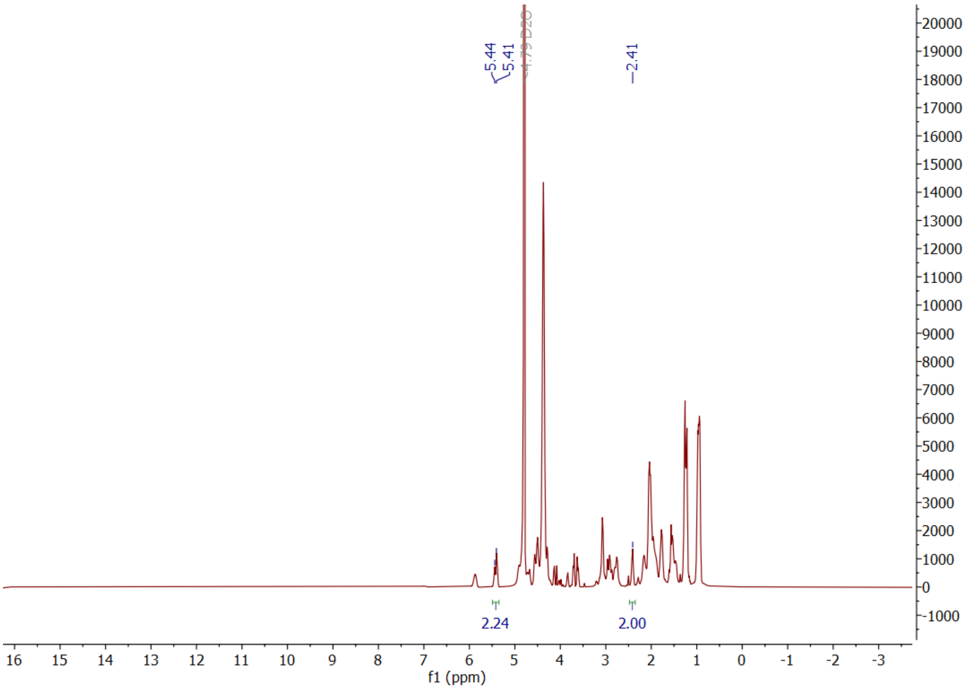

Figure 95: ^{1}H-NMR-spectrum of PDH2 (**XVI**) in D_2O (700 MHz).

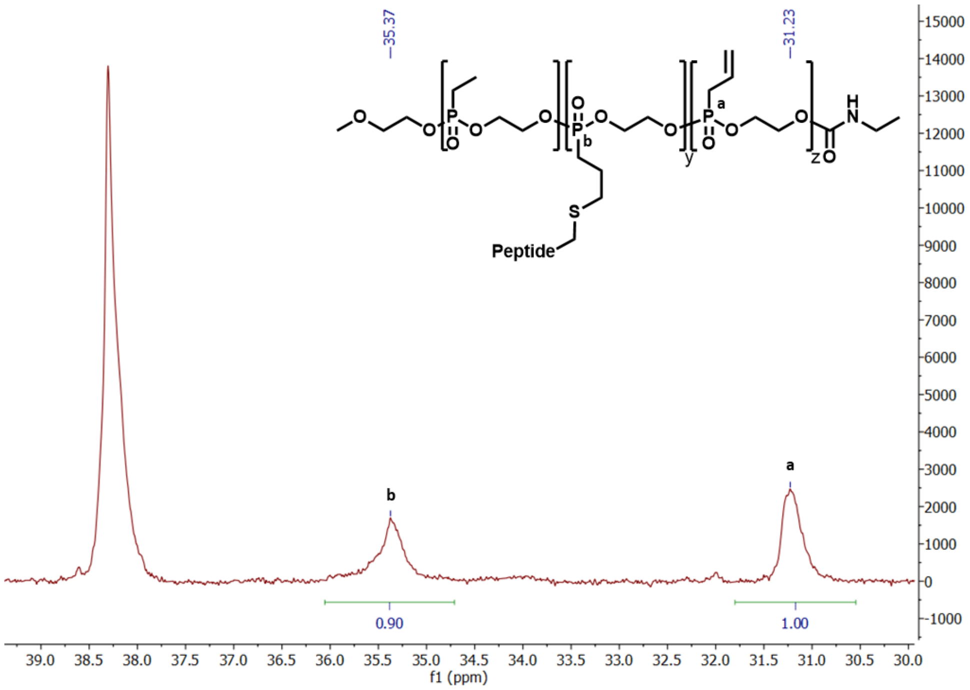

Figure 96: ^{31}P-NMR-spectrum of PDH2 (**XVI**) in D_2O (700 MHz) with the molecular structure and the relevant assigned phosphorus atoms.

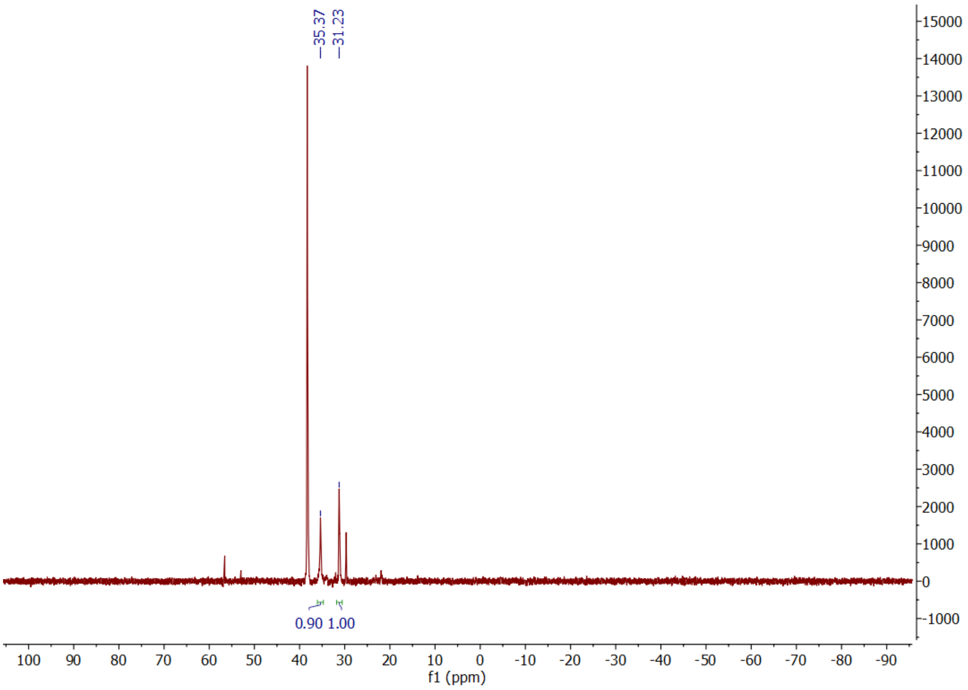

Figure 97: ^{31}P-NMR-spectrum of PDH2 (**XVI**) in D_2O (700 MHz).

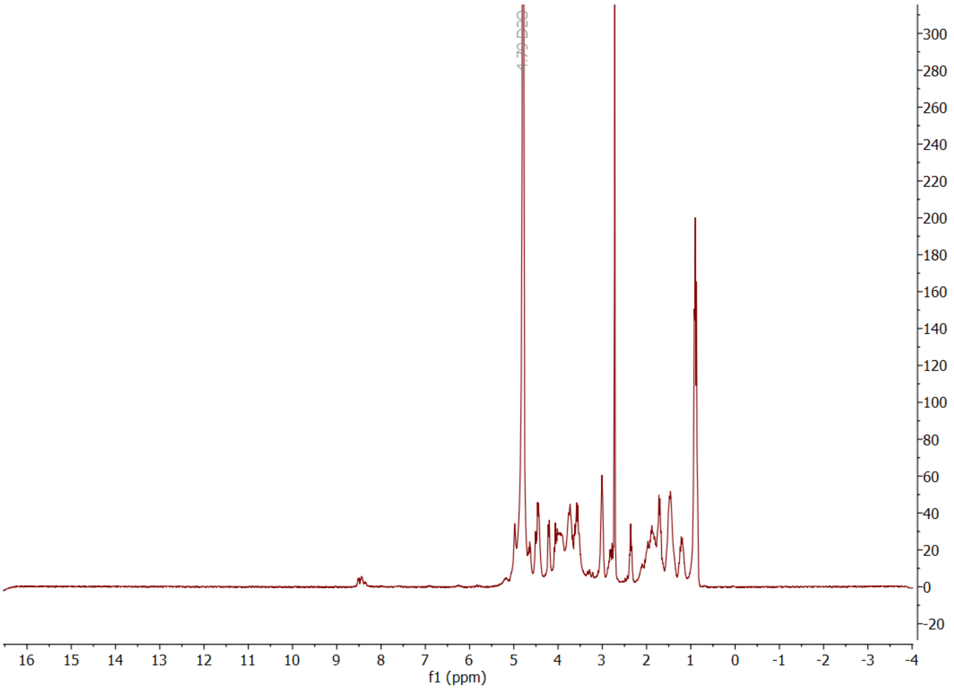

Figure 98: ^{1}H-NMR-spectrum of highly functionalized DexGMA1 DDH1 (**XIV**) in D_2O (700 MHz).

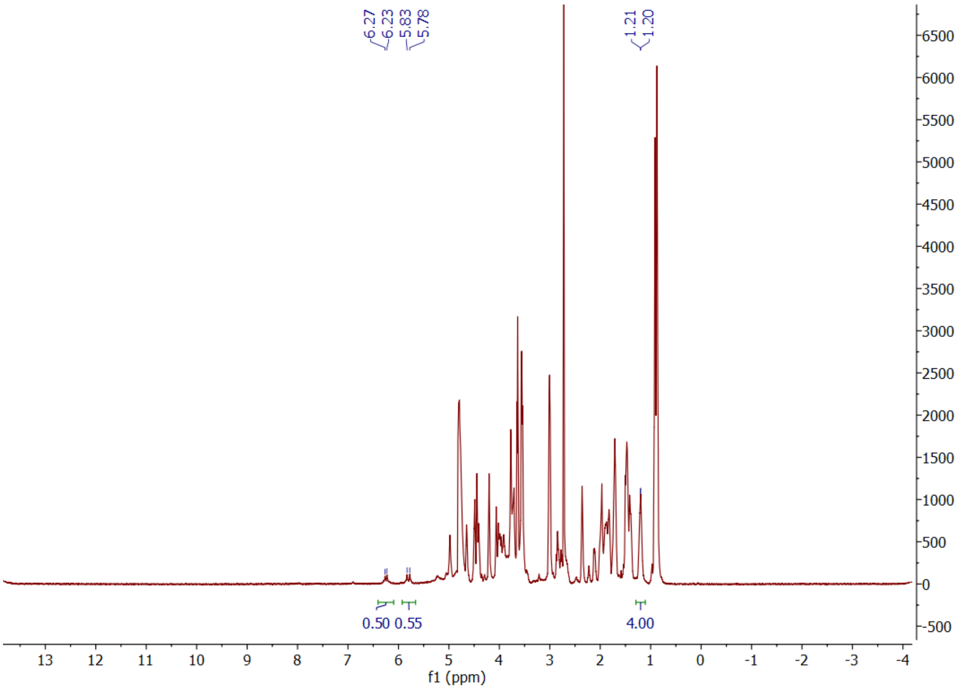

Figure 99: ^{1}H-NMR-spectrum of low functionalized DexGMA1 DDH2 (**XVIII**) in D_2O (700 MHz).

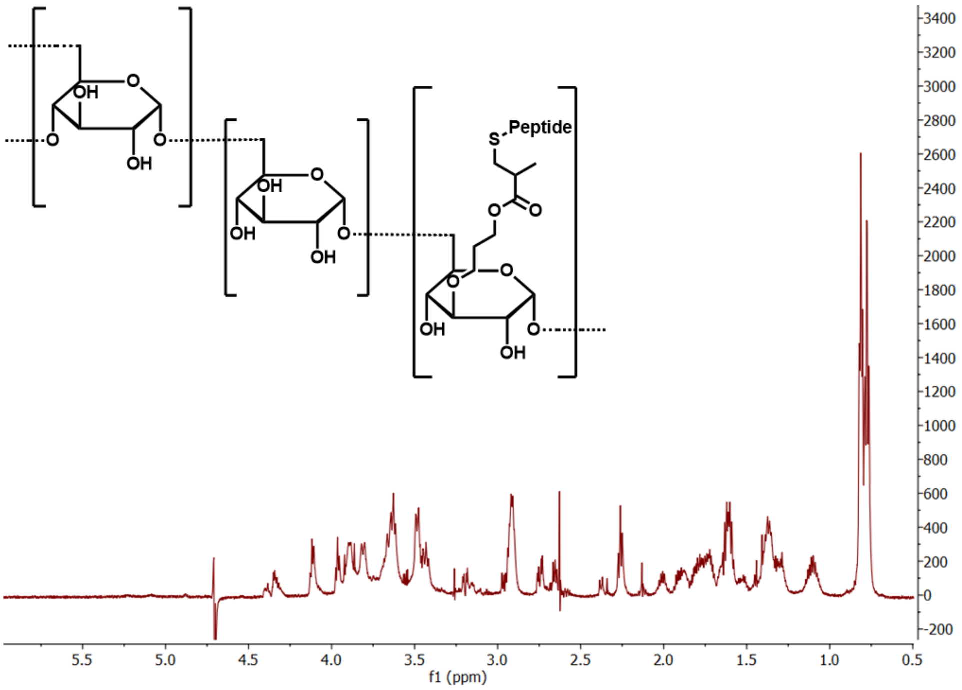

Figure 100: ^{1}H-NMR-spectrum of highly functionalized DexGMA2 DDH3 (**XIX**) with D3^C in D_2O with the suppression of water (700 MHz).

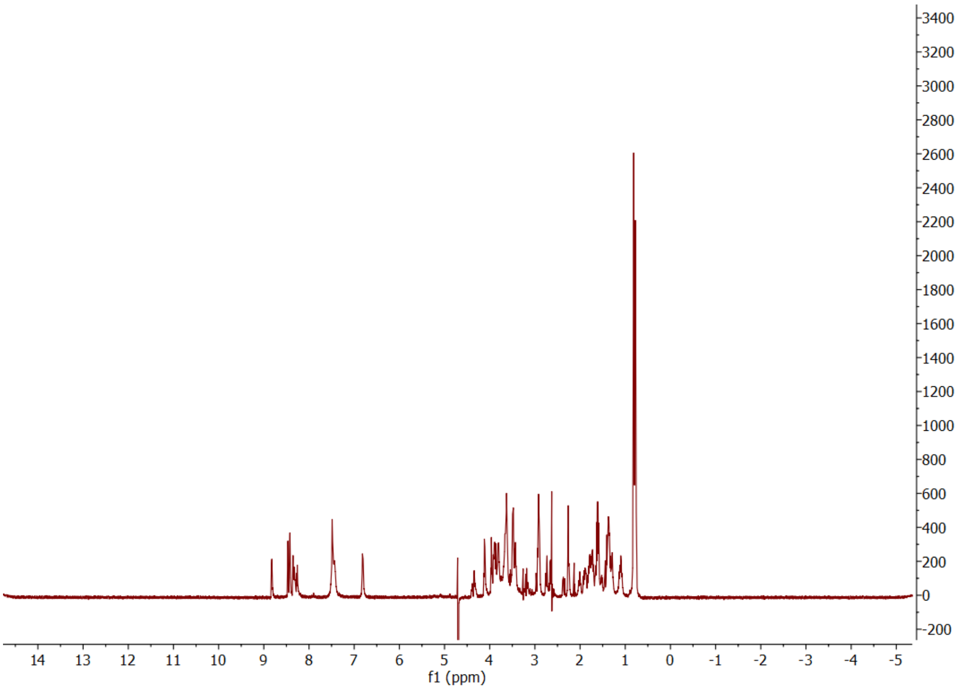

Figure 101: ^{1}H-NMR-spectrum of highly functionalized DexGMA2 DDH3 (**XV**) in D_2O (700 MHz).

8.2 List of Abbreviations

AA	Amino acid
$\mathrm{A}^{\mathrm{Pip}}$	3-(1-piperidinyl)alanine
ATP	Adenosine triphosphate
ATR	Attenuated total reflection
Boc	*tert*-Butyloxy carbonyl
Cbz	Benzyloxy carbonyl
CD	Circular dichroism
CHCA	α-Cyano-4-hydroxycinnamic acid
Clt	2-Chlorotrityl
DBU	1,8-Diazabicyclo-[5.4.0]undec-7-ene
DCC	*N,N'*-Dicyclohexylcarbodiimide
DCM	Dichloromethane
DexGMA	Glycidyl methacrylate-functionalized dextran
DHBA	2,4-Dihydroxybenzoic acid
DIC	Diisopropylcarbodiimide, *N,N'*-Diisopropylcarbodiimide
DMAP	*N,N*-Dimethylpyridin-4-amine
DMF	Dimethylformamide, *N,N*-Dimethylformamide
DMPAP	2,2-Dimethoxy-2-phenylacetophenone
DMSO	Dimethyl sulfoxide
DNA	Deoxyribonucleic acid
DOSY	Diffusion ordered spectroscopy
DP	Degree of polymerization
EDT	Ethane-1,2-dithiol
Fmoc	Fluorenylmethylenoxycarbonyl
FT	Fourier transformation
GMA	Glycidyl methacrylate
HA	Hyaluronic acid
HCCA	α-Cyano-4-hydroxycinamic acid
HCl	Hydrochloric acid

HOAt	1-Hydroxy-7-azabenzotriazole
HPLC	High performance liquid chromatography
HSA	Human serum albumin
HUVEC	Human umbilical vein endothelial cell
IR	Infrared
MALDI	Matrix-assisted laser desorption/ionization
MS	Mass spectroscopy
MWCO	Molecular weight cut-off
NCA	α-Amino acid N-carboxyanhydrides
Oxyma	Ethyl 2-cyano-2-(hydroxyimino)acetate
PBS	Phosphate buffered saline
PEG	Poly(ethylene glycol)
PPE	Poly(phosphoester)
RNA	Ribonucleic acid
RP-HPLC	Reversed-Phase High performance liquid chromatography
SEC	Size-exclusion chromatography
SPPS	solid-phase peptide synthesis
TCEP	Tris(2-carboxyethyl)phosphine
TEM	Transmission electron microscopy
TFA	Trifluoroacetic acid
ThT	Thioflavin T
TIPS	Triisopropylsilane
TOF	Time of flight
UV	Ultraviolet
VA-044	1,2-Bis(2-(4,5-dihydro-1*H*-imidazol-2-yl)propan-2-yl)diazene dihydrochloride

8.3 List of Figures

8.4 List of Tables

8.5 Bibliography

[1] J. M. Berg, J. L. Tymoczko, L. Stryer, G. J. Gatto, *Biochemie,* 7. Aufl., Springer Spektrum, Berlin, Heidelberg, **2014**.

[2] J. L. BAILEY, *Nature* **1949**, *164*, 889.

[3] R. B. Merrifield, *J. Am. Chem. Soc.* **1963**, *85*, 2149.

[4] S. Doonan, E. W. Abel (Hrsg.) *Tutorial Chemistry Texts*, Royal Society of Chemistry, Cambridge, **2007**.

[5] H. Bannwarth, B. P. Kremer, A. Schulz, *Basiswissen Physik, Chemie und Biochemie*. *Vom Atom bis zur Atmung - für Biologen, Mediziner und Pharmazeuten,* 2. Aufl., Springer-Verlag Berlin Heidelberg, Berlin, Heidelberg, **2011**.

[6] a) S. Jun, Y. Hong, H. Imamura, B.-Y. Ha, J. Bechhoefer, P. Chen, *Biophysical journal* **2004**, *87*, 1249; b) P. Arosio, M. Owczarz, H. Wu, A. Butté, M. Morbidelli, *Biophysical journal* **2012**, *102*, 1617.

[7] C. J. Bowerman, B. L. Nilsson, *Biopolymers* **2012**, *98*, 169.

[8] J. Gačanin, J. Hedrich, S. Sieste, G. Glaßer, I. Lieberwirth, C. Schilling, S. Fischer, H. Barth, B. Knöll, C. V. Synatschke et al., *Advanced materials (Deerfield Beach, Fla.)* **2019**, *31*, e1805044.

[9] M. Pieszka, A. M. Sobota, J. Gačanin, T. Weil, D. Y. W. Ng, *Chembiochem : a European journal of chemical biology* **2019**, *20*, 1376.

[10] M. Sunde, L. C. Serpell, M. Bartlam, P. E. Fraser, M. B. Pepys, C. C. Blake, *Journal of molecular biology* **1997**, *273*, 729.

[11] F. J. Blanco, G. Rivas, L. Serrano, *Nature structural biology* **1994**, *1*, 584.

[12] R. V. Rughani, J. P. Schneider, *MRS bulletin* **2008**, *33*, 530.

[13] A. D. MacNaught, A. Wilkinson, *Compendium of chemical terminology*. *IUPAC recommendations,* 2. Aufl., Blackwell Science, Oxford, **1997**.

[14] L. J. Smith, K. M. Fiebig, H. Schwalbe, C. M. Dobson, *Folding and Design* **1996**, *1*, R95-R106.

[15] G. Houen, *Peptide antibodies*. *Methods and protocols,* 1. Aufl., Humana Press, New York, **2015**.

[16] H. Rink, *Tetrahedron Letters* **1987**, *28*, 3787.

[17] S. S. Wang, *J. Am. Chem. Soc.* **1973**, *95*, 1328.

[18] K. Barlos, O. Chatzi, D. Gatos, G. Stavropoulos, *International journal of peptide and protein research* **1991**, *37*, 513.

[19] Y. Han, S. L. Bontems, P. Hegyes, M. C. Munson, C. A. Minor, S. A. Kates, F. Albericio, G. Barany, *J. Org. Chem.* **1996**, *61*, 6326.

[20] R. Sheppard, *Journal of peptide science : an official publication of the European Peptide Society* **2003**, *9*, 545.

[21] G. B. Fields, *Current protocols in protein science* **2002**, *Chapter 18*, Unit 18.1.

[22] L. A. Carpino, A. El-Faham, *Tetrahedron* **1999**, *55*, 6813.

[23] F. Albericio, J. M. Bofill, A. El-Faham, S. A. Kates, *J. Org. Chem.* **1998**, *63*, 9678.

[24] S. N. Khattab, *Chemical & pharmaceutical bulletin* **2010**, *58*, 501.

[25] R. Subiros-Funosas, S. N. Khattab, L. Nieto-Rodriguez, A. El-Faham, F. Albericio, *ChemInform* **2014**, *45*, 21-41.

[26] I. Ramos-Tomillero, H. Rodríguez, F. Albericio, *Organic letters* **2015**, *17*, 1680.

[27] Y. Fujiwara, K. Akaji, Y. Kiso, *Chemical & pharmaceutical bulletin* **1994**, *42*, 724.

[28] P. Stathopoulos, S. Papas, C. Pappas, V. Mousis, N. Sayyad, V. Theodorou, A. G. Tzakos, V. Tsikaris, *Amino acids* **2013**, *44*, 1357.

[29] a) C. M. Berac, L. Zengerling, D. Straβburger, R. Otter, M. Urschbach, P. Besenius, *Macromolecular rapid communications* **2020**, *41*, e1900476; b) J. D. Hartgerink, E. Beniash, S. I. Stupp, *Self-assembly and mineralization of peptide-amphiphile nanofibers*, **2011**.

[30] R. E. Moore, *Journal of industrial microbiology* **1996**, *16*, 134.

[31] I. Coin, *Journal of peptide science : an official publication of the European Peptide Society* **2010**, *16*, 223.

[32] Y. Sohma, Y. Hayashi, M. Kimura, Y. Chiyomori, A. Taniguchi, M. Sasaki, T. Kimura, Y. Kiso, *Journal of peptide science : an official publication of the European Peptide Society* **2005**, *11*, 441.

[33] J. K. Sahoo, C. Nazareth, M. A. VandenBerg, M. J. Webber, *Soft matter* **2018**, *14*, 9168.

[34] S. Zhang, M. A. Greenfield, A. Mata, L. C. Palmer, R. Bitton, J. R. Mantei, C. Aparicio, M. O. de La Cruz, S. I. Stupp, *Nature materials* **2010**, *9*, 594.

[35] G. A. Silva, C. Czeisler, K. L. Niece, E. Beniash, D. A. Harrington, J. A. Kessler, S. I. Stupp, *Science (New York, N.Y.)* **2004**, *303*, 1352.

[36] V. K. Thakur, M. K. Thakur, *Hydrogels*, Springer Singapore, Singapore, **2018**.

[37] R. M. Ottenbrite, K. Park, T. Okano, *Biomedical Applications of Hydrogels Handbook*, Springer New York, New York, NY, **2010**.

[38] P. M. Kharkar, K. L. Kiick, A. M. Kloxin, *Chemical Society reviews* **2013**, *42*, 7335.

[39] S. K. H. Gulrez, S. Al-Assaf, G. O in *Progress in Molecular and Environmental Bioengineering - From Analysis and Modeling to Technology Applications* (Hrsg.: A. Carpi), InTech, **2011**.

[40] K. M. Shakesheff, S. M. Cannizzaro, R. Langer, *Journal of Biomaterials Science, Polymer Edition* **1998**, *9*, 507.

[41] R. Dong, Y. Pang, Y. Su, X. Zhu, *Biomaterials science* **2015**, *3*, 937.

[42] G. W. M. Vandermeulen, H.-A. Klok, *Macromol. Biosci.* **2004**, *4*, 383.

[43] Z. Q. Liu, Z. Wei, X. L. Zhu, G. Y. Huang, F. Xu, J. H. Yang, Y. Osada, M. Zrínyi, J. H. Li, Y. M. Chen, *Colloids and surfaces. B, Biointerfaces* **2015**, *128*, 140.

[44] T. Steinbach, F. R. Wurm, *Angewandte Chemie (International ed. in English)* **2015**, *54*, 6098.

[45] C. B. Rodell, A. L. Kaminski, J. A. Burdick, *Biomacromolecules* **2013**, *14*, 4125.

[46] Q. Li, J. Wang, S. Shahani, D. D. N. Sun, B. Sharma, J. H. Elisseeff, K. W. Leong, *Biomaterials* **2006**, *27*, 1027.

[47] Z. Yang, G. Liang, L. Wang, B. Xu, *Journal of the American Chemical Society* **2006**, *128*, 3038.

[48] A. K. Sinha, D. Equbal, *Asian J. Org. Chem.* **2019**, *8*, 32.

[49] Y.-C. Wang, L.-Y. Tang, T.-M. Sun, C.-H. Li, M.-H. Xiong, J. Wang, *Biomacromolecules* **2008**, *9*, 388.

[50] J. Baran, S. Penczek, *Macromolecules* **1995**, *28*, 5167.

[51] J. Liu, W. Huang, Y. Pang, X. Zhu, Y. Zhou, D. Yan, *Biomacromolecules* **2010**, *11*, 1564.

[52] J. Wu, X.-Q. Liu, Y.-C. Wang, J. Wang, *J. Mater. Chem.* **2009**, *19*, 7856.

[53] K. Zarour, M. G. Llamas, A. Prieto, P. Rúas-Madiedo, M. T. Dueñas, P. F. de Palencia, R. Aznar, M. Kihal, P. López, *Carbohydrate polymers* **2017**, *174*, 646.

[54] D. Kim, J. F. Robyt, S.-Y. Lee, J.-H. Lee, Y.-M. Kim, *Carbohydrate Research* **2003**, *338*, 1183.

[55] Ș. Moldoveanu, V. David (Hrsg.) *Essentials in modern HPLC separations*, Elsevier, Waltham, Mass., **2013**.

[56] F. Hillenkamp, J. Peter-Katalinić (Hrsg.) *MALDI MS*. *A practical guide to instrumentation, methods and applications*, Wiley - VCH, Weinheim, **2009**.

[57] A. Wieser, S. Schubert, *TrAC Trends in Analytical Chemistry* **2016**, *84*, 80.

[58] C. Xue, T. Y. Lin, D. Chang, Z. Guo, *R. Soc. open sci.* **2017**, *4*, 160696.

[59] V. I. Stsiapura, A. A. Maskevich, V. A. Kuzmitsky, K. K. Turoverov, I. M. Kuznetsova, *J. Phys. Chem. A* **2007**, *111*, 4829.

[60] N. Amdursky, Y. Erez, D. Huppert, *Accounts of chemical research* **2012**, *45*, 1548.

[61] M. Biancalana, S. Koide, *Biochimica et biophysica acta* **2010**, *1804*, 1405.

[62] S. Udenfriend, S. Stein, P. Böhlen, W. Dairman, W. Leimgruber, M. Weigele, *Science (New York, N.Y.)* **1972**, *178*, 871.

[63] D. B. Williams, C. B. Carter, *Transmission electron microscopy*. *A textbook for materials science,* 2. Aufl., Springer, New York, **2008**.

[64] B. R. Singh (Hrsg.) *ACS symposium series*, *Vol. 750*, American Chemical Society, Washington, DC, **2000**.

[65] V. Cabiaux, R. Brasseur, R. Wattiez, P. Falmagne, J. M. Ruysschaert, E. Goormaghtigh, *The Journal of biological chemistry* **1989**, *264*, 4928.

[66] D. M. Byler, H. Susi, *Biopolymers* **1986**, *25*, 469.

[67] J. Fahrenfort, *Spectrochimica Acta* **1961**, *17*, 698.

[68] A. F. Drake, *J. Phys. E: Sci. Instrum.* **1986**, *19*, 170.

[69] W. W. Parson, *Modern Optical Spectroscopy*, Springer Berlin Heidelberg, Berlin, Heidelberg, **2015**.

[70] C. Wrana, *Polymerphysik*, Springer Berlin Heidelberg, Berlin, Heidelberg, **2014**.

[71] M. D. Lechner, K. Gehrke, E. H. Nordmeier, *Makromolekulare Chemie*. *Ein Lehrbuch für Chemiker, Physiker, Materialwissenschaftler und Verfahrenstechniker,* 4. Aufl., Birkhäuser Basel, Basel, **2010**.

[72] J. Mewis, N. J. Wagner, *Advances in colloid and interface science* **2009**, *147-148*, 214.

[73] J. L. J. L. L. Wiechmann, *Master thesis*, University of Ulm, Ulm, **2019**.

[74] X. Wang, Y. Zhou, J.-J. Ren, N. D. Hammer, M. R. Chapman, *Proceedings of the National Academy of Sciences of the United States of America* **2010**, *107*, 163.

[75] T. Wolf, T. Rheinberger, J. Simon, F. R. Wurm, *Journal of the American Chemical Society* **2017**, *139*, 11064.

[76] F. Hofmeister, *Archiv f. experiment. Pathol. u. Pharmakol* **1888**, *24*, 247.

[77] R. Beckert, E. Fanghänel, W. D. Habicher, H.-J. Knölker, P. Metz, K. Schwetlick, *Organikum*. *Organisch-chemisches Grundpraktikum,* 24. Aufl., Wiley-VCH Verlag, Weinheim, **2015**.

[78] N. P. Rodina, M. I. Sulatsky, A. I. Sulatskaya, I. M. Kuznetsova, V. N. Uversky, K. K. Turoverov, *Journal of Spectroscopy* **2017**, *2017*, 1.

[79] H. Kakwere, R. J. Payne, K. A. Jolliffe, S. Perrier, *Soft matter* **2011**, *7*, 3754.